University of Copenhagen

Niels Bohr Institute

Master's Thesis

Higgs Decay to Two Leptons and a Photon in the Standard Model Effective Field Theory

Author:
Thor Blokker Rasmussen

Supervisors:
Poul Henrik Damgaard
& Tyler Corbett

November, 2021

Acknowledgements

I would like to thank Poul Henrik Damgaard for allowing me the opportunity of writing my masters thesis within a very exciting field of research. Secondly I am profoundly grateful to Tyler Corbett for his guidance and great patience in answering my many questions.

Abstract

In this thesis we first introduce the concepts of the standard model and renormalization. We then discuss effective field theories where we introduce the four-Fermi theory and the chiral Lagrangian of pions as examples. We then discuss a simple method for deriving the effective action at tree-level from a ultraviolet theory. We also discuss how one might use effective field theories to infer the nature of new heavy physics and how these shift the predictions of low energy, or infrared, theories such as the standard model. Motivated by the discussion of effective field theories and how they can provide tools for exploring new physics, we discuss the standard model effective field theory (SMEFT).

Next we apply these concepts in order to derive the main result of this thesis, the Higgs decay to two leptons and a photon $H \to \bar{\ell}\ell\gamma$ at tree and one-loop level in the standard model and the shifts to this from the SMEFT at tree-level. We discuss how this decay at tree-level is chirally suppressed as m_ℓ/v due to the smallness of the leptonic Yukawa couplings and how this presents an interesting phenomenological application of the SMEFT. We calculate the matrix elements for the Higgs decays $H \to \gamma\gamma$ and $H \to \gamma Z$. We then discuss the remaining one-loop contributions from the standard model and then calculate the full standard model decay width at one-loop. We then move on to discuss the SMEFT contributions to the Higgs decay to two leptons and a photon. We do this by assembling matrix elements of the squares of tree-level SMEFT contributions as well as the SMEFT interference with the standard model tree and loop amplitudes. We then calculate the total decay width including the SMEFT contributions and normalize this to the standard model decay width. We expand this result in terms of the Wilson coefficients from the SMEFT. We then produce Dalitz-like plots showing the different SMEFT contributions normalized to the standard model. We use these plots in order to find cuts in the invariant mass of the di-lepton system suitable for emphasizing specific SMEFT contributions. Finally, we study five regions in phase space where we consider either weakly interacting new physics or an assumed new physics scale. We use this to demonstrate that the contributions of different operators within the SMEFT can be emphasized when using these regions and the aforementioned assumptions about new physics.

Contents

1 Standard Model

In this section we will outline certain aspects of the standard model of particle physics. First we discuss the underlying Lagrangian formalism which is used when working with relativistic particles, where quantum field theory is needed. We then discuss the Higgs mechanism and spontaneous symmetry breaking. Using this we discuss the process of spontaneous symmetry breaking in the context of electro-weak theory, responsible for massive vector bosons in the standard model.

1.1 The Lagrangian formalism

This section derives the Euler-Lagrange equations based on Refs. [1] and [2].
In quantum field theory one is using quantum mechanics paired with special relativity. This enables a quantum description of objects moving comparable to the speed of light where Newtonian mechanics fail. In a theory, where special relativity is needed, the formulation must be Lorentz invariant such that it is consistent across inertial systems. For these purposes quantum field theory, based on the Lagrangian formalism, is commonly used. One of the applications of the Lagrangian is the Euler-Lagrange equation which we now discuss in the context of field theory. Consider a Lagrangian density as a function of a scalar field $\phi(x)$ and its derivative $\partial_\mu\phi(x)$, $\mathcal{L}(x) = \mathcal{L}(\phi, \partial_\mu\phi)$. By infinitesimally varying the fields, as: $\phi \to \phi + \delta\phi$, we then obtain:

$$\delta\mathcal{L}(x) = \frac{\partial\mathcal{L}}{\partial\phi}\delta\phi(x) + \frac{\partial\mathcal{L}}{\partial(\partial_\mu\phi(x))}\delta(\partial_\mu\phi(x)) \tag{1}$$

The Euler-Lagrange equations for the field formalism can then be obtained by applying the principle of least action as one would do in classical mechanics:

$$\delta S = \int d^4x \delta\mathcal{L}(x) = 0\,. \tag{2}$$

Plugging in the varied Lagrangian density:

$$0 = \int d^4x \left[\frac{\partial\mathcal{L}}{\partial\phi}\delta\phi(x) + \frac{\partial\mathcal{L}}{\partial(\partial_\mu\phi(x))}\delta(\partial_\mu\phi(x))\right]\,. \tag{3}$$

This we can write as:

$$0 = \int d^4x \left(\left[\frac{\partial\mathcal{L}}{\partial\phi}\delta\phi(x) - \frac{\partial\mathcal{L}}{\partial(\partial_\mu\phi(x))}\delta(\partial_\mu\phi(x))\right] + \partial_\mu\left[\frac{\partial\mathcal{L}}{\partial(\partial_\mu\phi(x))}\delta\phi(x)\right]\right)\,. \tag{4}$$

Since the last term is the total derivative it only depends on the fixed end points and the Euler-Lagrange equations consequently becomes:

$$0 = \frac{\partial\mathcal{L}(\phi(x), \partial_\mu\phi(x))}{\partial\phi} - \partial_\mu\frac{\partial\mathcal{L}(\phi(x), \partial_\mu\phi(x))}{\partial(\partial_\mu\phi(x))}\,. \tag{5}$$

From this this equation the classical equations of motion can be found for the field ϕ. As we will see later in Section 3, the classical equations can be useful in th context of effective field theories.

1.2 Electroweak Symmetry Breaking

The weak force is mediated by the massive vector bosons $W^{\pm}, Z$. One problem with massive particles is that their Lagrangian is not invariant under local symmetries, i.e. gauge symmetries. Which leads to their Lagrangian being non-renormalizable. A solution to the experimental observation of massive gauge bosons is the Higgs mechanism. This will make it possible for particles in the Lagrangian to acquire mass through spontaneous symmetry breaking.

1.2.1 Example of Higgs mechanism with only U(1)

This section is based on discussions in Ref.[3].

Defining the Higgs potential as a complex scalar field potential:

$$V(\phi) = \frac{1}{2}\mu^2\phi^2 + \frac{1}{4}\lambda\phi^4\,, \tag{6}$$

then the corresponding Lagrangian reads:

$$\mathcal{L} = -\frac{1}{4}F^{\mu\nu}F_{\mu\nu} + (D_\mu\phi)(D^\mu\phi^*) - \mu^2\phi^2 - \lambda\phi^4\,. \tag{7}$$

Where D_μ is the covariant derivative defined as:

$$D_\mu = \partial_\mu + igB_\mu\,, \tag{8}$$

and B_μ is a new gauge field which has the field strength:

$$F^{\mu\nu} = (\partial^\nu B^\mu - \partial^\mu B^\nu)\,. \tag{9}$$

The Lagrangian is invariant under the local gauge transformations of $U(1)$ defined as:

$$\phi(x) \to \exp\left(igG(x)\right)\phi(x)\,,\ B_\mu \to B_\mu - \partial_\mu G(x)\,. \tag{10}$$

Plotting Eq. 6 for $\mu^2 < 0$ (Figure 1), we see that there is a degenerate minima in a continuous circle of radius $|\phi| = v$ away from $|\phi| = 0$. Expanding the field ϕ as a perturbation about the minimum v in Figure 1 we find:

$$\phi(x) = \frac{1}{\sqrt{2}}\left(v + h(x) + i\xi(x)\right)\,. \tag{11}$$

Where ξ is a Goldstone boson. The Goldstone boson ξ can be removed by an appropriate gauge fixing choice, as such we neglect them in the discussion below. As a result we use the field expanded as:

$$\phi(x) = \frac{1}{\sqrt{2}}\left(v + h(x)\right)\,. \tag{12}$$

We expand the Lagrangian about vacuum expectation value v by inserting Eq. 12 in Eq. 7 and we take $\mu^2 = \lambda v^2$. This yields two new mass terms in the Lagrangian. First we get a massive Higgs scalar with Lagrangian terms:

$$\mathcal{L} = \frac{1}{2}(\partial_\mu h)(\partial^\mu h) - \lambda h^2 v^2 + \mathcal{L}_{int}\,, \tag{13}$$

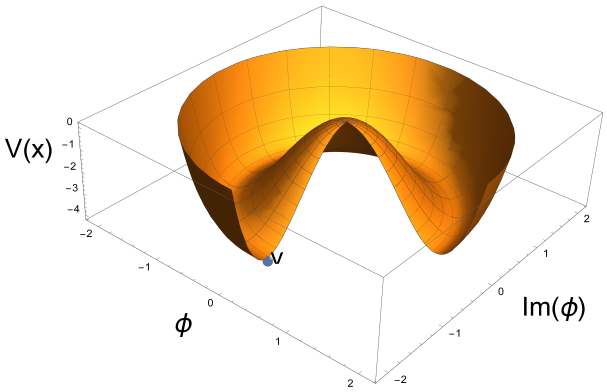

Figure 1: Example of complex scalar Higgs potential of the form in Eq. 6 with $\mu^2 < 0$ showing symmetric minima v around $\phi = 0$

giving a Higgs mass, $m_h^2 = 2\lambda v^2$. We also get a massive gauge boson:

$$\mathcal{L} = -\frac{1}{4}F^{\mu\nu}F_{\mu\nu} + \frac{1}{2}g^2v^2B_\mu B^\mu + \mathcal{L}_{int}\,, \tag{14}$$

Where the mass of the gauge boson is $m_B^2 = g^2v^2$. The Higgs mechanism thus allows for massive particles within in a locally gauge invariant Lagrangian, facilitated by *spontaneous symmetry breaking* where Higgs takes on constant vacuum expectation value v.

1.2.2 The Standard Model Vector bosons

The discussion in this section follows that of Ref. [2]. In the standard model the Higgs is instrumental in allowing for the famous electroweak unification where a $SU(2)\times U(1)$ symmetry is spontaneously broken. The Lagrangian is:

$$\mathcal{L} = -\frac{1}{4}(W_{\mu\nu}^a)^2 - \frac{1}{4}B_{\mu\nu}^2 + (D_\mu H)^\dagger(D_\mu H) - V(H)\,. \tag{15}$$

Where the Higgs potential is:

$$V(H) = -\mu^2 H^\dagger H + \lambda(H^\dagger H)^2\,, \tag{16}$$

with μ being positive definite and

$$H = \exp\left(2i\frac{\pi^a\tau^a}{v}\right)\begin{pmatrix}0\\ \frac{v}{\sqrt{2}}+\frac{h}{\sqrt{2}}\end{pmatrix}\,, \tag{17}$$

is the Higgs multiplet.

Employing the unitary gauge we can set $\pi^a = 0$. $W_{\mu\nu}^a$ is the $SU(2)$ gauge boson and $B_{\mu\nu}$ is the $U(1)$ gauge boson. The covariant derivative is:

$$D_\mu H = \partial_\mu H + ig_2W_\mu^a\tau^a H + \frac{1}{2}ig_1B_\mu H\,, \tag{18}$$

where $\tau^a = \frac{1}{2}\sigma^a$ with σ^a the Pauli matrices and g_2, g_1 are the $SU(2)$ and $U(1)$ coupling constants respectively.
Now expanding the covariant derivative term of the Lagrangian, which contains the Higgs interactions with $B_{\mu\nu}$ and $W^a_{\mu\nu}$

$$\begin{aligned}(D_\mu H)^\dagger D_\mu H = (g_2^2 W^a_\mu \tau^a H^\dagger W^a_\mu \tau^a H + \frac{1}{2} g_1 g_2 B_\mu W^a_\mu \tau^a H H^\dagger) + \\ (g_2 g_1 \frac{1}{2} W^a_\mu \tau^a H^\dagger B_\mu H + \frac{1}{4}(g_1)^2 B_\mu H^\dagger B_\mu H)\,.\end{aligned} \tag{19}$$

We then expand the Higgs doublet in Eq. 19 around the vacuum expectation value v. Additionally we disregard terms with the Higgs scalar h in the following and find:

$$\mathcal{L}_{\text{mass}} = \frac{v^2 g_2^2}{8} \begin{pmatrix} 0 & 1 \end{pmatrix} \left(W^a_\mu \sigma^a W^a_\mu \sigma^a + \frac{g_1}{g_2} B_\mu W^a_\mu \sigma^a + \frac{g_1}{g_2} W^a_\mu \sigma^a B_\mu + \left(\frac{g_1}{g_2}\right)^2 B_\mu B_\mu \right) \begin{pmatrix} 0 \\ 1 \end{pmatrix}\,. \tag{20}$$

The Pauli matrices satisfy:

$$\begin{pmatrix} 0 & 1 \end{pmatrix} \sigma^a \begin{pmatrix} 0 \\ 1 \end{pmatrix} = -\delta_{3,a}\,, \tag{21}$$

so that:

$$\mathcal{L}_{\text{mass}} = \frac{v^2 g_2^2}{8} \left((W^1_\mu)^2 + (W^2_\mu)^2 + \left(\frac{g_1}{g_2} B_\mu - W^3_\mu \right)^2 \right)\,. \tag{22}$$

Then to diagonalize the masses we define:

$$\begin{pmatrix} Z_\mu \\ A_\mu \end{pmatrix} = \begin{pmatrix} c_W & -s_W \\ s_W & c_W \end{pmatrix} \begin{pmatrix} W^3_\mu \\ B_\mu \end{pmatrix} \iff \begin{pmatrix} B_\mu \\ W^3_\mu \end{pmatrix} = \begin{pmatrix} c_W & -s_W \\ s_W & c_W \end{pmatrix} \begin{pmatrix} A_\mu \\ Z_\mu \end{pmatrix}, \tag{23}$$

where c_W and s_W are $\cos(\phi_w)$ and $\sin(\phi_w)$ with ϕ_w being the weak mixing angle defined by the ratio between g_1 and g_2 in Eq. 24. Using:

$$W^\pm_\mu = \frac{1}{\sqrt{2}} \left(W^1_\mu \mp i W^2_\mu \right)^2\,,\ \frac{g_1}{g_2} = \tan(\theta_w)\,, \tag{24}$$

we get

$$\mathcal{L}_{\text{mass}} = \frac{v^2 g_2^2}{8} \left(2 W^+_\mu W^-_\mu + \frac{Z^2_\mu}{c^2_W} \right) = m^2_W W^+_\mu W^-_\mu + \frac{1}{2} m^2_Z Z^2_\mu\,, \tag{25}$$

with:

$$m_Z = \frac{v g_2}{2 c_W},\quad m_W = \frac{v g_2}{2}\,, \tag{26}$$

and

$$m_Z = \frac{m_W}{c_W}\,. \tag{27}$$

We see that the physical massive gauge bosons Z and W emerge from the Higgs coupling to the electro weak $SU(2)$ and $U(1)$ gauge bosons. We also note that $U(1)_{QED}$ remains unbroken and the photon remains massless. Furthermore Eq. 27 predicts a mass splitting between the W and Z boson masses which is an important precision test of the standard model.

1.3 Standard Model Searches

In this section we present a summary of standard model data collected at the Large Hadron Collider (LHC). With this we want to motivate our standard model effective field theory studies by noting the large uncertainty there still is on Higgs production, as seen in Figure 2. In fact among the observables shown in Figure 2, the Higgs measurements represent the least well measured. Therefore we infer that the Higgs sector is a good place for new physics to be hiding within experimental uncertainties. To reinforce this we have calculated the relative uncertainty of the Higgs branching ratios from the plot on the left of Figure 3. Doing this we used the average of the upper and lower bound of the total uncertainties. These relative uncertainties are shown in Table 1, where we see just how large these are. However in the future, after the current run of the LHC, it will be upgraded to the High luminosity-LHC (HL-LHC). By the end of the HL-LHC 3000/fb of integrated luminosity is expected to be collected. This data is then expected to reduce the uncertainty on the Higgs decays. The HL-LHC projections for the Higgs branching ratio measurements, assuming the standard model Higgs, are shown on the right in Figure 3 from Ref.[4]. Especially relevant to this thesis is the branching ratio for the Higgs decay to a Z–boson and a photon, which has not yet been measured but is expected to be measured to 19.1% relative uncertainty at HL-LHC as seen on the right in Figure 3.

Branching ratios	Relative Uncertainty [%]
$\sigma_{ggF}^{ZZ^*}$	11.50%
$\sigma_{VBF}/\sigma_{ggF}$	23.79%
σ_{WH}/σ_{ggF}	41.94%
σ_{ZH}/σ_{ggF}	40.10%
$\sigma_{t\bar{t}+tH}/\sigma_{ggF}$	24.17%
$B_{\gamma\gamma}/B_{ZZ^*}$	14.97%
B_{WW^*}/B_{ZZ^*}	19.64%
$B_{\tau\tau}/B_{ZZ^*}$	27.91%
$B_{\bar{b}b}/B_{ZZ^*}$	34.95%

Table 1: Table of the relative uncertainty of the branching ratios in Figure 3. In calculation these we have used the average of the uncertainties lower and upper bound.

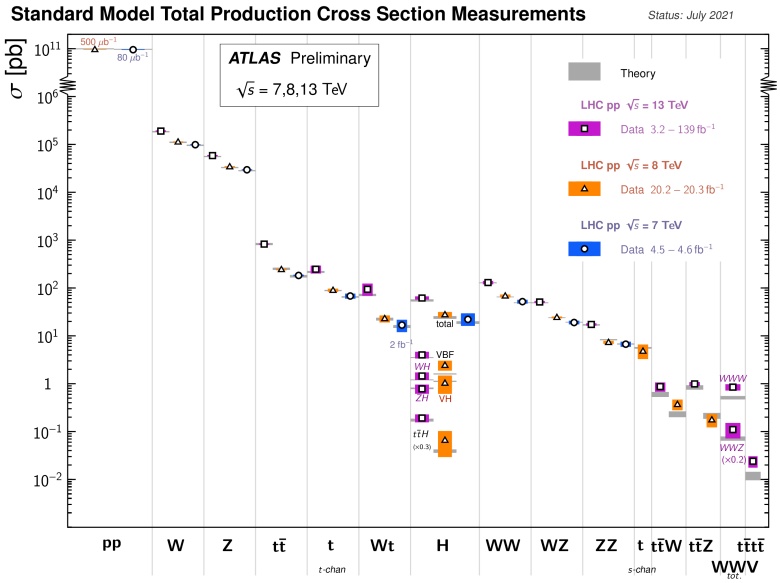

Figure 2: Plot taken from Ref. [5]. This plot contains total production cross section measurements for standard model particles, including the Higgs

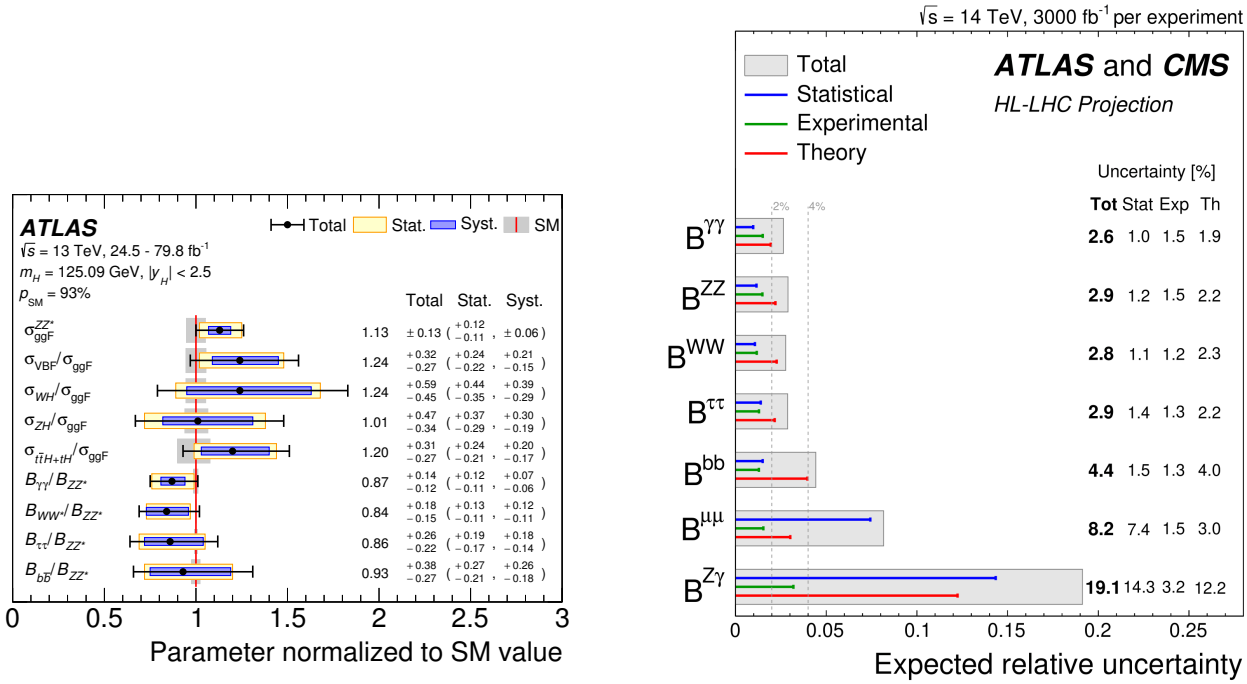

Figure 3: Figure on the left is taken from Ref. [6], showing the different Higgs decay branching ratios and their experimental error. Figure on the right is taken from Ref. [4], showing relative uncertainties on Higgs branching ratios expected from HL-LHC

2 Renormalization

In this section we briefly discuss renormalization in quantum field theory. We first discuss how loops give rise to divergences and how this motivates the concept of renormalization through a ϕ^4-theory example. We then discuss how some loops in a renormalizable theory with no possible counter term must be free of divergences, here we refer to these as non-divergent. Finally we explore how adding higher dimensional terms to the ϕ^4-theory makes for a non-renormalizable theory and what non-renormalizability actually means. This section is based on discussions from Refs. [1] and [2].

2.1 Renormalizable Theories

2.1.1 ϕ^4-theory

Suppose we have a theory with Lagrangian:

$$\mathcal{L} = \frac{1}{2}(\partial^\mu \phi)(\partial_\mu \phi) - \frac{1}{2}m^2\phi^2 - \frac{\lambda}{4!}\phi^4 \,. \tag{28}$$

The kinetic term gives the Feynman rule for the propagator of a ϕ going to a ϕ:

$$\phi \to \phi = \frac{i}{p^2 - m^2} \,. \tag{29}$$

The interaction term proportional to ϕ^4 gives the Feynman rule for the interaction of 4 ϕ fields, i.e. the 4ϕ scattering event ($\phi\phi \to \phi\phi$), e.g. the matrix element for 4ϕ scattering at tree level is simply given by:

$$i\mathcal{M}_{4\phi} = -i\lambda \,, \tag{30}$$

resulting in the square amplitude:

$$|\mathcal{M}|^2_{4\phi} = \lambda^2 \,. \tag{31}$$

At one loop we then have two propagators and an additional vertex factor. (see Figure 4)

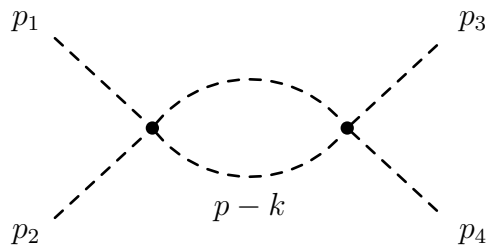

Figure 4: One-loop diagram from the ϕ^4 vertex

With momentum conventions defined in Figure 4, the matrix element would look like:

$$i\mathcal{M} = -\frac{\lambda^2}{2}\int \frac{dk^4}{(2\pi)^4}\frac{i}{(p-k)^2 - m^2}\frac{i}{k^2 - m^2}\,. \tag{32}$$

Where the internal momentum k is not constrained by momentum conservation $p_1 + p_2 = p_3 + p_4 = p$ and we therefore have to integrate over it. A naive dimensional analysis of the integrand indicates this integral is ill-defined. However, if we define a high energy, or ultraviolet (UV) scale, Λ at which the momenta is cut off we can define a superficial degree of divergence. The superficial degree of divergence is then logarithmic:

$$\propto \lim_{\Lambda\to\infty}\int_{-\Lambda}^{\Lambda}\frac{dk}{k} \sim \log\left(\frac{\Lambda}{c}\right) \to \infty\,, \tag{33}$$

where c is some constant.

In order to remove divergences such as this, it is common to redefine the parameters of the Lagrangian in a manner that allows for the introduction of counter terms which will cancel the UV divergences. Writing the Lagrangian as:

$$\mathcal{L} \to \mathcal{L}_0 \equiv \frac{1}{2}(\partial^\mu\phi)(\partial_\mu\phi) - \frac{1}{2}m_0^2\phi_0^2 - \frac{\lambda_0}{4!}\phi_0^4\,, \tag{34}$$

with:

$$\lambda_0 \equiv Z_\lambda\lambda_R\,, \tag{35}$$

λ_R is referred to as the renormalized coupling constant and Z_λ the renormalization constant. The fields and parameters with subscript 0 are referred to as *bare*, likewise the fields and parameters with subscript R are the renormalized ones. In order to regulate the one-loop divergence in Eq.32 we take:

$$Z_\lambda = 1 + \delta\lambda\,. \tag{36}$$

With this definition we find two terms in the potential:

$$V = \frac{\lambda_0}{4!}\phi_0^4 \;\rightarrow \frac{\lambda_R}{4!}\phi_0^4 \; + \frac{\lambda_R \delta\lambda}{4!}\phi_0^4 \,. \tag{37}$$

The first term is the tree level interaction and the second term is a counter term. The counter term is treated as formally of one-loop order. Writing the matrix element again, now with the counter term:

$$i\mathcal{M} = -i\lambda_R - \frac{\lambda_R^2}{2}\int \frac{dk^4}{(2\pi)^4}\frac{i}{(p-k)^2 - m^2}\frac{i}{k^2 - m^2} - i\lambda_R\delta\lambda \,. \tag{38}$$

By defining a subtraction scheme we can remove the UV divergences in the theory:

$$i\mathcal{M} = -i\lambda_R - \frac{\lambda_R^2}{2}\lim_{\Lambda\to\infty}\log\left(\frac{\Lambda}{c}\right) - i\lambda_R\delta\lambda \,, \tag{39}$$

$$\delta\lambda \equiv \frac{i\lambda_R}{2}\lim_{\Lambda\to\infty}\log\left(\frac{\Lambda}{c}\right) \,, \tag{40}$$

$$i\mathcal{M} = -i\lambda_R \,. \tag{41}$$

In general it is not necessarily the entire loop contribution which is subtracted off in this manner. This discussion is meant as a simplified example of how UV divergences are removed from a quantum field theory. In addition to divergences in interactions, the one loop corrections to two-point functions (propagators) can be UV divergent, a combination of rewriting $\phi_0 \rightarrow Z_\phi\phi_R$ and the counter term from m_0 are used to regulate these divergences. In this way there is one counter term for each divergence, we say the theory is renormalizable. More generally we define: A theory is renormalizable if its UV divergences can be removed with a finite amount of counter terms. Vice versa: A theory is non-renormalizable if its UV divergences require an infinite number of counter terms to be removed. Non-renormalizable theories are therefore technically able to be renormalized given an infinite number of counter terms. In section 2.2 we discuss that these theories are still well defined for phenomenological purposes in the correct kinematic limit. A general theory of space-time dimension d is renormalizable if its operators $\mathcal{Q}$ are of dimension $0 \leq [\mathcal{Q}] \leq d$. We discuss this further in Section 2.2.

2.1.2 Non-Divergent loops

In a renormalizable theory such as the ϕ^4 theory in Eq.28 the divergences of loop diagrams are canceled by counter terms which comes from interactions in the Lagrangian. If a loop diagram forms a process that does not have a corresponding tree-level interaction term in the Lagrangian, there is also no possibility for a counter term. If the corresponding Lagrangian

is renormalizable, it then follows that the process cannot be divergent since no counter term exists. Examples of this is the Higgs decay to 2 gluons or 2 photons which is not allowed at tree level but is through the loop diagrams(fig. 5, fig. 6):

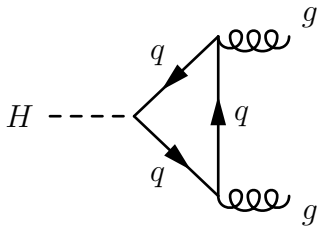

Figure 5: Diagram of the non-divergent loop process allowing for gluon production from Higgs decay

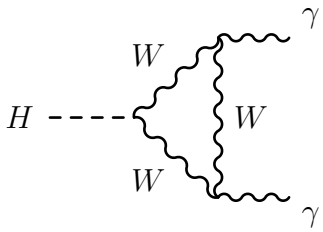

Figure 6: Example diagram of the non-divergent loop process allowing for photon production from Higgs decay

2.2 Non-renormalizable theories

In section 2.1.1 renormalizable and non-renormalizable theories were defined by how many counter terms were needed to renormalize them, more specifically if there was an finite or infinite number of counter terms needed. Here is a simple example of how an infinite number of required counter terms could arise. Consider this Lagrangian:

$$\mathcal{L} = \frac{1}{2}(\partial^\mu\phi)(\partial_\mu\phi) - \frac{1}{2}m^2\phi^2 - \frac{\lambda}{4!}\phi^4 - \frac{c^{(1)}}{6!\,M^2}\phi^6 - \frac{c^{(2)}}{8!\,M^4}\phi^8 - \frac{c^{(3)}}{10!\,M^6}\phi^{10} - \frac{c^{(4)}}{12!\,M^8}\phi^{12}\,, \quad (42)$$

with $c^{(i)}$ being dimensionless coupling constants and M is a relevant scale of mass dimension one. In the following we imagine that we are adding the terms of dimension six and higher one at a time.
Starting with the ϕ^6 term, a one-loop diagram of a 8ϕ interaction can be formed by two ϕ^6 vertices as seen in the diagram in Figure 7.

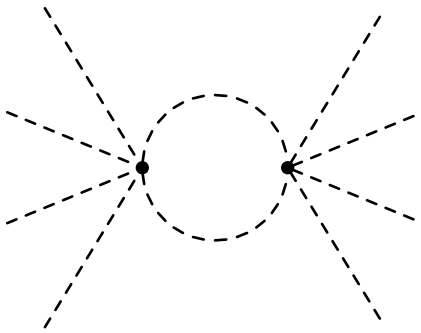

Figure 7: One-loop diagram from the ϕ^6 vertex

To cancel the divergence in Figure 7 we need, as in section 2.1.1, a one-loop order counter term. For such a counter term we need a tree-level equivalent process, i.e. a $4\phi \to 4\phi$ interaction at tree-level. This means a ϕ^8 term in the Lagrangian as one 8ϕ vertex would provide the $4\phi \to 4\phi$ at tree-level as seen in Figure 8. Already this is worrying since this tree-level equivalent process needed for a counter term, originates from a higher order term in the Lagrangian. This is unlike the one-loop process from the ϕ^4 term in section 2.1.1.

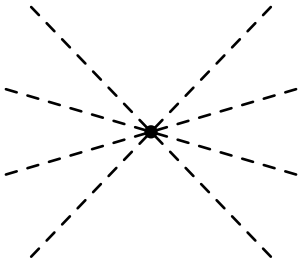

Figure 8: Tree-level diagram from the ϕ^8 vertex, with the same number of external lines as the one-loop diagram from the ϕ^6 term in Figure 7

We have discussed the addition of a ϕ^6 term to the Lagrangian and how this, for renormalization purposes, needs the ϕ^8 which we then added. Combining these two terms we are now able to create a one-loop diagram for a 10ϕ process with one ϕ^6 vertex and one ϕ^8 vertex (see Figure 9). Since this is a 10ϕ process we would then need, as discussed previously, a tree-level equivalent process in order to have a suitable counter term for this process. For a such a counter term we need a ϕ^{10} term in the Lagrangian.

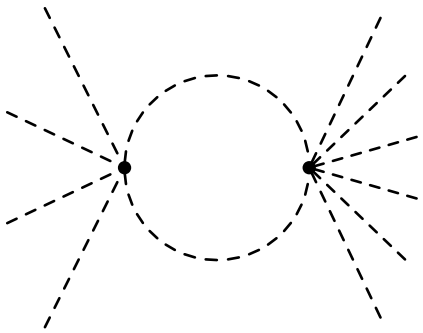

Figure 9: one-loop diagram of a $5\phi \to 5\phi$ scattering process formed from one ϕ^6 and one ϕ^8 vertex

We can continue this idea by considering the ϕ^8 term we now have in our Lagrangian. This term itself sources a one-loop 12ϕ process which needs a counter term from the tree-level equivalent process sourced by a ϕ^{12} term. By now it is evident that every time we add a term to the Lagrangian in order to source a counter term, this term itself has no such counter term which results in adding even more terms. In fact, a theory like this needs an infinite number of counter terms and is therefore non-renormalizable. Additionally, from this simple analysis it is apparent that the ϕ^4 term is special in that it sources its own tree-level equivalent process to its one-loop process, allowing for a one-loop order counter term.

Using dimensional analysis, we see from the Lagrangian in Eq. 2.1.1 that, since the Lagrangian has mass dimension $[\mathcal{L}]_M = 4$, the non-renormalizable terms have coupling constants of negative mass dimension: $[\lambda_6]_M$, $[\lambda_8]_M$, $[\lambda_{12}]_M < 0$. The renormalizable terms on the other hand have coupling constants with either positive or 0 mass dimension: $[m^2]_M = 2$, $[\lambda]_M = 0$. This can be generalized and added to the definition of renormalizable theories in section 2.1.1, such that renormalizable theories have coupling constants of mass dimension $d \geq [\lambda]_M \geq 0$, where d is the space-time dimension.

Despite theories being non-renormalizable they can still be predictive and of use to us. Generally the divergences arising from loop diagrams will always be polynomial in external momenta p.[2] This means that the theory is perturbative given the momentum of a process in consideration, is small relative to the mass m. This means that in this regime where $p \ll M$, i.e. low energy regime, only a finite number of these divergences are relevant by order in the $\frac{p}{M}$ power counting. As such perturbation theory is still well defined. Non-renormalizable theories therefore constitute well defined and systematically improvable quantum field theories. This leads us to discuss the utility of non-renormalizable theories, which within a certain energy regime are both well defined and predictive, in order to approach important problems in particle physics.

3 Effective Field Theories

In this section we introduce effective field theories as low energy effective theories obtained by the assumption that some field(s) has a very large mass compared to the other fields in the theory. These heavy fields can therefore be treated as a constant when looking at interactions among the remaining light fields. We introduce this process integrating out the heavy field. We discuss how the remaining fields in the effective field theory has corrections to them from the heavy field which was integrated out. As a result some effects of the heavy field can still be present in the effective field theory. We then introduce a way of obtaining an effective action at tree-level expanding the action around its equation of motion. Finally we use a method to obtain and effective action for the standard model Higgs modified by a heavy singlet scalar field which is integrated out at tree-level. We use this example to discuss how such field theories can be used and explore new physics their effects on standard model fields, possibly providing predictions of new heavy fields.

3.1 Introduction

Effective field theories are theories that use effective actions such as[7]:

$$\Gamma = \int dx^4 \mathcal{L}_{\text{eff}}(x)\,, \tag{43}$$

where $\mathcal{L}_{\text{eff}}(x)$ is the effective Lagrangian. The effective action is produced by integrating out fields in the action formed from the full theory, also known as the UV theory, thereby narrowing the degrees of freedom. For example[7]:

$$\int \mathcal{D}\phi\, e^{i\int d^4x \mathcal{L}_{\text{eff}}(\phi(x))} = \int \mathcal{D}\phi\, \mathcal{D}H\, e^{i\int d^4x \mathcal{L}(\phi(x),H)}\,, \tag{44}$$

where H is some heavy field integrated out. It is notable that even though H is integrated out of the theory thus producing an effective theory, H can still have effects on the remaining fields. These effects come as corrections to existing operators consisting of the so-called Wilson coefficients. These effective actions therefore depend on fewer fields, only valid in a limited regime and notably are non-renormalizable. These theories are often favored over full theories because easier calculations and little loss in predictability when applied in the correct range of validity. Effective field theories can also be used to probe for new physics. This is done by exploring the effects of new potential particles integrated out at current energy levels of experiments. Then if any predictions from a theory with a heavy field that has been integrated out, match experimental data, it could hint new heavy physics. These predictions would then be in the form of Wilson coefficients and their correlations as corrections to the UV theory.

3.1.1 Effective Action at Tree Level

Following B.Henning et al.[8] we define the effective action:

$$e^{i\int d^4x\mathcal{L}_{\text{eff}}(\phi)} = \int \mathcal{D}\Phi\, e^{i\int d^4x\mathcal{L}(\phi,\Phi)}\,, \tag{45}$$

where Φ is a heavy real scalar field we want to integrate out. Then expanding Φ around its minima Φ_c, which is determined by its equations of motion i.e.:

$$\frac{\delta S(\phi,\Phi)}{\delta\Phi} = 0 \implies \Phi_c\,. \tag{46}$$

The expansion then reads to tree-level order:

$$\int d^4x\mathcal{L}(\phi,\Phi+\eta) = S(\phi,\Phi+\eta) = S(\Phi_c) + \mathcal{O}(\eta^2)\,. \tag{47}$$

From this we compute the effective action as:

$$e^{i\int d^4x\mathcal{L}_{\text{eff}}(\phi)} = \int \mathcal{D}\eta\, e^{i\int d^4x\mathcal{L}(\phi,\Phi_c+\eta)} \approx e^{i\int d^4x\mathcal{L}(\Phi_c)}\,, \tag{48}$$

such that:

$$\mathcal{L}_{\text{eff}} \approx \mathcal{L}(\Phi_c)\,. \tag{49}$$

We can therefore obtain an effective Lagrangian at tree-level by solving for the Lagrangian's classical equations of motion and plugging them back into the Lagrangian.

3.2 Effective Field Theory as a Probe for New Physics

In effective field theories heavy particles, that are otherwise integrated out, can still influence physics in a measurable way. This enables effective field theory to be a useful tool in the search for new physics beyond. As we can theorize a new particle that is heavy so that we can integrate it out and then perform measurement at energy scales well below its mass. Then compare the effective theory to these measurement to see if there are signs of this new particle.

Following Corbett et al. [9] we can use the method introduced in Section 3.1.1, to calculate an effective field theory at tree level. This effective theory is based on a UV complete theory of the standard model Higgs with the addition of a heavy real singlet scalar, which is then integrated out. We discuss UV completions in the next section in the context of four-Fermi theory.
The new field added is S and the Higgs doublet is:

$$\Phi = \exp\left(i\frac{\omega(x)\cdot\tau}{v}\right)\begin{pmatrix}0\\ \frac{v+h}{\sqrt{2}}\end{pmatrix}\,, \tag{50}$$

where $\omega(x)$ is the Goldstone bosons and τ is the Pauli matrices. The lagrangian is

$$\mathcal{L} = (D^\mu \Phi)^\dagger (D_\mu \Phi) + \frac{1}{2}(\partial_\nu S)^2 - V(\Phi, S)\,, \tag{51}$$

with potential:

$$V(\Phi, S) = -\tilde{\mu}_H^2 |\Phi|^2 + \lambda |\Phi|^4 + \frac{1}{2} M_S^2 S^2 + \lambda_m v_S |\Phi|^2 S + \frac{1}{2}\lambda_m |\Phi|^2 S^2 + \frac{6\lambda_S v_s}{3!} S^3 - \frac{6}{4!}\lambda_S S^4\,. \tag{52}$$

The S dependent part of the Lagrangian can then be written:

$$\Delta\mathcal{L} = \frac{1}{2}(\partial_\nu S)^2 - \frac{1}{2} M_S^2 S^2 - A|\Phi|^2 S - \frac{1}{2} k |\Phi|^2 S^2 - \frac{1}{3!}\mu S^3 - \frac{1}{4!}\tilde{\lambda}_S S^4\,, \tag{53}$$

where:

$$\mu = 6\lambda_S v_S\,,\ A = \lambda_m v_S\,,\ k = \lambda_m\,,\ \tilde{\lambda}_S = 6\lambda\,. \tag{54}$$

As in Section 3.1.1 we can integrate out the S-field at tree level by solving for its classical equations of motion and plugging that back into the Lagrangian. Using the Euler-Lagrange equation of Section 1.1:

$$\frac{\partial \mathcal{L}}{\partial \phi} - \partial_\mu \frac{\partial \mathcal{L}}{\partial(\partial^\mu \phi)} = 0\,. \tag{55}$$

Evaluating each term separately we find:

$$\frac{\partial \Delta\mathcal{L}}{\partial S} = -M_S^2 S - A|\Phi|^2 - k|\Phi|^2 S - \frac{1}{2}\mu S^2 - \frac{1}{3!}\tilde{\lambda}_S S^3\,, \tag{56}$$

and

$$\partial_\mu \frac{\partial \Delta\mathcal{L}}{\partial(\partial_\mu S)} = \partial_\mu(\partial_\mu S)\,. \tag{57}$$

We obtain for our Euler-Lagrange equation:

$$-M_S^2 S - A|\Phi|^2 - \frac{1}{2} k |\Phi|^2 S - \frac{1}{2}\mu S^2 - \frac{1}{3!}\tilde{\lambda}_S S^3 - \partial_\mu(\partial_\mu S) = 0\,. \tag{58}$$

Solving to linear order in S and using the definitions, $U = k|\Phi|^2$ and $B = -A|\Phi|^2$ we find the equation of motion(EOM):

$$S_C = \frac{1}{\partial_\mu \partial^\mu + M_S^2 + U} B \tag{59}$$

Solving to linear order because the effects of solving to higher orders would only manifest at $1/M^{10}$ order in the effective Lagrangian. Therefore solving the EOM to higher than linear order would not have any effect on terms of dimension 8 and lower, and in the following we will just be keeping terms of dimension 8 and below.

In "integrating the S-field out" we assume that the mass M_S is very large which, lets us expand around $\frac{1}{M_S^2}$:

$$S_C \approxeq \frac{B}{M_S^2} - \frac{\partial_\mu \partial^\mu B + Bk|\Phi|^2}{M_S^4}\,. \tag{60}$$

Here we have expanded to an order which gives us terms of dimension 8 or lower in inverse mass, as explained above. Evaluating the terms of $\Delta\mathcal{L}$ one at a time:

$$\begin{aligned}
\frac{1}{2}(\partial_\nu S_C)^2 &\approx \frac{A^2\partial_\nu|\Phi|^2\partial_\nu|\Phi|^2}{2M_S^4} - \frac{A^2\partial_\nu|\Phi|^2\partial_\mu\partial^\mu\partial_\nu|\Phi|^2 + 2A^2k|\Phi|^2\partial_\nu|\Phi|^2\partial_\nu|\Phi|^2}{M_S^6} \\
-\frac{1}{2}M_S^2S_C^2 &\approx -\frac{A^2|\Phi|^4}{2M_S^2} - \frac{A^2\partial_\mu|\Phi|^2\partial^\mu\partial_\mu|\Phi|^2 + A^2|\Phi|^4k^2|\Phi|^4 - 4A^2k|\Phi|^2\partial_\mu|\Phi|^2\partial^\mu|\Phi|^2}{2M_S^6} + \frac{-A^2\partial_\mu|\Phi|^2\partial^\mu|\Phi|^2 + A^2k|\Phi|^6}{M_S^4} \\
-A|\Phi|^2S_C &\approx \frac{A^2|\Phi|^4}{M_S^2} - \frac{A^2|\Phi|^4\partial_\mu\partial^\mu + A^2|\Phi|^4k|\Phi|^2}{M_S^4} \\
-\frac{1}{2}k|\Phi|^2S_C^2 &\approx -\frac{A^2k|\Phi|^6}{2M_S^4} + \frac{-2A^2k|\Phi|^2\partial_\mu|\Phi|^2\partial^\mu|\Phi|^2 + A^2k^2|\Phi|^8|\Phi|^2}{M_S^6} \\
-\frac{1}{3!}\mu S_C^3 &\approx \frac{1}{3!}\mu\frac{A^3|\Phi|^6}{M_S^6} + \frac{1}{2}\mu\frac{A^3|\Phi|^2\partial_\mu|\Phi|^2\partial^\mu|\Phi|^2 - A^3k|\Phi|^8}{M_S^8} \\
-\frac{1}{4!}\tilde{\lambda}_S S_C^4 &\approx -\frac{1}{4!}\tilde{\lambda}_S\frac{A^4|\Phi|^8}{M_S^8}
\end{aligned} \tag{61}$$

Now Putting the terms together to get $\Delta\mathcal{L}(S_C)$ from Eq. 53

$$\begin{aligned}
&\frac{1}{2}(\partial_\nu S_C)^2 - \frac{1}{2}M_S^2S_C^2 - A|\Phi|^2S_C - \frac{1}{2}k|\Phi|^2S_C^2 - \frac{1}{3!}\mu S_C^3 - \frac{1}{4!}\tilde{\lambda}_S S_C^4 \\
&\quad\to \frac{A^2}{2M_S^2}|\Phi|^4 + \frac{A^2}{2M_S^4}\partial_\nu|\Phi|^2\partial^\nu|\Phi|^2 + \frac{A^2}{2M_S^4}\left(\frac{A\mu}{3M_S^2} - k\right)|\Phi|^6 + \frac{A^2}{2M_S^6}\left(-\frac{\tilde{\lambda}_S A^2}{12M_S^2} + k^2 - \frac{A\mu k}{M_S^2}\right)|\Phi|^8 \\
&\qquad + \frac{2A^2}{M_S^6}\left(\frac{A\mu}{2M_S^2} - k\right)|\Phi|^2\partial_\nu|\Phi|^2\partial^\nu|\Phi|^2 + \frac{A^2}{2M_S^6}\partial_\nu\partial^\nu|\Phi|^2\partial_\mu\partial^\mu|\Phi|^2
\end{aligned} \tag{62}$$

This effective Lagrangian provides predictions for the Wilson coefficients of the various effective higher dimensional operators of the Higgs doublet Φ. These can then be compared to experiment to see if there is an indication of the correlation of between the Wilson coefficients, i.e. the coefficients for the effective operators, that this theory predicts. The discovery of such correlations could then be indirect evidence of there being a real heavy scalar singlet. This is an example of how useful effective field theories can be at producing predictions to look for new physics.

3.3 Weak interaction & Fermi-Theory

This discussion of the Fermi theory follows that of [2].
The four-Fermi interaction:

$$\mathcal{L}_{\text{4-Fermi},\beta} = G_F\bar{\psi}_p\psi_n\bar{\psi}_e\psi_\nu\,, \tag{63}$$

can be used to model proton β-decay at low energy compared to $1/\sqrt{G_F}$. Where:

$$G_F = 1.1663787\times10^{-5}\text{GeV}^{-2}\,.[10][11] \tag{64}$$

In section 2.2 a renormalizable theory was defined to have coupling of mass dimension $0 \leq [\lambda] \leq d$. This means, since the mass dimension of the Fermi constant $[G_F] = -2$, four-Fermi

theory is non-renormalizable. In general we would then have to add all operators consistent with the symmetries of quantum electro-dynamics, i.e. an infinite number of terms, to this theory in order to fully renormalize it.

We might have Lagrangian terms of the form:

$$\hat{\mathcal{L}}_{\text{4-Fermi},\beta} = G_F\bar{\psi}_p\psi_n\bar{\psi}_e\psi_\nu + c^{(1)}G_F^2\bar{\psi}_p\Box\psi_n\bar{\psi}_e\psi_\nu + c^{(2)}G_F^3\partial\!\!\!/\bar{\psi}_p\partial\!\!\!/\psi_n\partial\!\!\!/\bar{\psi}_e\partial\!\!\!/\psi_\nu + c^{(3)}G_F^4\bar{\psi}_p\Box\psi_n\Box\bar{\psi}_e\Box\psi_\nu + \dots . \tag{65}$$

Here, following the symmetries we cannot add more fields. It is therefore apparent that each higher order term must be as such due to additional derivatives. The terms will, as a result, be suppressed by powers of external momentum from the derivatives, compared to G_F as $c^{(n)}\left(G_F p^2\right)^n$. Since the energies typical in β-decay ($\mathcal{O}(1\text{MeV})$ [12]) are much less than G_F, i.e. $p^2 \propto s \ll G_F^{-1}$. The higher order terms will be negligible at typical energy scales and consequently the leading-order term can be used predictively. As the four-Fermi theory is only predictive at low energies a theory consistent at higher energies, a UV completion, is required to make predictions at these energies. A UV completion is a theory that works above the effective theory's energy scale of validity, and reduces to an equivalent theory at low energies. There are many possible UV completions of the four-Fermi theory, however the predictions, and measurements of the W bosons properties indicate that the UV completion consistent with nature is the electroweak sector of the standard model.

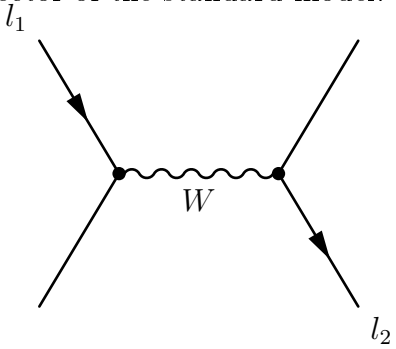

Figure 10: lepton interaction through charged current W boson

Since the W only couples to left-handed fermion we get, at tree level:

$$\mathcal{M} = \frac{-e^2}{2s_w^2}\left(\bar{l}_L\gamma^\mu\nu_{lL}\right)\frac{\left(g^{\mu\nu} - \frac{p^\mu p^\nu}{M_W^2}\right)}{q^2 - M_W^2}\left(\bar{\nu}_{lL}\gamma^\nu l_L\right) , \tag{66}$$

where s_w^2 is $\sin^2(\theta_w)$ and θ_w is the weak mixing angle. In the limit $M_W^2 \gg q^2$ this becomes:

$$\mathcal{M} = \frac{-e^2}{2M_W^2 s_w^2}\left(\bar{l}\gamma^\mu P_L\nu_l\right)\left(\bar{\nu}_l\gamma^\mu P_L l\right) , \tag{67}$$

where $P_L = \frac{1}{2}\left(1-\gamma^5\right)$ is the left-hand projection operator. This amounts to integrating out the W and we are now left with a four-Fermi interaction of the form $\bar{\psi}\gamma^\mu P_L\psi\bar{\psi}\gamma^\mu P_L\psi$, with

$$\frac{4G_F}{\sqrt{2}} \equiv \frac{e^2}{2M_W^2 s_w} \tag{68}$$

Thus this shows how a UV completion reduces to a low energy effective, or infrared (IR), theory when energy is below the threshold of the effective theory. This IR theory notably contains the symmetries of the UV theory. Where the W only couples to left handed fermions, the four-Fermi couples two left handed fermion currents. The originally proposed four-Fermi theory in Eq. 63 did not have this symmetry by default. We can therefore obtain a symmetry consistent effective theory by going from a UV theory to an IR theory. However, if we went the other way we would have no way of knowing this symmetry except by inferring from experimental data. Yet comparing experiments with four-Fermi theory was how the V-A structure of the weak sector was discovered[2]. As such IR theories can be instrumental in finding hints of the structure of a UV model consistent with nature.

3.4 Strong interaction and the effective field theory of pions

This discussion on pions follows that of [2]. As was explored in Section 3.3 we found that an IR theory deduced from a UV theory obeys the original symmetries of the UV theory. Using this we will motivate an effective field theory based on the symmetries of quarks and gluons. The theory describing the strong interaction is that of Quantum Chromodynamics (QCD) which has the Lagrangian (including just up and down quarks):

$$\mathcal{L}_{\text{QCD, quarks}} = -\frac{1}{4}(F^a_{\mu\nu})^2 + i\bar{u}^L \not{D} u^L + i\bar{u}^R \not{D} u^R + i\bar{d}^L \not{D} d^L + i\bar{d}^R \not{D} d^R \tag{69}$$

This Lagrangian is symmetric under separate left and right handed rotations between the up and down quarks. This symmetry is called a chiral symmetry, written $SU(2)_L \times SU(2)_R$ in group theory. Below a certain energy we do not observe quarks but instead observe hadrons. In describing pions, hadrons formed of a quark and anti quark, we will assume they are composite particles which behave as the Goldstone bosons of the spontaneously broken symmetry $SU(2)_L \times SU(2)_R \to SU(2)_V$. However we also have:

$$SU(2)_L \times SU(2)_R = SU(2)_V \times SU(2)_A \,. \tag{70}$$

This implies that the $SU(2)_A$ symmetry has been spontaneously broken. Spontaneous symmetry break of a continuous group is associated with Goldstone bosons[13]. Goldstones' theorem states for every broken generator of a broken gauge group a massless degree of freedom follows. $SU(2)_A$ has 3 generators, as such we have three massless Goldstone bosons: the pions $(\pi^0, \pi^\pm)$. We can put the pions in a field that transforms linearly under $SU(2)_L \times SU(2)_R$:

$$U(x) = \exp\left[\frac{i}{f_\pi}\sigma^a \pi^a\right] , \tag{71}$$

where f_π is called the pion decay constant, σ^a are the Pauli matrices and π^a are the pion field components: $\pi^0 = \pi^3$ and $\pi^\pm = \frac{1}{\sqrt{2}}(\pi^1 \pm i\pi^2)$. It should be noted that pions have been observed to be massive, this can be incorporated into the theory using spurions. Spurions are treated as fields with symmetry properties, however they are later set to appropriate constant

values which break the symmetry allowing for, e.g. pion masses, while allowing a consistent treatment of an effective Lagrangian based on the UV symmetries.

Effective low energy theories like the four-Fermi theory have the advantage of being much easier to actually use and produce predictions. Producing predictions in QCD is generally difficult as the coupling constant, g_3, is large. The coupling constant is known to grow as the energy decreases, and at some energy this coupling constant becomes much larger than one, causing perturbation theory to fail. At these low energies where perturbation theory fails the theory should still work, but we lack mathematical techniques to produce predictions. This has led to advances like lattice QCD which is able to make limited predictions in the low energy regime. Therefore effective low energy non-renormalizable theories, like the chiral Lagrangian, are useful in making predictions. The chiral Lagrangian to leading order is:

$$\mathcal{L}_{\chi,1} = \frac{f_\pi^2}{4} Tr\left[D_\mu U D^\mu U^\dagger\right] . \tag{72}$$

With covariant derivative:

$$D_\mu = \partial_\mu - iQ_i A_\mu \,, \tag{73}$$

where Q_i is the charge of the pion, A_μ is the photon field.

The form of the chiral Lagrangian in Eq. 72 is the lowest order effective Lagrangian in $U(x)$ obeying its symmetries. Expanding the exponential in Eq 72 for small $1/f_\pi$ we find the kinetic terms:

$$\mathcal{L}_{kin} = \frac{1}{2}\left(\partial_\mu \pi^0 \partial^\mu \pi^0\right) + (D_\mu \pi^+)(D^\mu \pi^-) \,. \tag{74}$$

Expanding to higher orders incurs more factors of $\frac{1}{f_\pi}$ with mass dimension $\left[\frac{1}{f_\pi}\right] = m^{-1}$, which is why this theory is non-renormalizable. Since $UU^\dagger = 1$ expansion of interaction terms in this theory must be a derivative expansion as:

$$\mathcal{L}_\chi = \frac{f_\pi^2}{4} Tr\left[D_\mu U D^\mu U^\dagger\right] + L_1 Tr\left[D_\mu U D^\mu U^\dagger\right]^2 + \cdots \tag{75}$$

for which each additional term will have increasing powers of $\frac{\sqrt{s}}{f_\pi}$. As such this theory is well behaved perturbatively given $\sqrt{s} \ll f_\pi$. The parameters of the model, e.g. f_π , L_1 can be measured experimentally and they can be used to make more predictions.

4 Standard Model Effective Field Theories

In this section we want to lay the groundwork of introducing the concepts of the standard model effective field theory (SMEFT). We first discuss the formulation and the definition of the SMEFT as well as motivate its use in the search for new heavy physics. We then go on to

discuss the finite field redefinitions that arise when reconstructing the canonical forms of the standard model after add the SMEFT operators. We discuss these finite field redefinitions through two examples one of which is the canonical form for the Higgs kinetic term. We then use this in our discussion of the Yukawa coupling where we show how redefining the Higgs to obtain a canonical kinetic term introduces shifts to all Higgs couplings. Finally we discuss the concept of the geoSMEFT as a way to write the SMEFT operators to all order in a compact fashion.

4.1 Formulation

The standard model is a successful model of many phenomena within the field of particle physics. A notable example is how it predicted the Higgs, which was later found, in order to explain particle masses. The standard model however, being renormalizable, gives us concrete predictions. When in search of physics beyond the standard model, the model itself is of little help. One way of trying to find new physics could be increasing the energy at particle colliders to see if anything new or unexplained appears. This trial and error approach has the disadvantage of being very expensive and hard to justify as one does not necessarily know what one is looking for. As discussed in section 3.1.1 effective field theories have heavy particles integrated out, yet effects of these heavy particles can still manifest in the effective field theory. The SMEFT is an effective field theory created as an extension of the standard model to be able to search for heavy new, beyond standard model, physics at current or near future experimentally achievable energies. The complete basis of operators in the SMEFT at dimension six was first written in [14]. The SMEFT Lagrangian can be defined to all orders in $1/\Lambda$ as[15]:

$$\mathcal{L} = \mathcal{L}_{Standard\,Model} + \mathcal{L}_{SMEFT}\,. \tag{76}$$

Where $\mathcal{L}_{SM}$ is the standard model Lagrangian. And the SMEFT extension is:

$$\mathcal{L}_{SMEFT} = \sum_{i}^{\infty}\sum_{j}\frac{c_j\mathcal{Q}_j^{(4+i)}}{\Lambda^{(i)}}\,. \tag{77}$$

The sum over j is the sum of all operators $\mathcal{Q}_j$ consistent with the symmetries of the standard model at dimension $d = i + 4$. We then sum over i to include operators of dimension $d > 4$ suppressed by Λ the mass scale of heavy new physics. The coefficients of each operator c_j are called Wilson coefficients and sometimes these have the $1/\Lambda^{(i)}$ absorbed into them such that the notation becomes:

$$\frac{c_j}{\Lambda^i} \to c_j^{(n)}\,, \tag{78}$$

where $i = n - 4$ so that n is the dimension of the operator. At leading order $d = 5$ there is only one operator, namely the neutrino mass operator[16]:

$$\mathcal{L}_5 = \frac{c_{\alpha\beta}}{\Lambda}(\bar{L}_\alpha^c\tilde{H})(\tilde{H}^\dagger L_\beta) \tag{79}$$

As this operator generates interactions between the Higgs boson and neutrinos which will not be visible at colliders like the LHC, this operator is not relevant to this thesis. At dimension $d = 6$ there exists 59(neglecting flavor) operator forms, with many of them given in Table 5 taken from [17]. The SMEFT is reminiscent of four-Fermi theory in section 3.3 where we added all symmetry consistent terms to the Lagrangian. In four-Fermi theory the higher order terms were suppressed by the Fermi coupling, $G_F \sim 1/M_W^2$. Likewise in SMEFT we have higher order corrections to the standard model which are suppressed by the mass scale of heavy new physics Λ. The SMEFT is therefore, as four-Fermi theory, a bottom-up approach to an effective field theory. In this context a bottom-up approach means that since we have added all possible operators to the Lagrangian we do not know or predict the values of Wilson coefficients. Using the SMEFT therefore amounts to finding what operators introduces shifts, or corrections, to standard model interactions. Where experiments can attempt to extrapolate values of Wilson coefficients and their predicted correlations among each other. The Wilson coefficients can then give hints of possible new physics.

4.2 Finite Field Redefinitions

The many operators from the SMEFT can have contributions to the canonical forms of the standard model Lagrangian when the Higgs attains a vacuum expectation value(vev). The canonical form for the kinetic and mass terms of the Higgs singlet are defined as:

$$\mathcal{L}_{\text{Canonical},\,h} = \frac{1}{2}\partial_\mu h \partial^\mu h - \frac{1}{2} m_h^2 h^2 \tag{80}$$

4.2.1 A class 3 operator example

Taking from Table 5, we can use a class 3 operator as an example of how the SMEFT shifts the canonical form of the Higgs singlet and how to make a field redefinition that results in a canonical form for the shifted Higgs singlet. We consider the operator $Q_{H\Box}$

$$C_3 = c_{H\Box}(H^\dagger H)\partial_\mu \partial^\mu (H^\dagger H)\,, \tag{81}$$

where H is the Higgs doublet. The Higgs attains a vev such that $H \to v + h$ (we are using unitary gauge):

$$C_3 = c_{H\Box}(h^\dagger h + v^2 + h^\dagger v + v h)\partial_\mu \partial^\mu (h^\dagger h + v^2 + h^\dagger v + v h)\,, \tag{82}$$

where h is the real part of the second component of the Higgs doublet so $h^\dagger = h$. We then have contributions to the canonical form for scalar of the form: $-c_{H\Box} v^2 \partial_\mu h \partial^\mu\, h$. Adding this to the standard model kinetic term and transforming $h \to \frac{h'}{\sqrt{C_{c_{H\Box}}}}$:

$$\mathcal{L}_{kin,\text{SMEFT}} = \frac{1}{C_{c_{H\Box}}}\left(\frac{1}{2}\partial_\mu h' \partial^\mu h' - c_{H\Box} v^2 \partial_\mu h' \partial^\mu h'\right). \tag{83}$$

Then taking $C_{c_{H\Box}} = 1 - 2c_{H\Box}v^2$ we then get a canonical kinetic form for the h':

$$\mathcal{L}_{kin,\text{SMEFT}_{\text{Canonical}}} = \frac{1}{2}\partial_\mu h' \partial^\mu h' \,. \tag{84}$$

We can expand $\frac{1}{C_{c_{H\Box}}}$ around $c_{H\Box} \ll 1$:

$$\frac{1}{C_{c_{H\Box}}} = 1 + 2c_{H\Box}v^2 + 2c_{H\Box}^2 v^4 + \cdots \,, \tag{85}$$

yielding an infinite series in $c_{H\Box}$. In this way we can parameterize the resulting shifts in the Higgs interaction terms (as discussed below) to any order in $c_{H\Box}$.

4.2.2 A class 4 operator example

As with the Higgs singlet in the previous section, we now describe a similar example for a class 4 operator from Table 5

$$C_4 = c_{HB}(H^\dagger H)(B_{\mu\nu}B^{\mu\nu}) \,, \tag{86}$$

where:

$$B_{\mu\nu} = \partial_\nu B_\mu - \partial_\mu B_\nu \,, \tag{87}$$

is the $U(1)$ gauge boson field strength from the weak sector of the standard model. The Higgs attains a vev such that $H \to v + h$,

$$C_4 = c_{HB}(v^2 + h^\dagger h + h^\dagger v + vh)B_{\mu\nu}B^{\mu\nu} \,. \tag{88}$$

We have shifts to the canonical form like: $c_{HB}v^2 B_{\mu\nu}B^{\mu\nu}$. The standard model canonical form kinetic term is:

$$\mathcal{L}_{kin} = -\frac{1}{4}B_{\mu\nu}B^{\mu\nu} \,. \tag{89}$$

Adding the two and transforming the field $B_{\mu\nu} \to \frac{B'_{\mu\nu}}{\sqrt{C}}$:

$$\mathcal{L}_{kin,\text{SMEFT}} = \frac{1}{C_{c_{HB}}}\left(-\frac{1}{4}B'_{\mu\nu}B'^{\mu\nu} + c_{HB}v^2 B'_{\mu\nu}B'^{\mu\nu}\right) \,. \tag{90}$$

Then taking $C_{c_{HB}} = 1 - 4c_{HB}v^2$ we get a canonical form for B':

$$\mathcal{L}_{kin,\text{SMEFT}_{\text{Canonical}}} = -\frac{1}{4}B'_{\mu\nu}B'^{\mu\nu} \,. \tag{91}$$

Expanding $\frac{1}{C_{cHB}}$ for $c_{HB} \ll 1$:

$$\frac{1}{C_{c_{HB}}} = 1 + 4c_{HB}v^2 + 8c_{HB}^2 v^4 + \cdots \,, \tag{92}$$

we have an infinite series in the Wilson coefficient c_{HB}. As with the Higgs shift we can now parameterize this shift to any order in the wilson coefficient c_{HB}. In addition to shifting the fields away from canonical kinetic and mass terms, Class 3 and 4 operators also affect the mixing between the neutral gauge bosons [18, 19]. We do not elaborate on this in this thesis.

4.2.3 Implications of the field redefinitions

In this section we will see how a shift to the canonical form of Higgs kinetic term, shifts all couplings to the Higgs. Taking the Yukawa coupling from the standard model as example, we have the Lagrangian[2]:

$$\mathcal{L}_{Yukawa} = -H\bar{q}_L Y_d d_R - \widetilde{H}\bar{q}_L Y_u u_R - H\bar{L}_L Y_e e_R + h.c.\,. \tag{93}$$

This Lagrangian is responsible for generation of the fermion masses by means of coupling them to the Higgs. Here Y_d, Y_u, Y_e are the Yukawa coupling matrices of the down type quarks, up-type quarks and leptons respectively. The subscripts L, R means left and right-handed field respectively. $\widetilde{H} = i\sigma_2 H$ is the conjugate Higgs doublet used for up-type quark couplings where σ_2 are the second Pauli matrix obeying $\sigma_2^* = -\sigma_2$. All the Yukawa couplings are of a similar form:

$$\mathcal{L}_{Yukawa} = -g_Y H\bar{\Psi}\psi + h.c.\,, \tag{94}$$

where Ψ represents a left-hand fermionic $SU(2)_L$ doublet and ψ represents a right-hand fermionic singlet. After spontaneous symmetry breaking we have:

$$\mathcal{L}_{Yukawa} = -g_Y(h+v)\bar{\Psi}\psi + h.c.\,. \tag{95}$$

Using $h \to \frac{h'}{\sqrt{C_{c_{H\Box}}}}$ from Eq 83 gives us:

$$\mathcal{L}_{Yukawa,\text{SMEFT}} = -g_Y(\frac{h'}{\sqrt{C_{c_{H\Box}}}} + v)\bar{\Psi}\psi + h.c.\,. \tag{96}$$

The shift from the class 3 operator in Eq 81 shifts all couplings to the Higgs. For this reason it is a tremendous task redefining all the interactions with shifts from the SMEFT, but the procedure can be simplified as well as generalized to all orders in $1/\Lambda$ using a methodology called the geoSMEFT.

4.3 geoSMEFT

In this section we briefly discuss the idea of the geoSMEFT theory described in Ref. [20] One can imagine how cumbersome it would be to write and work with the operators of the SMEFT to all orders. Indeed, in the previous discussion of Sections 4.2.1 and 4.2.2 we only considered two of the five operators which shift the kinetic and mass terms of the fields. Additionally, at dimension eight there are six operators further complicating the procedure. geoSMEFT is a method in which this process is simplified. In the standard model we have, for example, the kinetic term for the Higgs:

$$\mathcal{L}_{H_{\text{kinetic}}} = (D_\mu H)(D^\mu H^\dagger)\,. \tag{97}$$

If we then write the Higgs doublet in real scalar field coordinates we find:

$$H = \frac{1}{\sqrt{2}}\begin{pmatrix}\phi_2 + i\phi_1 \\ \phi_4 - i\phi_3\end{pmatrix}\,. \tag{98}$$

In this way we can write Eq.97 as:

$$\mathcal{L}_{H_{\text{kinetic}}} = \delta_{IJ}(D_\mu\phi)^I(D^\mu\phi)_J\,. \tag{99}$$

The geoSMEFT uses this idea to encode the operators of the SMEFT to all orders in $1/\Lambda$ within an object that corrects the δ-function, $\delta_{IJ} \to h_{IJ}$. The Lagrangian with all of the SMEFT corrections can the be written[20]:

$$\mathcal{L}_{H_{kinetic},\text{SMEFT}} = h_{IJ}(D_\mu\phi)^I(D^\mu\phi)_J\,. \tag{100}$$

Where:

$$\begin{aligned} h_{IJ} = &\left[1 + \phi^2\frac{c_{H\Box}}{\Lambda^2} + \sum_{n=0}^{\infty}\left(\frac{\phi^2}{2}\right)^{n+2}\left(\frac{c_{HD}^{(8+2n)} - c_{H,D2}^{(8+2n)}}{\Lambda^{2+2n}}\right)\right]\delta_{IJ} \\ &+ \frac{\Gamma^I_{A,J}\phi_K\Gamma^K_{A,L}\phi_L}{2}\left(\frac{c_{HD}^{(6)}}{2\Lambda^2} + \sum_{n=0}^{\infty}\left(\frac{\phi^2}{2}\right)^{n+1}\frac{c_{H,D2}^{(8+2n)}}{\Lambda^{2+2n}}\right)\,. \end{aligned} \tag{101}$$

In similar fashion we can define:

$$\mathcal{W}^A_\mu = \{W^1_\mu, W^2_\mu, W^3_\mu, B^1_\mu\}\,. \tag{102}$$

So that the standard model W and B fields kinetic terms, can be generalized to all orders SMEFT:

$$\mathcal{L}_{\mathcal{W}_{\text{kinetic}},\text{SM}} = -\frac{1}{4}\delta_{AB}\mathcal{W}^A_{\mu\nu}\mathcal{W}^{B,\mu\nu} \to \mathcal{L}_{\mathcal{W}_{\text{kinetic}},\text{SMEFT}} = -\frac{1}{4}g_{AB}\mathcal{W}^A_{\mu\nu}\mathcal{W}^{B,\mu\nu}\,. \tag{103}$$

These definitions can then be used to redefine the fields to all orders in the mass eigenstate basis with:

$$A^C_\mu \equiv \{W^+, W-, Z, \gamma\} = \sqrt{g^{CB}}U_{BA}W^A_\mu\,, \tag{104}$$

and

$$\Phi^K \equiv \{\Phi^+, \Phi-, \chi, h\} = \sqrt{h^{KJ}}V_{JI}\phi^I\,. \tag{105}$$

Where U and V are the matrices which in the standard model rotate the weak eigenstate fields to their mass eigenstates. Further, U includes shifts in the definition of the Weinberg angle (Weak mixing angle) and is therefore an implicit function of $\sqrt{g}$. This gives us the Lagrangian with canonically normalized fields to all order in the SMEFT:

$$\mathcal{L}_{\mathcal{W}_{\text{kinetic}},\text{SMEFT}} = -\frac{1}{4}g_{AB}\mathcal{W}^{B,\mu\nu} \to -\frac{1}{4}A^{B,\mu\nu}A^B_{\mu\nu}\,. \tag{106}$$

$$\mathcal{L}_{\mathcal{H}_{\text{kinetic}},\text{SMEFT}} = h_{IJ}(D_\mu\phi)^I(D^\mu\phi^\dagger)_J \to (D_\mu\Phi)^I(D^\mu\Phi)^I\,. \tag{107}$$

In this way we are able to transform all fields such that they have canonical kinetic terms while keeping track of the interaction terms in a much more straightforward manner than that outlined in Section 4.2. This is the methodology that was employed in deriving the Feynman rules of Appendix C.1, using the FeynRules package of [21].

5 $H \to \bar{\ell}\ell\gamma$ in the Standard Model

The standard model calculation of $H \to \bar{\ell}\ell\gamma$ has been discussed extensively in the literature [22, 23, 24, 25, 26, 27, 28]. In this thesis we present results also published in [29].

In this section we discuss the standard model Higgs decay to two leptons and a photon, $H \to \bar{\ell}\ell\gamma$. We will discuss the contributions from tree-level, how they are chirally suppressed and calculate the decay width at tree-level. We then go on to discuss the contributions at one-loop, here we go into more depth about the contributions from loops of top-quarks and calculate the matrix elements of the Higgs decay via top quark loop to two photons and to a photon and a Z boson respectively, allowing the Z and one of the photons to be off-shell. We then discuss the rest of the one-loop contributions of the $H \to \bar{\ell}\ell\gamma$ based on Ref.[29] to later be able to use their calculations of the total one-loop standard model contribution to this particular Higgs decay. We use a parameterization of the total one-loop amplitude from Ref.[29] to perform the decay width integral. We note that the decay widths obtained at one-loop are of same or larger order of magnitude compared to the tree-level decay width for muons and electrons respectively. With this in mind we also introduce Dalitz plots as a way to obtain more information about at what energies, which contributions affect the decay width the most.

The results in this section have also been published in [29].

5.1 Standard model at Tree-level

In the standard model the Higgs decays at tree level to two leptons through the Yukawa coupling. If one of these leptons radiate a photon we find that the Higgs can decay to two leptons and a photon, $H \to \bar{\ell}\ell\gamma$ at tree-level. Feynman diagrams for this decay are shown in Figures 11 and 12. The Yukawa coupling as defined in Section 4.2.3 couples left and right handed leptons together and is proportional ot m_f/v. As a result the production of leptons from the Yukawa coupling is chirally suppressed as m_ℓ/v.

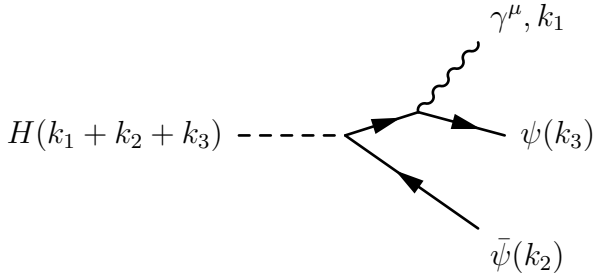

Figure 11: Higgs to two leptons and photon through radiation of photon

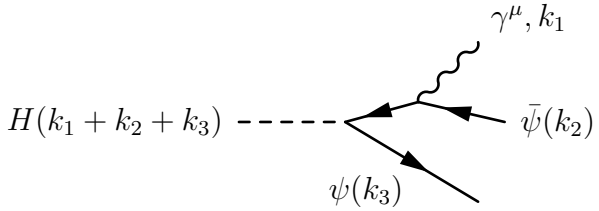

Figure 12: Higgs to two leptons and photon through radiation of photon

The two diagrams in Figures 11 and 12 correspond to the two cases of $H \to \bar{\ell}\ell\gamma$ at tree-level, where either the lepton or the anti-lepton radiates a photon. To find the matrix elements for this decay we need the following Feynman rules defined in Appendix C: The Higgs coupling to fermions, the photon coupling of leptons and the fermion propagator. For the first diagram in Figure 11 we obtain the matrix element:

$$\mathcal{M}_1 = -\frac{Q_f e m_f}{v}\epsilon^*_\mu(k_1)\bar{u}(k_3)_a\gamma^\mu_{ab}\left(\frac{(\not{k}_3+\not{k}_1)_{bc}+m_f}{(k_3+k_1)^2-m_f^2+i\epsilon}\right)v(k_2)_c\,. \tag{108}$$

Where $\epsilon_\mu(k_1)$ is the photon polarization associated with the external photon with momentum k_1 and Q_f is the fermion charge. For the second diagram, Figure 12, we obtain:

$$\mathcal{M}_2 = -\frac{Q_f e m_f}{v}\epsilon^*_\mu(k_1)\bar{u}(k_3)_a\left(\frac{(-\not{k}_2-\not{k}_1)_{ab}+m_f}{(k_2+k_1)^2-m_f^2+i\epsilon}\right)\gamma^\mu_{bc}v(k_2)_c\,. \tag{109}$$

We are interested in calculating the squared matrix element, and since the total matrix element is the sum of the two matrix elements i.e.: $\mathcal{M}_{Total} = \mathcal{M}_1 + \mathcal{M}_2$, the squared matrix element will be:

$$|\mathcal{M}_{Total}|^2 = |\mathcal{M}_1|^2 + |\mathcal{M}_2|^2 + \mathcal{M}_1\mathcal{M}_2^\dagger + \mathcal{M}_2\mathcal{M}_1^\dagger = |\mathcal{M}_1|^2 + |\mathcal{M}_2|^2 + 2\mathbb{R}\left[\mathcal{M}_1\mathcal{M}_2^\dagger\right]\,. \tag{110}$$

Where $\mathbb{R}(x)$ takes the real part of x. Evaluating the terms separately we find the following:

$$|\mathcal{M}_1|^2 = \frac{-Q_f^2e^2\bar{m}_f^2}{v^2\left((k_3+k_1)^2\right)^2}g_{\rho\mu}Tr\left(\not{k}_3\gamma^\mu\left(\not{k}_3+\not{k}_1\right)\not{k}_2\left(\not{k}_3+\not{k}_1\right)\gamma^\rho\right)\,. \tag{111}$$

$$|\mathcal{M}_2|^2 = \frac{-Q_f^2e^2\bar{m}_f^2}{v^2\left((k_2+k_1)^2\right)^2}g_{\rho\mu}Tr\left(\not{k}_3\left(\not{k}_2+\not{k}_1\right)\right)\gamma^\mu\not{k}_2\gamma^\rho\left(\not{k}_2+\not{k}_1\right))\,. \tag{112}$$

$$\mathcal{M}_1\mathcal{M}_2^\dagger = \frac{-Q_f^2e^2\bar{m}_f^2}{v^2(k_3+k_1)^2(k_2+k_1)^2}g_{\rho\mu}Tr\left(\not{k}_3\gamma^\mu\left(\not{k}_3+\not{k}_1\right)\not{k}_2\gamma^\rho\left(-\not{k}_2-\not{k}_1\right)\right)\,. \tag{113}$$

From these squared matrix elements we see the chiral suppression in the prefactor as $(\bar{m}_f/v)^2$. Employing the rules in Table 7 for traces over γ-matrices and contracting the Lorentz-indices we take the lepton's mass to be $m_f \to 0$ except in the leading order from the Yukawa coupling. This is done be able to write the equations in a publication friendly way, however the masses are used in the calculation of the decay widths below. Furthermore, we introduce the invariant variables defined in Appendix D, which with our momentum assignment becomes:

$s_1 = (k_1 + k_2)^2$, $s_2 = (k_2 + k_3)^2$ and $s_3 = (k_3 + k_1)^2$. Finally, using the relation between these variables and masses, $s_3 = M_H^2 - s_1 - s_2$ to eliminate s_3 we find:

$$|\mathcal{M}_{\text{Total}}|^2 = \frac{4e^2 m_f^2 \left(M_H + s_2^2\right)}{v^2 s_1 (s_1 + s_2 - M_H^2)} \,. \tag{114}$$

Where M_H is the mass of the Higgs introduced as the square root of the center of mass energy, $\sqrt{s} = M_H$. Using the definition of the decay width in three body phase space of Section D we find:

$$\Gamma^{(0)}_{H\to\bar{l}l\gamma} = \frac{1}{2M_H}\frac{1}{(2\pi)^5}\frac{8\pi^2}{32M_H^2}\int ds_1 ds_2 \Theta[-G(s_1, s_2, M_H^2, m_l^2, 0, m_l^2)]\frac{4e^2 m_f^2 \left(M_H + s_2^2\right)}{v^2 s_1 (s_1 + s_2 - M_H^2)} \,. \tag{115}$$

Here the superscript (0) denotes that this is the tree level result. Eq. 115 has an IR divergence because of the s_1 in the denominator which makes the integral ill defined at $s_1 \to 0$. As a result we use a minimum photon energy of 5GeV. To see how this works we use the expression for s_2 from Appendix D but written in terms of the decaying particle's momentum in its center of mass frame $p = [\sqrt{s}, 0]$:

$$s_2 = (p - p_1)^2 \,. \tag{116}$$

Where our momentum assignment has p_1 as the photon momentum. This then lets us write the photon energy as[30]:

$$E_1 = \frac{s - s_2}{2\sqrt{s}} \,. \tag{117}$$

Taking the photon energy to a minimum of 5GeV therefore corresponds to:

$$5\text{GeV} \leq \frac{M_H^2 - s_2}{2M_H} \,. \tag{118}$$

The parameters used are presented in Table 2. The integral was performed with the Vegas algorithm from the CUBA library for Mathematica[31].

$$\Gamma^{(0)}_{H\to\bar{e}e\gamma} = 3.44 \times 10^{-12}\,\text{GeV} \,, \tag{119}$$

$$\Gamma^{(0)}_{H\to\bar{\mu}\mu\gamma} = 1.01 \times 10^{-7}\,\text{GeV} \,, \tag{120}$$

$$\Gamma^{(0)}_{H\to\bar{\tau}\tau\gamma} = 2.10 \times 10^{-5}\,\text{GeV} \,. \tag{121}$$

We have calculated the tree-level decay width for the Higgs decay $H \to \bar{\ell}\ell\gamma$. We found these to be chirally suppressed and it is therefore interesting to compare these to the loop contributions.

5.2 Standard Model Loops

At the order of one loop in the standard model the Higgs can decay to two leptons and one photon through many processes. Two examples of one-loop Higgs decay are the top quark loop processes producing either two photons from which a photon can convert into a lepton pair, or a photon and a Z boson which can produce a lepton pair. See Figure 13. Since top-quarks have Yukawa coupling of order one $Y_t \propto m_t/v \approx \mathcal{O}(1)$, the top-quark loop has a large contribution from the Yukawa coupling compared to other lighter fermions.

e	0.308253
M_H	125.10 GeV
m_e	$0.51099895 \times 10^{-3}$ GeV
m_μ	$105.6583745 \times 10^{-3}$ GeV
m_τ	1.77686 GeV
m_t	172.4 GeV
M_Z	91.1876 GeV
G_F	1.1663787×10^{-5} GeV^{-2}

Table 2: Parameters used in numerical integration of decay width see Refs. [32] , [33] , [34], [10] and [11]

5.2.1 $H \to \gamma\gamma$ at through top-quark loop

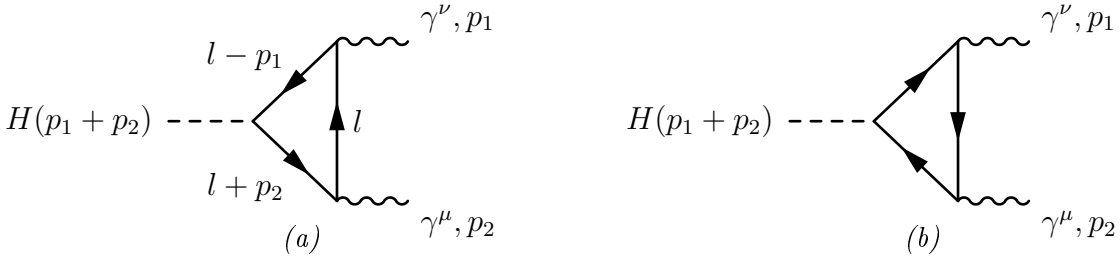

Figure 13: (a) Feynman diagram of the non-divergent top-quark loop process allowing for double photon production from Higgs decay. (b)Second Feynman diagram for the $H \to \gamma\gamma$ process through top-quark loop it is identical to Figure a, except it has reversed fermion flow in the top-quark loop, amounting to a reversal p_1 and p_2

To calculate the top-quark one-loop matrix element for the process $H \to \gamma\gamma$, we use the Feynman rules from Appendix C. For the Feynman diagram in Figure 13a we obtain the matrix element:

$$\mathcal{M}^{(1)}_{H\gamma\gamma} = -im_t \frac{4g_2 N_c e^2}{9m_W} \epsilon^*_\mu(p_2)\epsilon^*_\nu(p_1) \int \frac{d^D l}{(2\pi)^D} \frac{Tr\left((-\not{l} + \not{p}_1 + m_t)\gamma^\nu(-\not{l} + m_t)\gamma^\mu(-\not{l} - \not{p}_2 + m_t)\right)}{(l^2 - m_t^2 + i\epsilon)((l - p_1)^2 - m_t^2 + i\epsilon)((l + p_2)^2 - m_t^2 + i\epsilon)} . \tag{122}$$

Where m_t is the top quark mass, $\epsilon_\mu\,, \epsilon_\nu$ are the on shell photon polarization and g_2 is as discussed in Section 1.2.2 the $SU(2)$ gauge coupling. Furthermore the top-quark charge $Q_t = \frac{2}{3}e$ has been introduced explicitly, and quark colors have been introduced as the number of colors N_c. The superscript (1) denotes that this is a one-loop order process. The second diagram, Figure 13b simply introduces a factor of two which is included in Eq. 122.

To compute this integral we use the `Package-X` library for Mathematica [35], which allows for fast loop calculations. In order to compare with Ref. [36] we parametrize the result and expand in terms of $a = \frac{M_H}{4m_t}$ keeping terms up to $\mathcal{O}(a)$ and obtain:

$$\mathcal{M}^{(1)}_{H\gamma\gamma} = -i\frac{e^2}{8\pi^2}\frac{4}{3}\epsilon^*_\mu(p_2)\epsilon^*_\nu(p_1)\left(\frac{p_{1,\mu}p_{2,\nu}}{3} + \left(\frac{7p_{1,\mu}p_{2,\nu}}{90} - \frac{2m_t^2}{3}g^{\mu\nu}\right)a + \mathcal{O}(a^2)\right) . \tag{123}$$

Where we have used$g_2 = \frac{2m_W}{v}$ and $N_c = 3$. We get similar momentum dependence as Ref.[36].

Allowing one of the photons to be off-shell would then allow for a $\gamma \to \bar{\ell}\ell$ vertex with lepton-photon Feynman rule from Appendix.C:

$$\gamma \to \bar{\ell}\ell = -iQ_\ell e\gamma^\mu \,. \tag{124}$$

5.2.2 $H \to Z\gamma$ at through top-quark loop

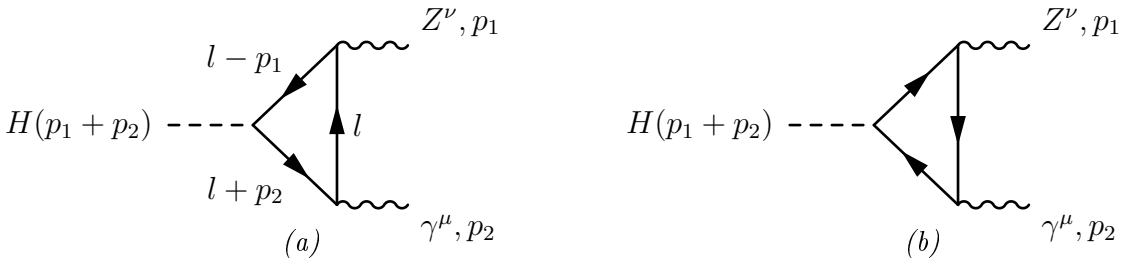

Figure 14: (a)Feynman diagram of Higgs decay to a Z boson and a photon through a top-quark loop. (b)Second Feynman diagram for the $H \to \gamma Z$ process through top-quark loop it is identical to Figure a, except it has reversed fermion flow in the top-quark loop, amounting to a reversal p_1 and p_2

We assemble the Feynman diagram in Figure 14a using Feynman rules in Appendix.C. We use the same conventions as for $H \to \gamma\gamma$ in Eq. 122, obtaining a factor two for the second diagram in Figure 14b. We find the matrix element:

$$\begin{aligned}\mathcal{M}^{(1)}_{H\gamma Z} = &-im_t \frac{2N_c g_2 e}{3c_w m_W} \epsilon^*_\mu(p_2)\epsilon^*_\nu(p_1) \\ &\times \int \frac{d^D}{(2\pi)^D} \frac{Tr\left((-\not{l} + \not{p}_1 + m_t)\gamma^\nu(g_L P_L + g_R P_R)(-\not{l} + m_t)\gamma^\mu(-\not{l} - \not{p}_2 + m_t)\right)}{(l^2 - m_t^2 + i\epsilon)((l - p_1)^2 - m_t^2 + i\epsilon)((l + p_2)^2 - m_t^2 + i\epsilon)} \,.\end{aligned} \tag{125}$$

We computing the integral with with `Package-X` as we did for the $H \to \gamma\gamma$ loop. We then parameterize the result as a series in $a = \frac{M_H^2}{4m_t^2}$, $b = \frac{M_Z^2}{4m_t^2}$ to order $\mathcal{O}\left(\frac{1}{m_t^2}\right)$, with M_Z being the Z-boson mass and find:

$$\begin{aligned}\mathcal{M}^{(1)}_{H\gamma Z} = &-i\frac{e^2}{4\pi^2}\left(\frac{1}{2} - \frac{4}{3}\sin(\theta_w)^2\right)\epsilon^*_\mu(p_2)\epsilon^*_\nu(p_1) \\ &\times \left(\frac{p_{1,\mu}p_{2,\nu}}{3} + \left(11\frac{p_{1,\mu}p_{2,\nu}}{90} + \frac{2m_t^2}{3}g^{\mu\nu}\right)b + \left(\frac{7p_{1,\mu}p_{2,\nu}}{90} - \frac{2m_t^2}{3}g^{\mu\nu}\right)a + \mathcal{O}\left((a+b)^2\right)\right) \,.\end{aligned} \tag{126}$$

Here θ_w is the weak mixing angle. We find similar momentum dependence as Ref. [36].

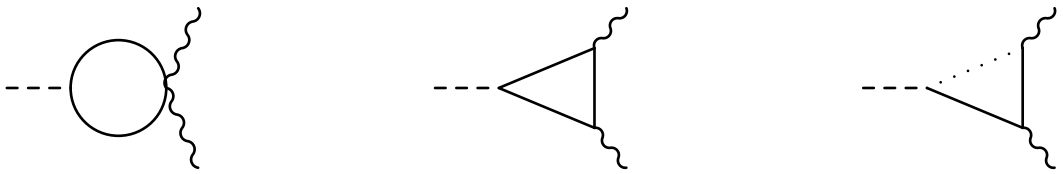

(a) (b) (c)

Figure 15: The rest of the diagrams contributing to the standard model Higgs decay with final states of either two photons or a photon a Z–boson taken from Ref. [29]. (a) and (b) have internal lines of either W–bosons, charged Goldstone bosons, charged ghosts[29], or fermions as we saw in the top-loop of Figures 13 and 14. If final state is a photon and a Z–boson (c) the loops can have internal lines from either one Goldstone boson and two W–bosons or two Goldstone bosons and one W–boson[29].

As with the $H \to \gamma\gamma$ process, if we let the Z-boson be off-shell it would allow for a $Z \to \bar{\ell}\ell$ vertex with Feynman rule as defined in Appendix.C:

$$Z \to \bar{\ell}\ell = -i\gamma^{\mu}(g_L P_L + g_R P_R)\,. \tag{127}$$

In the following applications we will use the full expressions for $H \to \gamma\gamma$ and $H \to \gamma Z$ and not the parameterized expressions in Eqs. 123 and 126.

5.2.3 Electro-weak Loops

As mentioned previously the two top-quark loops are not the only loops contributing to $H \to \bar{\ell}\ell\gamma$ at one-loop level in the standard model. The other possible standard model one-loop diagrams contributing to $H \to \bar{\ell}\ell\gamma$ consists of the electro-weak bosonic or fermionic loops to final states containing either two photons or a photon and a Z–boson[29], see Figures 15 and 16a. These contribute to $H \to \bar{\ell}\ell\gamma$ by a photon or a Z–boson going off shell and decaying to two leptons like the top-quark loops from Sections 5.2.1 5.2.2 did. Among these are the top-quark loops as discussed in the previous section. The rest of the electro-weak loops, shown in Figures 16a through 16c, are the Higgs decaying to two external fermions via loops of two W or Z–bosons and a fermion. Then either an external fermion or the internal fermion line can radiate a photon and thereby contribute to $H \to \bar{\ell}\ell\gamma$ at one-loop. It should be noted that these electroweak loops are not chiral in nature but bosonic. This means that they are not suppressed as m_f/v as chirally suppresed tree-level contribution, but proportional to M^2_{Boson}/v which is large for gauge bosons of the standard model.

5.3 Full Standard model loop calculation

As discussed above, there are more processes than the $H \to \gamma\gamma$ and $H \to \gamma Z$, that can contribute to the $H \to \bar{\ell}\ell\gamma$ at one-loop level, these are the electro-weak loops discussed in

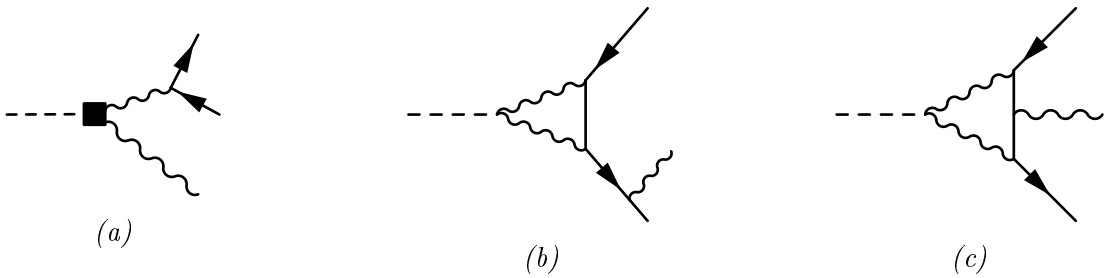

Figure 16: Feynman diagrams from Ref. [29] (a) are diagrams of one-loop order Higgs decays resulting in a either two photons or a photon and a Z-boson the box therefore represents all possible loops for those final states. Figure 15 shows the possible loops which are represented by the box in Figure a. (a) contains the top-loops from Sections 5.2.1 5.2.2. The diagrams of (b) and (c) have decays of the Higgs boson to loops of two W or Z-bosons resulting in two external fermions. A photon can radiate from either one of the external fermions (b) or the internal fermion line in the loop(c).

Section 5.2.3. The total one-loop amplitude can parametrized as[29]:

$$\begin{aligned} i\mathcal{M}_{1-\text{loop}} = &(c_{1L}\eta^{\mu\nu} + c_{2L}k_2^\mu k_1^\nu + c'_{2L}k_3^\mu k_1^\nu)\bar{u}_a(k_2)(\gamma_\nu P_L)_{ab}v_b(k_3) \\ &+ (c_{1R}\eta^{\mu\nu} + c_{2R}k_2^\mu k_1^\nu + c'_{2R}k_3^\mu k_1^\nu)\bar{u}_c(k_2)(\gamma_\nu P_R)_{cd}v_d(k_3)\,. \end{aligned} \tag{128}$$

Where we have the same momentum configuration as in Figures 13 and 14. The $c_{iL,R}$ are the coefficients of the kinematic structures from the full one-loop matrix element for $H \to \bar{l}l\gamma$ in the standard model. Squaring this matrix element in the limit $m_l \to 0$ we obtain:

$$|\mathcal{M}_{1-\text{loop}}|^2 = \frac{1}{2}s_2(4c_{1L}c_{1L}^* + 4c_{1R}c_{1R}^* + (c_{2L}^{'*}c_{2L} + c'_{2L}c_{2L}^* + c_{2R}^*c_{2R} + c'_{2R}c_{2R}^*)s_1(s_1 + s_2 - M_H^2))\,. \tag{129}$$

Where we have used the invariant variables defined in Appendix.D. We supplement our calculation of the top loop contribution from Sections 5.2.1 and 5.2.2, with the electroweak loops as calculated in Ref. [29] to obtain the coefficients $c_{i,L,R}$ of Eq. 129. We then go on to calculate the decay width. The numerical integration was done with Mathematica libraries CollierLink[35] and CUBA[31] with error at the level of less than a per mil ($< ‰$). The parameter used are those in Table 2 We find:

$$\Gamma^{(1)}_{H\to\bar{e}e\gamma} = 5.70 \times 10^{-7}\,\text{GeV}\,, \tag{130}$$

$$\Gamma^{(1)}_{H\to\bar{\mu}\mu\gamma} = 3.73 \times 10^{-7}\,\text{GeV}\,, \tag{131}$$

$$\Gamma^{(1)}_{H\to\bar{\tau}\tau\gamma} = 2.84 \times 10^{-7}\,\text{GeV}\,, \tag{132}$$

It is interesting to compare these results with the tree level results. Since the tree-level process is chirally suppressed we find that the one-loop result is very significant in comparison. In particular we find that for electrons the one-loop contributions is far more significant than the tree-level and for the muon the two are of the same order of magnitude. To learn more about the processes one can make a Dalitz plot. We produce Dalitz plots by plotting the integrand of the decay width, as defined in Eq. D.8, over the physical region defined by $G[x, y, z, u, v, w]$ in Eq.D.6 on the (s_1, s_2) plane. Such a plot will then show what part of the

integrand of the decay width has the most impact on the total decay width. As an example, take the tree-level decay width for $H \to \bar{\ell}\ell\gamma$ in Eq. 115. Plotting:

$$\frac{d\Gamma^{(0)}_{H\to\bar{l}l\gamma}}{ds_1 ds_2} = \frac{1}{2M_H}\frac{1}{(2\pi)^5}\frac{8\pi^2}{32M_H^2}\Theta[-G(s_1,s_2,M_H^2,m_l^2,0,m_l^2)]\frac{4e^2m_f^2\,(M_H+s_2^2)}{v^2 s_1(s_1+s_2-M_H^2)}\,, \tag{133}$$

for muons gives the plot on the left in Figure 17. The Dalitz plots presented in this section are also published in Ref [29]. The plot on the right in Figure 17 is the Dalitz plot of the

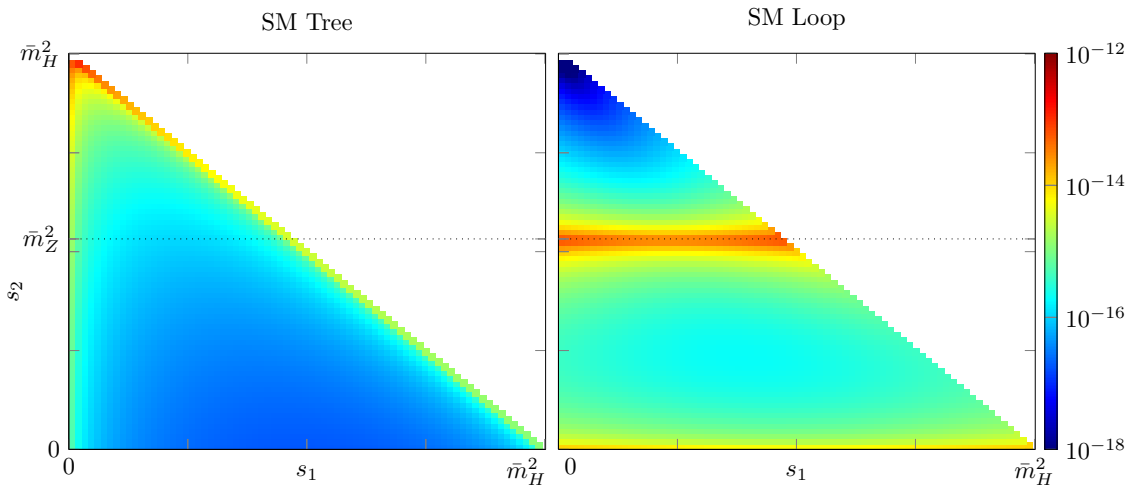

Figure 17: Dalitz of the standard model Higgs decay to two fermions and a photon. The dotted line marking the Z-boson mass are to compare with the one-loop, which has a pole at m_Z^2 from the $H \to \gamma Z$ processes where the Z–boson decays to two fermions. An example of this is the top loops to a photon and a Z–boson in Figure 14. Units are $[GeV]^{-3}$. Also published in Ref [29].

one-loop decay width from Eq. 129. Dalitz plots such as those in Figure 17 are incredibly useful in learning about the kinematics of a given process. We note that in Figure 17 we can see, for the one-loop case, a resonance in s_2 at the mass of the Z-boson squared m_Z^2. Since $s_2 = (p_2 + p_3)^2$ corresponds to the squared center of mass energy of the two final state leptons, this pole corresponds to the case where the Z–boson from a $H \to \gamma Z$ process, such as the ones in Figure 14, are allowed to be off-shell and convert to a lepton pair. We also see the differential width is peaked as the photon corresponding to the lepton pair goes off shell, i.e. $s_2 \to 0$ and produce the lepton pair, corresponding processes with $H \to \gamma\gamma \to \bar{\ell}\ell\gamma$. An example of such a process is the top-quark loop to two photons in Figure 13 Finally the tree level process seems to have increasing effect at higher s_2 where the one-loop contribution falls off. It is evident Dalitz plots such as those in Figure 17 can be instrumental for experiments, guiding their search and helping distinguish specific processes by isolating particular regions of s_2. In particular it is evident that we can study the standard model of different loop contributions as well as tree level separately by using cuts in s_2 on the differential width in Eq.133, Ref. [37].

5.4 Conclusions from the Standard Model Calculations

In this section we discussed the Higgs decay to two leptons and a photon, $H \to \bar{\ell}\ell\gamma$ at both tree and one-loop level. We went on to calculate the tree-level decay width we also note that the tree-level decay is chirally suppressed. We assembled the matrix elements of the Higgs decay via top-quarks loops in the standard model and explained how the two cases $H \to \gamma\gamma$ and $H \to \gamma Z$ could contribute to $H \to \bar{\ell}\ell\gamma$ at one loop. We then discussed the rest of the one-loop contributions of the $H \to \bar{\ell}\ell\gamma$ and using a parameterization of the total one-loop amplitude we calculated the total decay width at one-loop in the standard model. We discovered that in the standard model the decay widths of $H \to \bar{\ell}\ell\gamma$ at one-loop can be of same order of magnitude or larger than the tree level depending on the flavor of the lepton. We then introduced Dalitz plots to obtain information about dominant contributions to the total decay width at different energies.

6 SMEFT Contributions at Tree-Level

In this section we discuss the tree-level SMEFT contributions to the Higgs decay $H \to \bar{\ell}\ell\gamma$. We then calculate the matrix elements for the tree-level SMEFT contributions to $H \to \bar{\ell}\ell\gamma$. These matrix elements are then used to calculate the SMEFT contribution to the decay width $H \to \bar{\ell}\ell\gamma$, normalized to the standard model. This is first done at tree-level in and then we include the interferences of the tree-level SMEFT and the one-loop standard model amplitudes. The result is expanded in terms of the Wilson coefficents for the different SMEFT operators involved. The results in this section are also published in collaboration with T.Corbett Ref. [29].

The SMEFT as discussed in Section 4 is a bottom-up EFT produces predictions with corrections to the standard model in terms of the SMEFT Wilson coefficients. In the case of the process $H \to \bar{\ell}\ell\gamma$ we have particular interest, because the tree-level amplitude is chirally suppressed. This means that the SMEFT contributions could have larger significance and might be more easily found through experiments. We are interested in finding the tree-level SMEFT corrections to $H \to \bar{\ell}\ell\gamma$.

6.1 Tree-level SMEFT

Following Ref.[29] we have the Tree-level squared matrix element with SMEFT corrections:

$$|\mathcal{M}_{\text{Tree}}|^2 = |\mathcal{M}^{(0)}_{\text{Standard Model}}|^2(1 + 2\Delta_{H\bar{\ell}\ell} + [\Delta^{(6)}_{H\bar{\ell}\ell}]^2) + |\mathcal{M}_{\text{C1}} + \mathcal{M}_{\text{C2}}|^2 \,. \tag{134}$$

The $\Delta_{H\bar{\ell}\ell}$ is the SMEFT correction to the standard model Yukawa coupling $H \to \bar{\ell}\ell$, coming from the finite field redefinitions (from class 3 operators) as was discussed in Section 4.2

as well as direct contributions from the Class 5 operators of 5 which are rescalings of the standard model Yukawa couplings. The corrections in the parenthesis of Eq. 134 are defined as[29]:

$$\Delta_{H\bar{\ell}\ell} = v^2\left[c^{(6)}_{H\Box} - \frac{1}{4}c^{(6)}_{HD} - \frac{v^2}{8}(c^{(8)}_{HD} + c^{(8)}_{HD,2}) + \frac{3v^2}{32}(c^{(6)}_{HD} - 4c^{(6)}_{H\Box})^2\right] - \frac{3v^3}{2\sqrt{2}\bar{m}_\ell}\left(c^{(6)}_{eH} + \frac{v^2}{2}c^{(8)}_{eH}\right). \tag{135}$$

The barred lepton mass $\bar{m}_\ell$ has implicit SMEFT shifts in it, and as lepton masses are among our input parameters this implicit dependence is absorbed into the input parameter. The term with superscript (6) in Eq. 134 is just the dimension 6 part, i.e. the part with superscript (6) in Eq. 135. This is simply a result of truncating the expansion in $1/\Lambda$ (see Section 4) at order $1/\Lambda^4$. Additionally, in Eq. 134, we have two new tree-level amplitudes $\mathcal{M}_{C1}, \mathcal{M}_{C2}$ for $H \to \bar{\ell}\ell\gamma$ from the SMEFT. These come from the class 4 operators in Table 5 and allow for the processes $H \to \gamma\gamma$ ($\mathcal{M}_{C1}$) and $H \to \gamma Z$ ($\mathcal{M}_{C2}$) at tree-level. Following Ref. [29] we define these tree-level SMEFT processes as the following numbered cases:

1. Higgs coupling directly to two photons as the $H \to \gamma\gamma$ vertex with Feynman rule Eq. C.5 where the photon then decays to a lepton pair via the standard model coupling modified by $e \to \bar{e}$. (Class 4 operators in Table 5).

2. Higgs coupling directly to a photon and a Z–boson as the $H \to \gamma Z$ vertex with Feynman rule Eq. C.6 where the Z–boson then decays to a lepton pair via the modified coupling of Eq. C.10. (Class 4 operators in Table 5).

Where the case numbers are represented as subscripts on matrix elements as $\mathcal{M}_{Ci}$. Using the Feynman rules for these couplings found in Appendix.C.1, we can reproduce the matrix elements $\mathcal{M}_{C1}$ $\mathcal{M}_{C2}$:

$$i\mathcal{M}_{C1} = -i\frac{\bar{e}Q_l g_{HAA} v}{s2}(k_1^\nu(k_2+k_3)^\mu - k_1\cdot(k_2+k_3)\eta^{\mu\nu})\bar{u}(k_2)\gamma^\nu v(k_3)\epsilon^{*\mu}(k_1)\,. \tag{136}$$

$$i\mathcal{M}_{C2} = i\mathcal{M}_{C2,L} + i\mathcal{M}_{C2,R}\,. \tag{137}$$

$$i\mathcal{M}_{C2,L} = \frac{-ivg_{HAZ}\bar{g}_Z(g_L+g'_L)}{4(s_2^2 - M_Z^2 + i\Gamma_Z M_Z)}(k_1^\nu(k_2+k_3)^\mu - k_1\cdot(k_2+k_3)\eta^{\mu\nu})\bar{u}(k_2)\gamma^\nu)P_L v(k_3)\epsilon^{*\mu}(k_1)\,. \tag{138}$$

$$i\mathcal{M}_{C2,R} = \frac{-ivg_{HAZ}\bar{g}_Z(g_R+g'_R)}{4(s_2^2 - M_Z^2 + i\Gamma_Z M_Z)}(k_1^\nu(k_2+k_3)^\mu - k_1\cdot(k_2+k_3)\eta^{\mu\nu})\bar{u}(k_2)\gamma^\nu)P_R v(k_3)\epsilon^{*\mu}(k_1)\,. \tag{139}$$

The barred parameters in these matrix elements as mentioned above correspond to implicitly shifted parameters due to the SMEFT operators. g'_L, g'_R are also such shifts to the left and right handed couplings. We see the tree-level SMEFT matrix elements are not chirally suppressed as the standard model tree-level matrix element. As mentioned earlier in this section, this makes the $H \to \bar{\ell}\ell\gamma$ a good place to look for SMEFT corrections to the standard model through experiment. The expression in Eq. 6 can be integrated numerically and used

to obtain the SMEFT contributions normalized to the standard model in terms of the Wilson coefficients, defining in the case of muons (our calculations henceforth will be with muons):

$$\Delta = \frac{\Gamma^{SMEFT}_{H\to\bar{\mu}\mu\gamma}}{\Gamma^{\text{Standard Model}}_{H\to\bar{\mu}\mu\gamma}} - 1\,. \tag{140}$$

Where the input parameters used are those given in Table 2. Using the tree level SMEFT contribution of Eq. 134 normalized to the standard model decay width of Sections 5.1and 5.3 as in Eq.140 we obtain:

$$\begin{aligned}\Delta = {} & 0.40\tilde{c}^{(6)}_{H\Box} - 0.10\tilde{c}^{(6)}_{HD} - 0.050\tilde{c}^{(8)}_{HD} - 0.050\tilde{c}^{(8)}_{HD,2} + 0.81[\tilde{c}^{(6)}_{H\Box}]^2 - 0.40\tilde{c}^{(6)}_{H\Box}\tilde{c}^{(6)}_{HD} + 0.050[\tilde{c}^{(6)}_{HD}]^2 \\ & - 0.43\frac{v}{\bar{m}_\mu}\tilde{c}^{(6)}_{eH} + 0.23\frac{v^2}{\bar{m}^2_\mu}[\tilde{c}^{(6)}_{eH}]^2 - 0.21\frac{v}{\bar{m}_\mu}\tilde{c}^{(8)}_{eH} - 0.43\frac{v}{\bar{m}_\mu}\tilde{c}^{(6)}_{eH}\tilde{c}^{(6)}_{H\Box} + 0.11\frac{v}{\bar{m}_\mu}\tilde{c}^{(6)}_{eH}\tilde{c}^{(6)}_{HD} \\ & + 10^4\left(5.9[\tilde{c}^{(6)}_{HB}]^2 + 1.9\tilde{c}^{(6)}_{HB}\tilde{c}^{(6)}_{HW} + 1.1[\tilde{c}^{(6)}_{HW}]^2 + 4.9\tilde{c}^{(6)}_{HB}\tilde{c}^{(6)}_{HWB} - 2.5\tilde{c}^{(6)}_{HW}\tilde{c}^{(6)}_{HWB} + 1.8[\tilde{c}^{(6)}_{HWB}]^2\right)\,.\end{aligned} \tag{141}$$

Where the following notation has been used:

$$\tilde{c}^{(6)}_i = v^2 c^{(6)}_i\,, \tag{142}$$

$$\tilde{c}^{(8)}_i = v^4 c^{(8)}_i\,. \tag{143}$$

The result in Eq.141 was obtained by integrating over all of phase space with the exception of the 5GeV minimum photon energy, as was done in the standard model section 5. However, in our discussion about Dalitz plots in Section 5.3 it was evident that some regions of phase-space can be more interesting than others. This is particularly so when looking for specific corrections such as those of the different Wilson coefficients. This will be explored further in Section 6.4. We have found in Eq. 141 the ratio of the SMEFT corrected decay width with the standard model decay width. As was discussed in Section 5 we expect the SMEFT contributions to be significant even at tree-level because of the chiral suppression of the tree-level interaction in the standard model. With some of the Wilson coefficients having contributions of order $\mathcal{O}(1)$ to the standard model this expectation seems to have been correct.

6.2 Tree-level SMEFT at one-loop

Beyond tree level we have the tree-level SMEFT contribution interfered with the standard model one-loop as[29]:

$$|\mathcal{M}_{\text{one-loop}}|^2 = \frac{1}{16\pi^2}2\text{Re}\left[\mathcal{M}^{(1)}_{\text{Standard Model}}\left(\mathcal{M}_{\text{C1}} + \mathcal{M}_{\text{C2}} + \mathcal{M}_{\text{C3}} + \mathcal{M}_{\text{C4}}\right)^*\right]\,, \tag{144}$$

with $\mathcal{M}_{C1}$, $\mathcal{M}_{C2}$ defined as in Eqs. 136, 137, 138 and 139. We have two new cases $\mathcal{M}_{C3}$ and $\mathcal{M}_{C4}$ in Eq.144, which we label as we did for the cases $\mathcal{M}_{C1}$ and $\mathcal{M}_{C2}$:

3. Higgs decay directly to $\bar{\ell}\ell\gamma$ through 4-point interaction vertex with Feynman rule Eq. C.17. (Class 11 operators of dimension 8, see Table 6).

4. Higgs decay directly to $\bar{\ell}\ell\gamma$ through 4-point interaction vertex with Feynman rule Eq. C.17 (Class 15 operators of dimension 8, see Table 6).

We note that standard model tree-level matrix, including its SMEFT shift is of the form $\bar{u}\gamma^\mu\gamma^\nu v$ (see Eq. 108). Therefore its interference with any other matrix elements in Eq. 144 is proportional to the fermion mass (see Table 8) and therefore negligible under $m_f \to 0$.

$\mathcal{M}_{C3}$ and $\mathcal{M}_{C4}$ can be constructed from the Feynman rules in Appendix. C.1:

$$\mathcal{M}_{Ci} = \mathcal{M}_{Ci,L} + \mathcal{M}_{Ci,R}\,. \tag{145}$$

$$i\mathcal{M}_{C3,L} = i\frac{A_{11}Q_l ev}{2}(k_1^\nu)(k_2+k_3)^\mu \bar{u}(k_2)\gamma_\nu P_L v(k_3)\epsilon^{*\mu}(k_1),\,. \tag{146}$$

$$i\mathcal{M}_{C3,R} = i\frac{B_{11}Q_l ev}{2}(k_1^\nu)(k_2+k_3)^\mu \bar{u}(k_2)\gamma_\nu P_R v(k_3)\epsilon^{*\mu}(k_1)\,. \tag{147}$$

$$i\mathcal{M}_{C4,L} = ivA_{15}(k_1^\nu(k_2+k_3)^\mu - k_1\cdot(k_2+k_3)g_{\mu\nu})\bar{u}(k_2)\gamma_\nu P_L v(k_3)\epsilon^{*\mu}(k_1)\,. \tag{148}$$

$$i\mathcal{M}_{C4,R} = ivB_{15}(k_1^\nu(k_2+k_3)^\mu - k_1\cdot(k_2+k_3)g_{\mu\nu})\bar{u}(k_2)\gamma_\nu P_R v(k_3)\epsilon^{*\mu}(k_1)\,. \tag{149}$$

These matrix elements, $\mathcal{M}_{C3}, \mathcal{M}_{C4}$, corresponds to the decay $H \to \bar{\ell}\ell\gamma$ happening at tree-level through a single four-point vertex. If we include Eq. 144 in Eq. 140 we obtain the full equation:

$$\begin{aligned}
\Delta =& 0.40\tilde{c}^{(6)}_{H\Box} - 0.10\tilde{c}^{(6)}_{HD} - 0.050\tilde{c}^{(8)}_{HD} - 0.050\tilde{c}^{(8)}_{HD,2} + 0.81[\tilde{c}^{(6)}_{H\Box}]^2 - 0.40\tilde{c}^{(6)}_{H\Box}\tilde{c}^{(6)}_{HD} + 0.050[\tilde{c}^{(6)}_{HD}]^2 \\
&-0.43\frac{v}{\bar{m}_\mu}\tilde{c}^{(6)}_{eH} + 0.23\frac{v^2}{\bar{m}_\mu^2}[\tilde{c}^{(6)}_{eH}]^2 - 0.21\frac{v}{\bar{m}_\mu}\tilde{c}^{(8)}_{eH} - 0.43\frac{v}{\bar{m}_\mu}\tilde{c}^{(6)}_{eH}\tilde{c}^{(6)}_{H\Box} + 0.11\frac{v}{\bar{m}_\mu}\tilde{c}^{(6)}_{eH}\tilde{c}^{(6)}_{HD} \\
&+10^4\left(5.9[\tilde{c}^{(6)}_{HB}]^2 + 1.9\tilde{c}^{(6)}_{HB}\tilde{c}^{(6)}_{HW} + 1.1[\tilde{c}^{(6)}_{HW}]^2 + 4.9\tilde{c}^{(6)}_{HB}\tilde{c}^{(6)}_{HWB} - 2.5\tilde{c}^{(6)}_{HW}\tilde{c}^{(6)}_{HWB} + 1.8[\tilde{c}^{(6)}_{HWB}]^2\right) \\
&-270(\tilde{c}^{(6)}_{HB} + \tilde{c}^{(8)}_{HB}) - 80(\tilde{c}^{(6)}_{HW} + \tilde{c}^{(8)}_{HW} + \tilde{c}^{(8)}_{HW,2}) + 150(\tilde{c}^{(6)}_{HWB} + \tilde{c}^{(8)}_{HWB}) \\
&-540[\tilde{c}^{(6)}_{HB}]^2 - 160[\tilde{c}^{(6)}_{HW}]^2 + 590\tilde{c}^{(6)}_{HB}\tilde{c}^{(6)}_{HWB} - 0.016\tilde{c}^{(6)}_{HW}\tilde{c}^{(6)}_{HWB} + 17[\tilde{c}^{(6)}_{HWB}]^2 \\
&-270\tilde{c}^{(6)}_{HB}\tilde{c}^{(6)}_{H\Box} + 130\tilde{c}^{(6)}_{HB}\tilde{c}^{(6)}_{HD} - 80\tilde{c}^{(6)}_{HW}\tilde{c}^{(6)}_{H\Box} - 43\tilde{c}^{(6)}_{HW}\tilde{c}^{(6)}_{HD} + 150\tilde{c}^{(6)}_{HWB}\tilde{c}^{(6)}_{H\Box} + 4\tilde{c}^{(6)}_{HWB}\tilde{c}^{(6)}_{HD} \\
&-5.2\tilde{c}^{(6)}_{HB}\tilde{c}^{(6)}_{He} - 8.1\tilde{c}^{(6)}_{HB}(\tilde{c}^{(6),1}_{Hl} + \tilde{c}^{(6),3}_{Hl}) + 5.2\tilde{c}^{(6)}_{HW}\tilde{c}^{(6)}_{He} + 8.1\tilde{c}^{(6)}_{HW}(\tilde{c}^{(6),1}_{Hl} + \tilde{c}^{(6),3}_{Hl}) \\
&-3.3\tilde{c}^{(6)}_{HWB}\tilde{c}^{(6)}_{He} - 5.2\tilde{c}^{(6)}_{HWB}(\tilde{c}^{(6),1}_{Hl} + \tilde{c}^{(6),3}_{Hl}) \\
&-1.3\tilde{c}^{(8),1}_{e^2BH^2D} - 0.24(\tilde{c}^{(8),1}_{e^2H^2D^3} + \tilde{c}^{(8),2}_{e^2H^2D^3}) + 0.72\tilde{c}^{(8),1}_{e^2WH^2D} - 0.13(\tilde{c}^{(8),1}_{l^2BH^2D} + \tilde{c}^{(8),5}_{l^2BH^2D}) \\
&+0.025(\tilde{c}^{(8),1}_{l^2WH^2D} + \tilde{c}^{(8),5}_{l^2WH^2D}) - 0.070(\tilde{c}^{(8),1}_{l^2WH^2D} + \tilde{c}^{(8),5}_{l^2WH^2D})\,.
\end{aligned} \tag{150}$$

We now have the SMEFT corrections to the standard model decay width expanded in terms of the Wilson coefficients. Expressions like this can be used when exploring how the ratios between different Wilson coefficients change as we restrict the phase space integral to certain regions. Additionally expression like this are also useful on their own when compared again large datasets of experimental measurements to hopefully in the future constrain the parameter space of the SMEFT and measure deviations from the standard model.

6.3 SMEFT Dalitz Plots

In this section we discuss Dalitz-like plots of the SMEFT contributions to the Higgs decay $H \to \bar{\ell}\ell\gamma$. Dalitz-like plots meaning the plots are normalized to the standard model as to ascertain the SMEFT contribution relative to the standard model. The Dalitz-like plots in this section are also published in collaboration with T.Corbett in Ref.[29]. See Figures 18 and 19. We will discuss how plots of the like can be used to distinguish which SMEFT operators might be dominant in a certain regime. These Dalitz-like plots are plotted as the ratio of the different tree-level SMEFT contributions to the total standard model squared matrix element much like Eq. 140 is normalized to the standard model:

$$\begin{aligned} R^{(0)}_{\mathrm{C}i} &= \frac{|\mathcal{M}_{\mathrm{C}i}|^2}{|\mathcal{M}^{(0)}_{\text{Standard Model}} + \mathcal{M}^{(1)}_{\text{Standard Model}}|^2}\,, \\ R^{(0)}_{\mathrm{C}i\mathrm{C}j^*} &= \frac{2\mathrm{Re}[\mathcal{M}_{\mathrm{C}i}\mathcal{M}^*_{\mathrm{C}j}]}{|\mathcal{M}^{(0)}_{\text{Standard Model}} + \mathcal{M}^{(1)}_{\text{Standard Model}}|^2}\,, \\ R^{(1)}_{\mathrm{C}i} &= \frac{2\mathrm{Re}[\mathcal{M}^{(1)}_{\text{Standard Model}}\mathcal{M}^*_{\mathrm{C}i}]}{|\mathcal{M}^{(0)}_{\text{Standard Model}} + \mathcal{M}^{(1)}_{\text{Standard Model}}|^2}\,. \end{aligned} \tag{151}$$

Where the superscript denotes tree-level for (0) and interference with the standard model at one-loop for (1). The C_i are the numbered cases as described previously. In Eq.150 the decay widths were integrated over the whole phase-space with the caveat that there was a minimum photon energy of 5GeV. Looking at the Dalitz-like plots in Figures 18 19 we see as in the standard model Dalitz plots (Figure 17) there are regions where the different operators have larger contributions to the total decay width this motivates the idea of making certain cuts in the kinematic invariant s_2 to emphasize certain operators. As such the Dalitz-like plots explored here present an opportunity of fine tuning predictions for experimentalists to test but that process also introduces more model dependence. Curiously some of the Dalitz-like plots have sign flips indicated by solid black line, where the top-most region has been taken to always be positive. The sign of interferences of the form $\mathcal{M}_i\mathcal{M}^*_j$ are not guaranteed to be positive as in the case of a squared matrix element of the form $|\mathcal{M}|^2$. As a results sign flips occurs as can occur as s_2 varies. It is interesting to note that in Figure 19 we see that there is two sign flips for the left handed parts whereas there are only one for the right handed part. In tandem with the above discussion about emphasizing certain SMEFT contributions these sign flips could provide a way of combining certain regions as to isolate SMEFT contributions of interest.

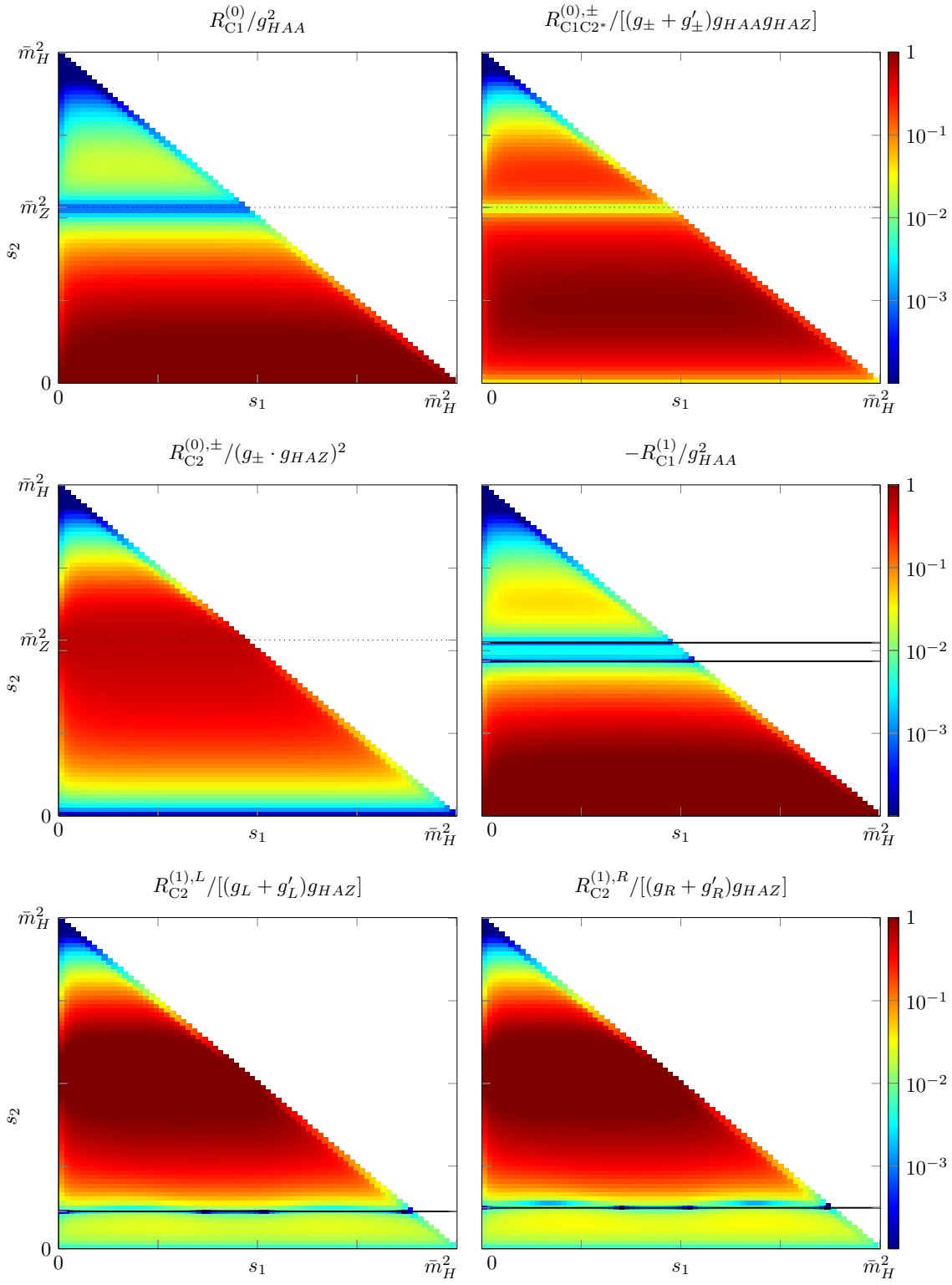

Figure 18: Dalitz-like plots defined in Eq. 151. Wilson coefficients have been pulled out of the ratios. The "±" indicates that the Left and right handed parts are are the same up to the normalization indicated by the plot title. Also published in Ref.[29]

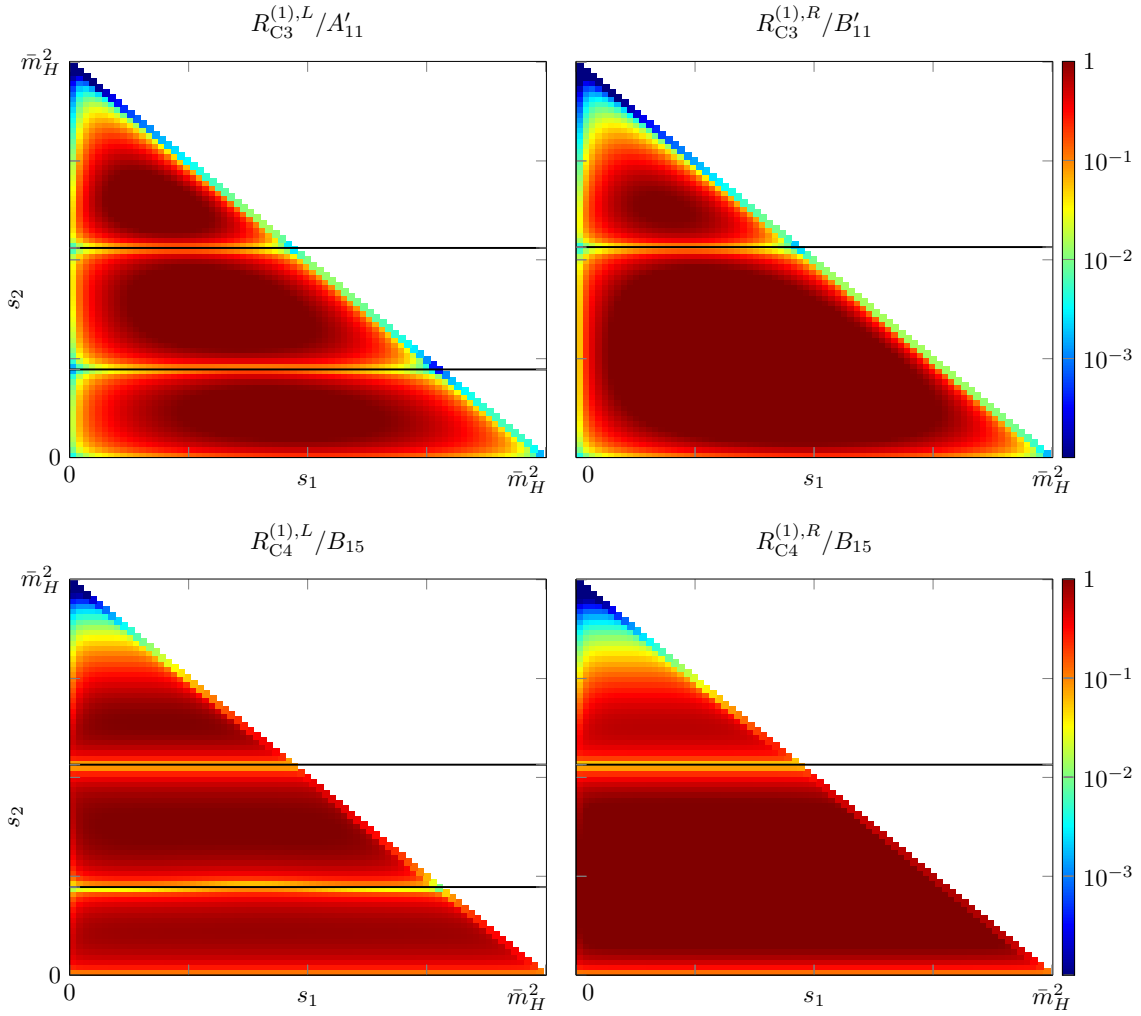

Figure 19: Second set of Dalitz-like with the same descriptions as in Figure 18. Also published in Ref.[29]

We now turn from our discussion of the Dalitz-like plots to proposing regions as cuts of s_2 in the phase space with the goal of emphasizing the different SMEFT contributions. We remind the reader that $s_2 = (k_2+k_3)^2$ is the invariant mass of the two final state leptons, i.e di-lepton system. We define a set of cuts in s_2 as regions R_1 through R_5 which are summarized in Table 3. The first region R_1 is just the full phase space yielding Eq. 150. For Region two our goal is to emphasize the C_1 contributions from the class 4 operators. Looking at Figure 18 we see that these are concentrated at low s_2 where the standard model is not resonant. Based on this we define R_2 as $[10^2 \leq s_2 \leq 40^2]$.

Region three R_3 has been designed to emphasize the C_2 contributions of the class 4 operators in addition to the standard model resonance at m_Z^2. Looking at Figures 18 and 17 we see that the region $[70^2 \leq s_2 \leq 100^2]\text{GeV}^2$ encapsulates the major contribution of C_2 in addition to capturing the Z-boson resonance of the standard model at one-loop.

A fourth region R_4 is designed to emphasize the contribution from the standard model at tree-level. This includes the shifts to it from the class 3 and 5 operators, contained in $\Delta_{H\bar{\ell}\ell}$

	Region $[\text{GeV}]^2$	Purpose of emphasis
R_1	$(0 \leq s_2 \leq \bar{m}_H^2)$	No cut/General
R_2	$(10^2 \leq s_2 \leq 40^2)$	Standard model non-resonant and C_1
R_3	$(70^2 \leq s_2 \leq 100^2)$	Standard model resonant, C_2 and C_3
R_4	$(100^2 \leq s_2 \leq \bar{m}_H^2)$	Standard model tree and its SMEFT correction
R_5	$(45^2 \leq s_2 \leq 50^2) - (65^2 \leq s_2 \leq 80^2)$	C_{3L} & C_{3L}
R_6	$(45^2 \leq s_2 \leq 50^2) + (65^2 \leq s_2 \leq 80^2)$	Control for R_5

Table 3: This table summarizes the different cuts in the phase space integral discussed in Section 6.4 as the regions $R_1, R_2, R_3, R_4, R_5, R_6$ and what features they attempt to emphasize.

as discussed in Sections 4.2 and 6.Looking at Figures 17 and 18 we find that a region $[100 \leq s_2 \leq \bar{m}_H^2]\text{GeV}^2$ encapsulates the standard model tree-level contribution, which is concentrated at high $s_2 \sim \bar{m}_H^2$.

In the attempt to emphasize the direct four point vertices coming the class 11 and 15 operators we construct a fifth region R_5. Looking at Figure 19 we see a large contribution from the left handed part of both C_3 and C_4 in the middle and bottom of the s_2 range. Additionally the right handed region also has a large contribution through out these two regions. However the left handed contribution has an additional sign flip. In region R_5 we attempt to use the second sign flip of the left hand C_{3L} and C_{4L}. This is done by subtraction of two ranges with contribution of different sign in the left handed case only due to the second sign flip. subtracting these regions should then have cancellations in all other cases than that of the C_{3L} and C_{4L}. Ranges chosen are $[45^2 \leq s_2 \leq 50^2]\text{GeV}^2$ and $[65^2 \leq s_2 \leq 80^2]\text{GeV}^2$. The region for R_5 is then $[45^2 \leq s_2 \leq 50^2]\text{GeV}^2 - [65^2 \leq s_2 \leq 80^2]\text{GeV}^2$.

Finally we present as a sanity check the region R_6 which is the sum of the subregions in R_5. This region should provide emphasize the opposite of R_5 which means we should see suppression of the cases C_3 and C_4 and enhancement of C_1 and C_2.

6.4 Optimizing SMEFT Searches

In this section we discuss the combination of Dalitz plots as discussed in Sections 5 and 6.3 and the SMEFT contributions discussed in Section 6. We are interested in providing experimentalists with as easily testable predictions as possible, but we are also interested in as little model dependence as possible. We present two assumptions based on the dependence of Eq. 150 on cuts in the kinematic invariant s_2 (invariant mass of the final state di-lepton system), where the third line without any assumptions seems dominant.

1. The first assumption is made by restoring the factor v^{i-4}/Λ^{i-4} absorbed into $\tilde{c}_j^{(i)}$, then assume that $c_j^{(i)} = 1$. Assuming Λ to some scale then lets us find a scale for which

the terms linear in dimension six Wilson coefficients $\tilde{c}_j^{(6)}$ in Eq. 150 could dominate the terms quadratic in those same Wilson coefficients e.g. line 3 of Eq. 150. This is because the quadratic dimension six and linear dimension eight terms would have $1/\Lambda^4$ dependence whereas the linear dimension six term would have $1/\Lambda^2$ scaling.

2. The second assumption is the assumption of weakly interacting new physics where operators of class 4 with Wilson coefficients: $(c_{HB}^{(6)}, c_{HW}^{(6)}, c_{HWB}^{(6)})$, only occur at loop level [38]. These will therefore be suppressed by a factor of $1/(16\pi^2)$ meaning we take $\left[c_{HB}^{(6)}, c_{HW}^{(6)}, c_{HWB}^{(6)}\right] \to 1/(16\pi^2)\left[c_{HB}^{(6)}, c_{HW}^{(6)}, c_{HWB}^{(6)}\right]$. This assumption leads to the third line remaining dominant but suppressed in the full phase space (Eq. 150).

A third assumption with parts of both of the previous two could be made but this would be very model dependent, therefore we do not consider it here. Additionally the Wilson coefficients $\tilde{c}_{eH}^{(6)}$ have been constrained[39] and we neglect them in the following discussion.

As mentioned above we present cuts in s_2, attempting to enhance different contributions from the SMEFT operators. In the case of the full phase space (region one R_1) except the minimum photon energy in Eq. 150, applying the first assumption the third line, corresponding to $|\mathcal{M}_{C1}|^2$ and $|\mathcal{M}_{C2}|^2$, remains dominant at a scale from $\Lambda \sim 1$TeV up to $\Lambda \sim 3.5$TeV. After this the class 4 operator terms linear in dimension six Wilson coefficients dominate. Using the loop assumption in R_1 i.e. the full phase space, we find that contributions from the class 4 operators remain dominant and that the terms quadratic in the class 4 operators become of same order as those linear in the class 4 operators. By using both assumptions class 4 operators will no longer be dominant at $\Lambda \sim 1$TeV.

We present the rest of the results for region R_2 to R_5. For region two in phase space R_2 (see Table 3) we obtain:

$$
\begin{aligned}
\Delta^{R_2} =& 0.12\tilde{c}_{H\Box}^{(6)} - 0.029\tilde{c}_{HD}^{(6)} - 0.015\tilde{c}_{HD}^{(8)} - 0.015\tilde{c}_{HD,2}^{(8)} + 0.23[\tilde{c}_{H\Box}^{(6)}]^2 - 0.12\tilde{c}_{H\Box}^{(6)}\tilde{c}_{HD}^{(6)} + 0.015[\tilde{c}_{HD}^{(6)}]^2 \\
& -0.12\frac{v}{\bar{m}_\mu}\tilde{c}_{eH}^{(6)} - 0.062\frac{v}{\bar{m}_\mu}\tilde{c}_{eH}^{(8)} + 0.066\frac{v^2}{\bar{m}_\mu^2}[\tilde{c}_{eH}^{(6)}]^2 - 0.12\frac{v}{\bar{m}_\mu}\tilde{c}_{eH}^{(6)}\tilde{c}_{H\Box}^{(6)} + 0.03\frac{v}{\bar{m}_\mu}\tilde{c}_{eH}^{(6)}\tilde{c}_{HD}^{(6)} \\
& +10^5\left(1.4[\tilde{c}_{HB}^{(6)}]^2 + 0.83\tilde{c}_{HB}^{(6)}\tilde{c}_{HW}^{(6)} + 0.13[\tilde{c}_{HW}^{(6)}]^2 - 1.5\tilde{c}_{HB}^{(6)}\tilde{c}_{HWB}^{(6)} - 0.46\tilde{c}_{HW}^{(6)}\tilde{c}_{HWB}^{(6)} + 0.42[\tilde{c}_{HWB}^{(6)}]^2\right) \\
& -720(\tilde{c}_{HB}^{(6)} + \tilde{c}_{HB}^{(8)}) - 220(\tilde{c}_{HW}^{(6)} + \tilde{c}_{HW}^{(8)} + \tilde{c}_{HW2}^{(8)}) + 400(\tilde{c}_{HWB}^{(6)} + \tilde{c}_{HWB}^{(8)}) \\
& -1400[\tilde{c}_{HB}^{(6)}]^2 - 430[\tilde{c}_{HW}^{(6)}]^2 + 150[\tilde{c}_{HWB}^{(6)}]^2 + 1600\tilde{c}_{HB}^{(6)}\tilde{c}_{HWB}^{(6)} + 4.2\tilde{c}_{HW}^{(6)}\tilde{c}_{HWB}^{(6)} \\
& -720\tilde{c}_{HB}^{(6)}\tilde{c}_{H\Box}^{(6)} + 340\tilde{c}_{HB}^{(6)}\tilde{c}_{HD}^{(6)} - 220\tilde{c}_{HW}^{(6)}\tilde{c}_{H\Box}^{(6)} - 110\tilde{c}_{HW}^{(6)}\tilde{c}_{HD}^{(6)} + 400\tilde{c}_{HWB}^{(6)}\tilde{c}_{H\Box}^{(6)} + 5.9\tilde{c}_{HWB}^{(6)}\tilde{c}_{HD}^{(6)} \\
& -18\tilde{c}_{HB}^{(6)}\tilde{c}_{He}^{(6)} - 14\tilde{c}_{HB}(\tilde{c}_{Hl}^{(6),1} + \tilde{c}_{Hl}^{(6),3}) + 18\tilde{c}_{HW}^{(6)}\tilde{c}_{He}^{(6)} + 14\tilde{c}_{HW}^{(6)}(\tilde{c}_{Hl}^{(6),1} + \tilde{c}_{Hl}^{(6),3}) \\
& -11\tilde{c}_{HWB}^{(6)}\tilde{c}_{He}^{(6)} - 8.7\tilde{c}_{HWB}^{(6)}(\tilde{c}_{Hl}^{(6),1} + \tilde{c}_{Hl}^{(6),3}) \\
& -3.1\tilde{c}_{e^2BH^2D}^{(8),1} - 0.55(\tilde{c}_{e^2H^2D^3}^{(8),1} + \tilde{c}_{e^2H^2D^3}^{(8),2}) + 1.7\tilde{c}_{e^2WH^2D}^{(8),1} - 2.4(\tilde{c}_{L^2BH^2D}^{(8),1} + \tilde{c}_{L^2BH^2D}^{(8),5}) \\
& -0.42(\tilde{c}_{l^2H^2D^3}^{(8),1} + \tilde{c}_{l^2H^2D^3}^{(8),2}) - 0.21(\tilde{c}_{l^2H^2D^3}^{(8),3} + \tilde{c}_{l^2H^2D^3}^{(8),4}) + 1.3(\tilde{c}_{l^2WH^2D}^{(8),1} + \tilde{c}_{l^2WH^2D}^{(8),5})
\end{aligned}
\tag{152}
$$

This region was designed to enhance the contributions of case one (C_1) coming from the class

4 operators as discussed in Section 4.2. This also emphasizes the non-resonant contribution from the standard model as seen in Figure 17. We obtain this region by looking at Figure 18 where we see that the chosen region $[10^2 \leq s_2 \leq 40^2]$ is where C_1 seems to have the largest contribution. Looking at Figure 19 we observe that the direct four point couplings of C_3 and C_4 also have a large contribution in the region. We therefore also see an enhancement in those cases. In particular we find that the squared class 4 operator contribution is increased by an order of magnitude. Using the assumption of a new physics scale $1/\Lambda$ the class 4 operator contributions linear in dimension six Wilson coefficients i.e. scaled as $1/\Lambda^2$ will begin to dominate over the otherwise dominant quadratic tree-level class 4 contributions at $\Lambda \sim 3.5$TeV. Using the weakly interacting new physics assumption, leading to loop suppression of class 4 operators, we find that the four-point vertex direct couplings of C_3 and C_4 become of the same order as the class 4 operators at tree-level. While these calculations are done for the muon, it is also possible to influence the contribution of class 3 operators (those with Wilson coefficients: $c_{HD}, c_{H\Box}$) by considering lepton flavor. This is because the class 3 operators contribute through the chirally Yukawa coupling. Here tau-leptons will have the largest contribution while the electron will have the smallest. In fact for tau leptons the class 3 operators will enhanced by $(m_\tau/m_\mu)^2 \sim 3 \times 10^2$, as such we could see the class 3 operators dominate under the loop-suppression assumption.

Using the region R_3 (see Table 3) we find:

$$
\begin{aligned}
\Delta^{R_3} =& 0.19\tilde{c}^{(6)}_{H\Box} - 0.047\tilde{c}^{(6)}_{HD} - 0.023\tilde{c}^{(8)}_{HD} - 0.023\tilde{c}^{(8)}_{HD,2} + 0.37[\tilde{c}^{(6)}_{H\Box}]^2 - 0.19\tilde{c}^{(6)}_{H\Box}\tilde{c}^{(6)}_{HD} + 0.023[\tilde{c}^{(6)}_{HD}]^2 \\
& 0.19\frac{v}{\bar{m}_\mu}\tilde{c}^{(6)}_{eH} + 0.10\frac{v^2}{\bar{m}_\mu^2}[\tilde{c}^{(6)}_{eH}]^2 - 0.010\frac{v}{\bar{m}_\mu}\tilde{c}^{(8)}_{eH} - 0.20\frac{v}{\bar{m}_\mu}\tilde{c}^{(6)}_{eH}\tilde{c}^{(6)}_{H\Box} + 0.049\frac{v}{\bar{m}_\mu}\tilde{c}^{(6)}_{eH}\tilde{c}^{(6)}_{HD} \\
& +10^4\left(1.4[\tilde{c}^{(6)}_{HB}]^2 - 2.5\tilde{c}^{(6)}_{HB}\tilde{c}^{(6)}_{HW} + 1.3[\tilde{c}^{(6)}_{HW}]^2 + 1.5\tilde{c}^{(6)}_{HB}\tilde{c}^{(6)}_{HWB} - 1.7\tilde{c}^{(6)}_{HW}\tilde{c}^{(6)}_{HWB} + 0.56[\tilde{c}^{(6)}_{HWB}]^2\right) \\
& -16(\tilde{c}^{(6)}_{HB} + \tilde{c}^{(8)}_{HB}) + 9.1(\tilde{c}^{(6)}_{HW} + \tilde{c}^{(8)}_{HW} + \tilde{c}^{(8)}_{HW,2}) - 3.9(\tilde{c}^{(6)}_{HWB} + \tilde{c}^{(8)}_{HWB}) \\
& -32[\tilde{c}^{(6)}_{HB}]^2 + 18[\tilde{c}^{(6)}_{HW}]^2 + 2.7\tilde{c}^{(6)}_{HB}\tilde{c}^{(6)}_{HWB} - 18\tilde{c}^{(6)}_{HW}\tilde{c}^{(6)}_{HWB} + 31[\tilde{c}^{(6)}_{HWB}]^2 \\
& -16\tilde{c}^{(6)}_{HB}\tilde{c}^{(6)}_{H\Box} + 8.9\tilde{c}^{(6)}_{HB}\tilde{c}^{(6)}_{HD} + 9.1^{(6)}\tilde{c}^{(6)}_{HW}\tilde{c}_{H\Box} - 7.2\tilde{c}^{(6)}_{HW}\tilde{c}^{(6)}_{HD} - 3.9\tilde{c}^{(6)}_{HWB}\tilde{c}^{(6)}_{H\Box} + 10\tilde{c}^{(6)}_{HWB}\tilde{c}^{(6)}_{HD} \\
& +4.5\tilde{c}^{(6)}_{HB}\tilde{c}^{(6)}_{He} - 16\tilde{c}^{(6)}_{HB}(\tilde{c}^{(6),1}_{Hl} + \tilde{c}^{(6),3}_{Hl}) - 4.5\tilde{c}^{(6)}_{HW}\tilde{c}^{(6)}_{He} + 16\tilde{c}^{(6)}_{HW}(\tilde{c}^{(6),1}_{Hl} + \tilde{c}^{(6),3}_{Hl}) \\
& +2.9\tilde{c}^{(6)}_{HWB}\tilde{c}^{(6)}_{He} - 10\tilde{c}^{(6)}_{HWB}(\tilde{c}^{(6),1}_{Hl} + \tilde{c}^{(6),3}_{Hl}) \\
& -1.0\tilde{c}^{(8),1}_{e^2BH^2D} + 0.57\tilde{c}^{(8),1}_{e^2WH^2D} - 0.18(\tilde{c}^{(8),1}_{e^2H^2D^3} + \tilde{c}^{(8),2}_{e^2H^2D^3}) + 0.51(\tilde{c}^{(8),1}_{l^2BH^2D} + \tilde{c}^{(8),5}_{l^2BH^2D}) \\
& +0.090(\tilde{c}^{(8),1}_{l^2H^2D^3} + \tilde{c}^{(8),2}_{l^2H^2D^3}) + 0.045(\tilde{c}^{(8),3}_{l^2H^2D^3} + \tilde{c}^{(8),4}_{l^2H^2D^3}) - 0.28(\tilde{c}^{(8),1}_{l^2WH^2D} + \tilde{c}^{(8),5}_{l^2WH^2D})
\end{aligned}
\tag{153}
$$

From this region we find that the SMEFT contribution from class 4 operators has decreased. This is because in emphasizing C_2 we have reduced the C_1 contribution which is larger than C_2 by two orders of magnitude. However, as seen in the two first plots of Figure 18, in this region we have that $\mathcal{M}_{C1}\mathcal{M}^*_{C2}$ has the opposite sign as $|\mathcal{M}_{C1}|^2$. This means that some destructive interference takes place and is the reason that the class 4 operators are not reduced by two orders of magnitude but only one. In introducing the assumptions in region R_3 we start with assuming a new physics scale we find that class 4 operator terms linear in dimen-

sion six Wilson coefficients, i.e. those with $1/\Lambda^2$ dependence, overtakes the squared class 4 operator terms with $1/\Lambda^4$ scaling at $\Lambda \sim 8\text{TeV}$. Invoking the second assumption suppressing the class 4 operators by the loop suppression factor $1/16\pi^2$ achieves a balance between all operators, with them all being close to the same size.

Using region R_4 (see Table 3) we find:

$$\begin{aligned}\Delta^{R_4} =& 1.9\tilde{c}^{(6)}_{H\Box} - 0.48\tilde{c}^{(6)}_{HD} - 0.24\tilde{c}^{(8)}_{HD} - 0.24\tilde{c}^{(8)}_{HD,2} + 3.9[\tilde{c}^{(6)}_{H\Box}]^2 - 1.9\tilde{c}^{(6)}_{H\Box}\tilde{c}^{(6)}_{HD} + 0.24[\tilde{c}^{(6)}_{HD}]^2 \\ &+2.1\frac{v}{\bar{m}_\mu}\tilde{c}^{(6)}_{eH} + 1.1\frac{v^2}{\bar{m}_\mu^2}[\tilde{c}^{(6)}_{eH}]^2 - 1.0\frac{v}{\bar{m}_\mu}\tilde{c}^{(8)}_{eH} - 2.1\frac{v}{\bar{m}_\mu}\tilde{c}^{(6)}_{eH}\tilde{c}^{(6)}_{H\Box} + 0.51\frac{v}{\bar{m}_\mu}\tilde{c}^{(6)}_{eH}\tilde{c}^{(6)}_{HD} \\ &+600[\tilde{c}^{(6)}_{HB}]^2 - 710\tilde{c}^{(6)}_{HB}\tilde{c}^{(6)}_{HW} + 470[\tilde{c}^{(6)}_{HW}]^2 + 320\tilde{c}^{(6)}_{HB}\tilde{c}^{(6)}_{HWB} - 700\tilde{c}^{(6)}_{HW}\tilde{c}^{(6)}_{HWB} + 256[\tilde{c}^{(6)}_{HWB}]^2 \\ &+5.5(\tilde{c}^{(6)}_{HB} + \tilde{c}^{(8)}_{HB}) - 7.4(\tilde{c}^{(6)}_{HW} + \tilde{c}^{(8)}_{HW} + \tilde{c}^{(8)}_{HW,2}) + 5.2(\tilde{c}^{(6)}_{HWB} + \tilde{c}^{(8)}_{HWB}) \\ &+11[\tilde{c}^{(6)}_{HB}]^2 - 15[\tilde{c}^{(6)}_{HW}]^2 + 14\tilde{c}^{(6)}_{HB}\tilde{c}^{(6)}_{HWB} + 6.9\tilde{c}^{(6)}_{HW}\tilde{c}^{(6)}_{HWB} - 17[\tilde{c}^{(6)}_{HWB}]^2 \\ &+5.5\tilde{c}^{(6)}_{HB}\tilde{c}^{(6)}_{H\Box} - 2.4\tilde{c}^{(6)}_{HB}\tilde{c}^{(6)}_{HD} - 7.4\tilde{c}^{(6)}_{HW}\tilde{c}^{(6)}_{H\Box} + 2.8\tilde{c}^{(6)}_{HW}\tilde{c}^{(6)}_{HD} + 5.2\tilde{c}^{(6)}_{HWB}\tilde{c}^{(6)}_{H\Box} - 5.8\tilde{c}^{(6)}_{HWB}\tilde{c}^{(6)}_{HD} \\ &-4.8\tilde{c}^{(6)}_{HB}\tilde{c}^{(6)}_{He} + 8.8\tilde{c}^{(6)}_{HB}(\tilde{c}^{(6),1}_{Hl} + \tilde{c}^{(6),3}_{Hl}) + 4.8\tilde{c}^{(6)}_{HW}\tilde{c}^{(6)}_{He} - 8.8\tilde{c}^{(6)}_{HW}(\tilde{c}^{(6),1}_{Hl} + \tilde{c}^{(6),3}_{Hl}) \\ &-3.1\tilde{c}^{(6)}_{HWB}\tilde{c}^{(6)}_{He} + 5.6\tilde{c}^{(6)}_{HWB}(\tilde{c}^{(6),1}_{Hl} + \tilde{c}^{(6),3}_{Hl}) \\ &+0.27\tilde{c}^{(8),1}_{e^2BH^2D} + 0.049(\tilde{c}^{(8),1}_{e^2H^2D^3} + \tilde{c}^{(8),2}_{e^2H^2D^3}) - 0.15\tilde{c}^{(8),1}_{e^2WH^2D} - 0.50(\tilde{c}^{(8),1}_{l^2BH^2D} + \tilde{c}^{(8),5}_{l^2BH^2D}) \\ &-0.090(\tilde{c}^{(8),1}_{l^2H^2D^3} + \tilde{c}^{(8),2}_{l^2H^2D^3}) - 0.045(\tilde{c}^{(8),3}_{l^2H^2D^3} + \tilde{c}^{(8),4}_{l^2H^2D^3}) + 0.28(\tilde{c}^{(8),1}_{l^2WH^2D} + \tilde{c}^{(8),5}_{l^2WH^2D}) \end{aligned} \quad (154)$$

While this region was designed to emphasize the standard model tree contribution, we also find that in this region, looking at Figure 18, class 4 operators are heavily suppressed, especially the tree-level contributions from squared class 4 operators ($|\mathcal{M}_{C1} + \mathcal{M}_{C2}|^2$). However, despite this we still find these class 4 operators dominant before applying further assumptions. We make the assumption of a new physics scale and find that as for region R_3 the class 4 operator terms linear in dimension six Wilson coefficients begins to dominate the quadratic terms at some scale. However here we find that this happens much earlier at $\Lambda \sim 2.5\text{TeV}$. Next we invoke the loop suppression assumption of the class 4 operators. Here we find that the large suppression from the chosen region in phase space combined with the loop suppression makes the class 3 contributions in line one, coming from the standard model shift $\Delta_{H\bar{\ell}\ell}$, dominate. It should be noted that this region could be enhanced further by considering the heavier lepton flavor of tau-leptons. As mentioned above this is because the class 3 operators enter the equation through corrections to the chirally suppressed Yukawa coupling. This leads to an enhancement of order $\mathcal{O}(10^2)$ for tau-leptons.

Using region R_5 (see Table 3) we find:

$$\begin{aligned}\Delta^{R_5} =& 0.85\tilde{c}^{(6)}_{H\Box} - 0.21\tilde{c}^{(6)}_{HD} - 0.11\tilde{c}^{(8)}_{HD} - 0.11\tilde{c}^{(8)}_{HD,2} + 1.7[\tilde{c}^{(6)}_{H\Box}]^2 - 0.85\tilde{c}^{(6)}_{H\Box}\tilde{c}^{(6)}_{HD} + 0.11[\tilde{c}^{(6)}_{HD}]^2 \\ & -0.90\frac{v}{\bar{m}_\mu}\tilde{c}^{(6)}_{eH} - 0.48\frac{v^2}{\bar{m}_\mu^2}[\tilde{c}^{(6)}_{eH}]^2 - 0.45\frac{v}{\bar{m}_\mu}\tilde{c}^{(8)}_{eH} - 0.90\frac{v}{\bar{m}_\mu}\tilde{c}^{(6)}_{eH}\tilde{c}^{(6)}_{H\Box} + 0.22\frac{v}{\bar{m}_\mu}\tilde{c}^{(6)}_{eH}\tilde{c}^{(6)}_{HD} \\ & +10^3\left(8.0[\tilde{c}^{(6)}_{HB}]^2 - 18.3\tilde{c}^{(6)}_{HB}\tilde{c}^{(6)}_{HW} + 7.4[\tilde{c}^{(6)}_{HW}]^2 + 12\tilde{c}^{(6)}_{HB}\tilde{c}^{(6)}_{HWB} - 8.6\tilde{c}^{(6)}_{HW}\tilde{c}^{(6)}_{HWB} - 2.2[\tilde{c}^{(6)}_{HWB}]^2\right) \\ & +160(\tilde{c}^{(6)}_{HB} + \tilde{c}^{(8)}_{HB}) - 130(\tilde{c}^{(6)}_{HW} + \tilde{c}^{(8)}_{HW} + \tilde{c}^{(8)}_{HW,2}) + 73(\tilde{c}^{(6)}_{HWB} + \tilde{c}^{(8)}_{HWB}) \\ & +330[\tilde{c}^{(6)}_{HB}]^2 - 260[\tilde{c}^{(6)}_{HW}]^2 - 120\tilde{c}^{(6)}_{HWB}\tilde{c}^{(6)}_{HW} - 170[\tilde{c}^{(6)}_{HWB}]^2 + 410\tilde{c}^{(6)}_{HB}\tilde{c}^{(6)}_{HWB} \\ & +160\tilde{c}^{(6)}_{HB}\tilde{c}^{(6)}_{H\Box} - 20\tilde{c}^{(6)}_{HB}\tilde{c}^{(6)}_{HD} - 130\tilde{c}^{(6)}_{HW}\tilde{c}^{(6)}_{H\Box} + 12\tilde{c}^{(6)}_{HW}\tilde{c}^{(6)}_{HD} + 73\tilde{c}^{(6)}_{HWB}\tilde{c}^{(6)}_{H\Box} - 80\tilde{c}^{(6)}_{HWB}\tilde{c}^{(6)}_{HD} \\ & -180\tilde{c}^{(6)}_{HB}\tilde{c}^{(6)}_{He} + 100\tilde{c}^{(6)}_{HB}(\tilde{c}^{(6),1}_{Hl} + \tilde{c}^{(6),3}_{Hl}) + 180\tilde{c}^{(6)}_{HW}\tilde{c}^{(6)}_{He} - 100\tilde{c}^{(6)}_{HW}(\tilde{c}^{(6),1}_{Hl} + \tilde{c}^{(6),3}_{Hl}) \\ & -64\tilde{c}^{(6)}_{HWB}\tilde{c}^{(6)}_{He} + 64\tilde{c}^{(6)}_{HWB}(\tilde{c}^{(6),1}_{Hl} + \tilde{c}^{(6),3}_{Hl}) \\ & -10\tilde{c}^{(8),1}_{e^2BH^2D} - 1.8(\tilde{c}^{(8),1}_{e^2H^2D^3} + \tilde{c}^{(8),2}_{e^2H^2D^3}) + 6.9(\tilde{c}^{(8),1}_{l^2BH^2D} + \tilde{c}^{(8),5}_{l^2BH^2D}) + 5.7\tilde{c}^{(8),1}_{e^2WH^2D} \\ & +1.2(\tilde{c}^{(8),1}_{l^2H^2D^3} + \tilde{c}^{(8),2}_{l^2H^2D^3}) + 0.6(\tilde{c}^{(8),3}_{l^2H^2D^3} + \tilde{c}^{(8),4}_{l^2H^2D^3}) - 3.8(\tilde{c}^{(8),1}_{l^2WH^2D} + \tilde{c}^{(8),5}_{l^2WH^2D}) \end{aligned} \tag{155}$$

With this region we see an enormous enhancement of the cases C_{3L} and C_{4L} but it is evident that class 4 operators still dominate. This is because, as seen in Figure 18 where C_1 and C_2 contributions are large at the middle and bottom of the s_2 range respectively. This means it is not possible to have one region cancel all class 4 operator contributions simultaneously. Additionally we note that the right handed contributions are also enhanced, because the region encompasses its largest contribution while the cancellation is not perfect. Invoking the two assumptions as we did for the other regions: First using assumption one, we find the scale at which the class 4 operator terms linear in dimension six Wilson coefficients overtake and dominate those quadratic in the class 4 operators to be $\Lambda \sim 3\text{TeV}$. The second assumption, namely, the loop suppression of the class 4 operators achieves the dominance of the cases C_3 and C_4 that we designed this region for. However, this only holds for muons and electrons as for the heaviest lepton flavor, the tau-lepton, the contribution from the class 3 operators would increase by order of magnitude $(m_\tau/m_\mu)^2 \sim \mathcal{O}(10^2)$ and dominate.

Finally region R_6 (see Table 3) yields:

$$\begin{aligned}
\Delta^{R_6} =& 0.75\tilde{c}^{(6)}_{H\Box} - 0.19\tilde{c}^{(6)}_{HD} - 0.093\tilde{c}^{(8)}_{HD} - 0.093\tilde{c}^{(8)}_{HD,2} + 1.5[\tilde{c}^{(6)}_{H\Box}]^2 - 0.75\tilde{c}^{(6)}_{H\Box}\tilde{c}^{(6)}_{HD} + 0.093[\tilde{c}^{(6)}_{HD}]^2 \\
&-0.79\frac{v}{\bar{m}_\mu}\tilde{c}^{(6)}_{eH} + 0.42\frac{v^2}{\bar{m}_\mu^2}[\tilde{c}^{(6)}_{eH}]^2 - 0.40\frac{v}{\bar{m}_\mu}\tilde{c}^{(8)}_{eH} - 0.79\frac{v}{\bar{m}_\mu}\tilde{c}^{(6)}_{eH}\tilde{c}^{(6)}_{H\Box} + 0.20\frac{v}{\bar{m}_\mu}\tilde{c}^{(6)}_{eH}\tilde{c}^{(6)}_{HD} \\
&+10^4\left(4.0[\tilde{c}^{(6)}_{HB}]^2 - 0.70\tilde{c}^{(6)}_{HB}\tilde{c}^{(6)}_{HW} + 0.82[\tilde{c}^{(6)}_{HW}]^2 + 2.8\tilde{c}^{(6)}_{HB}\tilde{c}^{(6)}_{HWB} - 1.7\tilde{c}^{(6)}_{HW}\tilde{c}^{(6)}_{HWB} + 1.2[\tilde{c}^{(6)}_{HWB}]^2\right) \\
&-53(\tilde{c}^{(6)}_{HB} + \tilde{c}^{(8)}_{HB}) - 140(\tilde{c}^{(6)}_{HW} + \tilde{c}^{(8)}_{HW} + \tilde{c}^{(8)}_{HW,2}) - 140(\tilde{c}^{(6)}_{HWB} + \tilde{c}^{(8)}_{HWB}) \\
&-110[\tilde{c}^{(6)}_{HB}]^2 - 64[\tilde{c}^{(6)}_{HW}]^2 + 158\tilde{c}^{(6)}_{HB}\tilde{c}^{(6)}_{HWB} - 130\tilde{c}^{(6)}_{HWB}\tilde{c}^{(6)}_{HW} - 87[\tilde{c}^{(6)}_{HWB}]^2 \\
&-53\tilde{c}^{(6)}_{HB}\tilde{c}^{(6)}_{H\Box} + 76\tilde{c}^{(6)}_{HB}\tilde{c}^{(6)}_{HD} - 140\tilde{c}^{(6)}_{HW}\tilde{c}^{(6)}_{H\Box} - 27\tilde{c}^{(6)}_{HW}\tilde{c}^{(6)}_{HD} + 144\tilde{c}^{(6)}_{HWB}\tilde{c}^{(6)}_{H\Box} - 49\tilde{c}^{(6)}_{HWB}\tilde{c}^{(6)}_{HD} \\
&-150\tilde{c}^{(6)}_{HB}\tilde{c}^{(6)}_{He} + 54\tilde{c}^{(6)}_{HB}(\tilde{c}^{(6),1}_{Hl} + \tilde{c}^{(6),3}_{Hl}) + 150\tilde{c}^{(6)}_{HW}\tilde{c}^{(6)}_{He} - 54\tilde{c}^{(6)}_{HW}(\tilde{c}^{(6),1}_{Hl} + \tilde{c}^{(6),3}_{Hl}) \\
&-94\tilde{c}^{(6)}_{HWB}\tilde{c}^{(6)}_{He} + 35\tilde{c}^{(6)}_{HWB}(\tilde{c}^{(6),1}_{Hl} + \tilde{c}^{(6),3}_{Hl}) \\
&-2.5\tilde{c}^{(8),1}_{e^2BH^2D} - 0.44(\tilde{c}^{(8),1}_{e^2H^2D^3} + \tilde{c}^{(8),2}_{e^2H^2D^3}) + 1.3\tilde{c}^{(8),1}_{e^2WH^2D} \\
&+0.67(\tilde{c}^{(8),1}_{l^2BH^2D} + \tilde{c}^{(8),5}_{l^2BH^2D}) + 0.11(\tilde{c}^{(8),1}_{l^2H^2D^3} + \tilde{c}^{(8),2}_{l^2H^2D^3}) \\
&+0.06(\tilde{c}^{(8),3}_{l^2H^2D^3} + \tilde{c}^{(8),4}_{l^2H^2D^3}) - 0.36(\tilde{c}^{(8),1}_{l^2WH^2D} + \tilde{c}^{(8),5}_{l^2WH^2D})\,. \qquad (156)
\end{aligned}$$

As expected we see a tree-level contribution from C_1 and C_2 which is on the same order of magnitude as for the full-phase space in region one Eq. 150. Additionally we find that the terms from cases C_3 and C_4 are suppressed.

In Tables 3 and 4 we summarize the regions and the corresponding dominant contributions under the two assumptions discussed in this section. From the above discussion we find that cases C_1 and C_2 coming from the class 4 operators of the SMEFT dominate in all described regions when no assumptions are applied. We find however that by assuming that the class 4 operators first occur at one-loop level, and therefore are suppressed by $1/16\pi^2$, suppresses the class 4 operators sufficiently so that we are able to emphasize other contributions. Additionally we find that the class 4 operators coming from the one-loop order interference with the standard model one-loop expression, can be distinguished from those contributing at tree-level at a larger new physics scale Λ. We also note that flavor of the final state leptons has a large impact on the contributions from the class 3 operators which shift the chirally suppressed standard model Yukawa coupling. With these considerations we conclude that it is possible to study $H \to \bar{\ell}\ell\gamma$ in the SMEFT and distinguish between tree and loop generated operators as well as resolve the direct contact four-point vertex which is first generated at dimension eight. Lastly we note that while the assumptions allow for more in depth studies of the individual SMEFT contributions they are inherent biases with which one should be careful making conclusions about UV physics.

	Class 4 operators	Class 3 operators	Class 11 and 15 operators	Λ
R_1	$D_{e,\mu,\tau}$	–	–	3.5 TeV
R_2	$C_{e,\mu}$	D_τ	$C_{e,\mu}$	3.5 TeV
R_3	C_μ	$C_\mu,\ D_\tau$	$C_\mu,\ D_e$	8 TeV
R_4	–	$D_{\mu,\tau}$	D_e	2.5 TeV
R_5	–	D_τ	$D_{e,\mu}$	3 TeV

Table 4: Table, showing for all five regions, the dominant operators D under the assumption that the Class 4 operators are generated at one loop and therefore suppressed by $1/16\pi^2$*. e, μ, τ indicates lepton-flavors. $C_{e,\mu,\tau}$ indicates that no particular contribution is dominant for the given flavor. Additionally two C's in the same row means that the two contributions marked are of the same order of magnitude. The last column shows the new physics scale Λ at which class 4 operator contributions linear in dimension six Wilson coefficients, begins to dominate those quadratic in the class 4 operators.*

7 Conclusion

In Section1 we introduced the electroweak sector of the standard model. We started with introducing the Lagrangian formalism but then went on to discuss the Higgs mechanism, spontaneous symmetry break and how this is needed for the standard model to include the observed massive gauge bosons. Then in Section 1.3 we discussed a summary of Higgs data from the LHC and noted the high uncertainty on this data. This motivated the idea that new physics could be hiding in these uncertainties. Based on this we deemed Higgs decays an interesting area in which to hunt for new physics using future data from HL-LHC. Effective field theories are a great way to do this, but before introducing effective field theories, we needed to introduce the idea of renormalizable and non-renormalizable theories.

In Section 2 we discuss renormalizability and how a non-renormalizable theory is still useful in the right context. This lead us to the concept of effective field theories. These are non-renormalizable field theories, but where higher order terms are suppressed by some scale under which the theory is perturbative. In Section 3 we discussed the effective action and the concept of integrating out a heavy field. We then discussed two famous examples of these effective field theories, the four-Fermi theory and the chiral Lagrangian of pions. We then followed a calculation of an effective Lagrangian based on a standard model Higgs modified by heavy singlet scalar. We used this example to discuss how effective field theories can be used to look for new physics.

Following the discussion of effective field theories and their use in predicting new physics, we discuss the standard model effective field theory(SMEFT) in Section 4. The SMEFT is introduced as an effective field theory extension of the standard model, to be used to look for new physics beyond the standard model. We discussed the construction of the SMEFT and the concept of the SMEFT operators shifting canonical forms of the standard model. We

discussed the redefinition of fields which lets us transform the Lagrangian to one where the fields have canonical kinetic terms. We also outline the idea of the geoSMEFT theory which provides a compact notation while including operators to all orders in the SMEFT.

We then moved on to explore the Higgs decay to two leptons and a photon in the standard model. In Section 5 we start off by calculating the squared matrix element for the process $H \to \bar{\ell}\ell\gamma$ at tree-level in the standard model. Using this we calculated the tree-level decay width. We also noted the chiral suppression of the tree-level decay by m_ℓ/v coming from the Yukawa coupling. Next we calculate the matrix elements for the processes $H \to \gamma\gamma$ and $H \to \gamma Z$ mediated by top-quark loops and discuss how these contribute to the Higgs decay $H \to \bar{\ell}\ell\gamma$ at one-loop. We then discuss the rest of the one-loop contributions to $H \to \bar{\ell}\ell\gamma$, namely the electroweak contributions, and using a parameterization we calculate the total decay width at one-loop in the standard model of $H \to \bar{\ell}\ell\gamma$. Then for the standard model we introduced Dalitz plots and produced such plots for the calculated standard model decay at both tree and one-loop level. We also discussed how the decay width at one-loop was larger than that at tree-level for electrons and on same order of magnitude for muons. This suppression of the tree-level decay width then provided motivation for our SMEFT studies.

In Section 6.4 we started by discussing the tree-level SMEFT contributions and assembling the matrix elements for these. We then used these matrix elements to calculate the total decay width shifted by the SMEFT which we normalized to the standard model. We expanded the result of this in terms of the Wilson coefficients from the contributing SMEFT operators. We then constructed Dalitz like plots of the SMEFT contributions normalized to the standard model. These Dalitz like plots then were used to guide us in designing cuts in the invariant mass of the final state di-lepton system. Using such cuts (see Table 3) in combination with the assumption of weakly interacting new physics or an assumed new physics scale, we were able to emphasize different SMEFT contributions(see Table 4). This was especially so when also considering flavor of the final state leptons. We found however that the contributions from class 4 operators dominate in all regions presented when no assumptions are made. Finally we note that these assumptions bring inherent bias, or model dependence, and should be taken with care.

Appendices

A SMEFT $\mathcal{L}_6$ Operators

$1:X^3$		$2:H^6$		$3:H^4D^2$		$5:\psi^2H^3+\text{h.c.}$	
Q_G	$f^{ABC}G_\mu^{A\nu}G_\nu^{B\rho}G_\rho^{C\mu}$	Q_H	$(H^\dagger H)^3$	$Q_{H\Box}$	$(H^\dagger H)\Box(H^\dagger H)$	Q_{eH}	$(H^\dagger H)(\bar{l}_p e_r H)$
Q_W	$\epsilon^{IJK}W_\mu^{I\nu}W_\nu^{J\rho}W_\rho^{K\mu}$			Q_{HD}	$\left(H^\dagger D^\mu H\right)^*\left(H^\dagger D_\mu H\right)$	Q_{uH}	$(H^\dagger H)(\bar{q}_p u_r \widetilde{H})$
						Q_{dH}	$(H^\dagger H)(\bar{q}_p d_r H)$

$4:X^2H^2$		$6:\psi^2XH+\text{h.c.}$		$7:\psi^2H^2D$	
Q_{HG}	$H^\dagger H\, G^A_{\mu\nu}G^{A\mu\nu}$	Q_{eW}	$(\bar{l}_p\sigma^{\mu\nu}e_r)\tau^I H W^I_{\mu\nu}$	$Q_{Hl}^{(1)}$	$(H^\dagger i\overleftrightarrow{D}_\mu H)(\bar{l}_p\gamma^\mu l_r)$
Q_{HW}	$H^\dagger H\, W^I_{\mu\nu}W^{I\mu\nu}$	Q_{eB}	$(\bar{l}_p\sigma^{\mu\nu}e_r)H B_{\mu\nu}$	$Q_{Hl}^{(3)}$	$(H^\dagger i\overleftrightarrow{D}^I_\mu H)(\bar{l}_p\tau^I\gamma^\mu l_r)$
Q_{HB}	$H^\dagger H\, B_{\mu\nu}B^{\mu\nu}$	Q_{uG}	$(\bar{q}_p\sigma^{\mu\nu}T^A u_r)\widetilde{H}\, G^A_{\mu\nu}$	Q_{He}	$(H^\dagger i\overleftrightarrow{D}_\mu H)(\bar{e}_p\gamma^\mu e_r)$
Q_{HWB}	$H^\dagger\tau^I H\, W^I_{\mu\nu}B^{\mu\nu}$	Q_{uW}	$(\bar{q}_p\sigma^{\mu\nu}u_r)\tau^I\widetilde{H}\, W^I_{\mu\nu}$	$Q_{Hq}^{(1)}$	$(H^\dagger i\overleftrightarrow{D}_\mu H)(\bar{q}_p\gamma^\mu q_r)$
		Q_{uB}	$(\bar{q}_p\sigma^{\mu\nu}u_r)\widetilde{H}\, B_{\mu\nu}$	$Q_{Hq}^{(3)}$	$(H^\dagger i\overleftrightarrow{D}^I_\mu H)(\bar{q}_p\tau^I\gamma^\mu q_r)$
		Q_{dG}	$(\bar{q}_p\sigma^{\mu\nu}T^A d_r)H\, G^A_{\mu\nu}$	Q_{Hu}	$(H^\dagger i\overleftrightarrow{D}_\mu H)(\bar{u}_p\gamma^\mu u_r)$
		Q_{dW}	$(\bar{q}_p\sigma^{\mu\nu}d_r)\tau^I H\, W^I_{\mu\nu}$	Q_{Hd}	$(H^\dagger i\overleftrightarrow{D}_\mu H)(\bar{d}_p\gamma^\mu d_r)$
		Q_{dB}	$(\bar{q}_p\sigma^{\mu\nu}d_r)H\, B_{\mu\nu}$	$Q_{Hud}+\text{h.c.}$	$i(\widetilde{H}^\dagger D_\mu H)(\bar{u}_p\gamma^\mu d_r)$

$8:(\bar{L}L)(\bar{L}L)$		$8:(\bar{R}R)(\bar{R}R)$		$8:(\bar{L}L)(\bar{R}R)$	
Q_{ll}	$(\bar{l}_p\gamma_\mu l_r)(\bar{l}_s\gamma^\mu l_t)$	Q_{ee}	$(\bar{e}_p\gamma_\mu e_r)(\bar{e}_s\gamma^\mu e_t)$	Q_{le}	$(\bar{l}_p\gamma_\mu l_r)(\bar{e}_s\gamma^\mu e_t)$
$Q_{qq}^{(1)}$	$(\bar{q}_p\gamma_\mu q_r)(\bar{q}_s\gamma^\mu q_t)$	Q_{uu}	$(\bar{u}_p\gamma_\mu u_r)(\bar{u}_s\gamma^\mu u_t)$	Q_{lu}	$(\bar{l}_p\gamma_\mu l_r)(\bar{u}_s\gamma^\mu u_t)$
$Q_{qq}^{(3)}$	$(\bar{q}_p\gamma_\mu\tau^I q_r)(\bar{q}_s\gamma^\mu\tau^I q_t)$	Q_{dd}	$(\bar{d}_p\gamma_\mu d_r)(\bar{d}_s\gamma^\mu d_t)$	Q_{ld}	$(\bar{l}_p\gamma_\mu l_r)(\bar{d}_s\gamma^\mu d_t)$
$Q_{lq}^{(1)}$	$(\bar{l}_p\gamma_\mu l_r)(\bar{q}_s\gamma^\mu q_t)$	Q_{eu}	$(\bar{e}_p\gamma_\mu e_r)(\bar{u}_s\gamma^\mu u_t)$	Q_{qe}	$(\bar{q}_p\gamma_\mu q_r)(\bar{e}_s\gamma^\mu e_t)$
$Q_{lq}^{(3)}$	$(\bar{l}_p\gamma_\mu\tau^I l_r)(\bar{q}_s\gamma^\mu\tau^I q_t)$	Q_{ed}	$(\bar{e}_p\gamma_\mu e_r)(\bar{d}_s\gamma^\mu d_t)$	$Q_{qu}^{(1)}$	$(\bar{q}_p\gamma_\mu q_r)(\bar{u}_s\gamma^\mu u_t)$
		$Q_{ud}^{(1)}$	$(\bar{u}_p\gamma_\mu u_r)(\bar{d}_s\gamma^\mu d_t)$	$Q_{qu}^{(8)}$	$(\bar{q}_p\gamma_\mu T^A q_r)(\bar{u}_s\gamma^\mu T^A u_t)$
		$Q_{ud}^{(8)}$	$(\bar{u}_p\gamma_\mu T^A u_r)(\bar{d}_s\gamma^\mu T^A d_t)$	$Q_{qd}^{(1)}$	$(\bar{q}_p\gamma_\mu q_r)(\bar{d}_s\gamma^\mu d_t)$
				$Q_{qd}^{(8)}$	$(\bar{q}_p\gamma_\mu T^A q_r)(\bar{d}_s\gamma^\mu T^A d_t)$

$$H^\dagger i\overleftrightarrow{D}_\mu H \equiv H^\dagger iD_\mu H - (iD_\mu H^\dagger)H$$
$$H^\dagger i\overleftrightarrow{D}^I_\mu H \equiv H^\dagger i\tau^I D_\mu H - (iD_\mu\tau^I H^\dagger)H$$

Table 5: The operators in the SMEFT at dimension $d = 6$ from [17].There are 59 unique operator forms that occur at dimension-six. In this table we have removed the CP odd operators as they are not relevant to our discussion. There are 5 four fermion operators which we have removed as they are not relevant to this thesis.

B Class 11 and 15 SMEFT Operators

Dimension eight we have the following operators from classes 11 and 15[29].

Class 11: $\psi^2 H^2 D^3$	
$Q^{(8),1}_{l^2H^2D^3}$	$i(\bar{l}\gamma^\mu D^\nu l)(D_{(\mu}D_{\nu)}H^\dagger H)$
$Q^{(8),2}_{l^2H^2D^3}$	$i(\bar{l}\gamma^\mu D^\nu l)(H^\dagger D_{(\mu}D_{\nu)}H)$
$Q^{(8),3}_{l^2H^2D^3}$	$i(\bar{l}\gamma^\mu \tau^I D^\nu l)(D_{(\mu}D_{\nu)}H^\dagger \tau^I H)$
$Q^{(8),4}_{l^2H^2D^3}$	$i(\bar{l}\gamma^\mu \tau^I D^\nu l)(H^\dagger \tau^I D_{(\mu}D_{\nu)}H)$
$Q^{(8),1}_{e^2H^2D^3}$	$i(\bar{e}_R\gamma^\mu D^\nu e_R)(D_{(\mu}D_{\nu)}H^\dagger H)$
$Q^{(8),2}_{e^2H^2D^3}$	$i(\bar{e}_R\gamma^\mu D^\nu e_R)(H^\dagger D_{(\mu}D_{\nu)}H)$

Class 15: $\psi^2 X H^2 D$	
$Q^{(8),1}_{e^2WH^2D}$	$(\bar{e}_R\gamma^\nu e_R)D^\mu(H^\dagger\tau^I H)W^I_{\mu\nu}$
$Q^{(8),1}_{e^2BH^2D}$	$(\bar{e}_R\gamma^\nu e_R)D^\mu(H^\dagger H)B_{\mu\nu}$
$Q^{(8),1}_{l^2WH^2D}$	$(\bar{l}\gamma^\nu l)D^\mu(H^\dagger\tau^I H)W^I_{\mu\nu}$
$Q^{(8),5}_{l^2WH^2D}$	$(\bar{l}\gamma^\nu\tau^I l)D^\mu(H^\dagger H)W^I_{\mu\nu}$
$Q^{(8),9}_{l^2WH^2D}$	$\epsilon^{IJK}(\bar{l}\gamma^\nu\tau^I l)D^\mu(H^\dagger\tau^J H)W^K_{\mu\nu}$
$Q^{(8),1}_{l^2BH^2D}$	$(\bar{l}\gamma^\nu\tau^I l)D^\mu(H^\dagger\tau^I H)B_{\mu\nu}$
$Q^{(8),5}_{l^2BH^2D}$	$(\bar{l}\gamma^\nu l)D^\mu(H^\dagger H)B_{\mu\nu}$

Table 6: SMEFT operators forms of dimension eight, taken from Ref.[29]. These are used in the calculation of tree-level SMEFT contributions to the Higgs decay to two leptons and a photon

C Feynman Rules

Higgs coupling to fermions:

$$H \to f\bar{f} = -im_f\frac{g_2}{2m_W}\,. \tag{C.1}$$

fermion propagator:

$$f \to f = \frac{i(\gamma^\mu p_\mu + m_f)}{p^2 - m_f^2 + i\epsilon}\,. \tag{C.2}$$

fermion coupling to photons:

$$ff \to \gamma = -iQ_f e\gamma^\mu\,. \tag{C.3}$$

Fermion coupling to Z boson:

$$\bar{f}f \to Z = -i\left(\frac{g_2}{c_w}\right)\gamma^\mu(c_L P_L + c_R P_R) = -i\gamma^\mu(g_L P_L + g_R P_R)\,. \tag{C.4}$$

C.1 SMEFT Feynman Rules

These are the tree-level SMEFT Feynman rules taken from Ref. [29]

Tree-level coupling of Higgs to two photons or a photon and a Z-boson:

$$\begin{pmatrix} H \\ A_1 \\ A_2 \end{pmatrix} = ig_{HAA}v(k_1^{\mu_2}k_2^{\mu_1} - k_1\cdot k_2\eta^{\mu_1\mu_2}) \tag{C.5}$$

$$\begin{pmatrix} H \\ A_1 \\ Z_2 \end{pmatrix} = -\frac{ig_{HAZ}v}{2}(k_1^{\mu_2}k_2^{\mu_1} - k_1\cdot k_2\eta^{\mu_1\mu_2}) \tag{C.6}$$

With definitions:

$$\begin{aligned} g_{HAZ} &= \left[8(c_{HB}^{(6)} - c_{HW}^{(6)})\bar{c}_W\bar{s}_W + 4c_{HWB}^{(6)}(\bar{c}_W^2 - \bar{s}_W^2)\right](1+\Delta_{HAZ}v^2) \\ &\quad + v^2\left[8(c_{HB}^{(8)} - c_{HW}^{(8)} - c_{HW,2}^{(8)})\bar{c}_W\bar{s}_W + 4c_{HWB}^{(8)}(\bar{c}_W^2 - \bar{s}_W^2)\right] \end{aligned} \tag{C.7}$$

$$\Delta_{HAZ} = 2c_{HB}^{(6)} + 2c_{HW}^{(6)} + c_{H\Box}^{(6)} - \frac{1}{4}c_{HD}^{(6)} \tag{C.8}$$

$$\begin{aligned} g_{HAA} &= 4\left[c_{HB}^{(6)}\bar{c}_W^2 + c_{HW}^{(6)}\bar{s}_W^2 - \bar{s}_W\bar{c}_W c_{HWB}^{(6)}\right] \\ &\quad + v^2\bar{c}_W^2\left[c_{HB}^{(6)}(8c_{HB}^{(6)} + 4c_{H\Box}^{(6)} - c_{HD}^{(6)}) + 2(\bar{c}_{HWB}^{(6)})^2\right] \\ &\quad + v^2\bar{s}_W^2\left[c_{HW}^{(6)}(8c_{HW}^{(6)} + 4c_{H\Box}^{(6)} - c_{HD}^{(6)}) + 2(\bar{c}_{HWB}^{(6)})^2\right] \\ &\quad - v^2\bar{c}_W\bar{s}_W c_{HWB}^{(6)}\left[8c_{HB}^{(6)} + 4c_{H\Box}^{(6)} - c_{HD}^{(6)} + 8c_{HW}^{(6)}\right] \\ &\quad + 4v^2\left[c_{HB}^{(8)}\bar{c}_W^2 + (c_{HW}^{(8)} + c_{HW,2}^{(8)})\bar{s}_W^2 - \bar{s}_W\bar{c}_W c_{HWB}^{(8)}\right] \end{aligned} \tag{C.9}$$

Class 7 operators shift the Z coupling to leptons yielding the rule Feynman rule:

$$\begin{pmatrix} \bar{\ell} \\ \ell \\ \hat{Z}_1 \end{pmatrix} = i\frac{\bar{g}_Z}{2}\gamma^{\mu_1}(g'_L P_L + g'_R P_R) \tag{C.10}$$

$$g'_L = v^2\left(c_{Hl}^{(6),1} + c_{Hl}^{(6),3}\right)(1+\Delta_{Z\ell\ell}) + \frac{v^4}{2}\left(c_{Hl}^{(8),1} + c_{Hl}^{(8),2} + c_{Hl}^{(8),3}\right) \tag{C.11}$$

$$g'_R = v^2 c_{He}^{(6)}(1+\Delta_{Z\ell\ell}) + \frac{v^4}{2}c_{He}^{(8)} \tag{C.12}$$

$$\Delta_{Z\ell\ell} = \frac{v^2}{2}\left[2\bar{c}_W g_2 c_{HW}^{(6)} + 2\bar{s}_W g_1 \bar{c}_{HB}^{(6)} + (g_2\bar{s}_W + g_1\bar{c}_W)c_{HWB}^{(6)}\right] \tag{C.13}$$

Class 11 operators shift the Z coupling to leptons yielding Feynman rule:

$$\begin{pmatrix} \bar{\ell} \\ \ell_1 \\ \hat{Z}_2 \end{pmatrix} = i\frac{\bar{g}_Z}{8}v^2\left[A_{11}(k_1\cdot k_2\gamma^{\mu_2} + k_1^{\mu_2}\not{k}_2)P_L + B_{11}(k_1\cdot k_2\gamma^{\mu_2} + k_1^{\mu_2}\not{k}_2)P_R\right] \tag{C.14}$$

$$A_{11} = 2c_{l^2H^2D^3}^{(8),1} - 2c_{l^2H^2D^3}^{(8),2} + c_{l^2H^2D^3}^{(8),3} - c_{l^2H^2D^3}^{(8),4} \tag{C.15}$$

$$B_{11} = 2c_{e^2H^2D^3}^{(8),1} - 2c_{e^2H^2D^3}^{(8),2} \tag{C.16}$$

Class 11 and Class 15 operators can generate a single vertex interaction $H \to \bar{\ell}\ell\gamma$:

$$\begin{pmatrix} \bar{\ell} \\ \ell \\ \hat{A}_1 \\ \hat{H}_2 \end{pmatrix} = \begin{array}{l} i\frac{Q_\ell \bar{e} v}{2} k_2^{\mu_1} \not{k}_2 (A'_{11} P_L + B'_{11} P_R) \\ -iv\left[A_{15}(k_1 \cdot k_2 \gamma^{\mu_1} - k_2^{\mu_1} \not{k}_1) P_L + B_{15}(k_1 \cdot k_2 \gamma^{\mu_1} - k_2^{\mu_1} \not{k}_1) P_R\right] \end{array} \tag{C.17}$$

$$A'_{11} = 2c^{(8),1}_{l^2H^2D^3} + 2c^{(8),2}_{l^2H^2D^3} + c^{(8),3}_{l^2H^2D^3} + c^{(8),4}_{l^2H^2D^3} \tag{C.18}$$

$$B'_{11} = 2c^{(8),1}_{e^2H^2D^3} + 2c^{(8),2}_{e^2H^2D^3} \tag{C.19}$$

$$A_{15} = \bar{c}_W (c^{(8),1}_{l^2BH^2D} + c^{(8),5}_{l^2BH^2D}) - \bar{s}_W (c^{(8),1}_{l^2WH^2D} + c^{(8),5}_{l^2WH^2D}) \tag{C.20}$$

$$B_{15} = \bar{c}_W c^{(8),1}_{e^2BH^2D} - \bar{s}_W c^{(8),1}_{e^2WH^2D} \tag{C.21}$$

D 3-body phase space

This section is based on Ref. [30] The three body phase space is relevant when calculating crosssections of $1 \to 3$ processes and can be modeled similarly to $2 \to 2$ processes. The physical region of phase space with in the $1 \to 3$ process can be described by the condition:

$$G(s_1, s_2, s, m_2^2, m_1^2, m_3^2) < 0\,. \tag{D.1}$$

Where $\{s_1, s_2, s, m_2^2, m_1^2, m_3^2\}$ are the masses and invariant variable defined as:

$$s_1 = (p_1 + p_2)^2\,. \tag{D.2}$$

$$s_2 = (p_2 + p_3)^2\,. \tag{D.3}$$

$$s_3 = (p_1 + p_3)^2\,. \tag{D.4}$$

The decaying particles center of mass energy is $\sqrt{s}$, and the labels $1, 2, 3$ refer to the decay products. These are related by:

$$s_1 + s_2 + s_3 = s + m_1^2 + m_2^2 + m_3^2\,. \tag{D.5}$$

The center of mass energy of the decaying particle is equal to it's mass when in its rest frame so that $\sqrt{s} = M_{\text{Decay}}$. The function G can be interpreted as a tetrahedron function defined as a Cayley determinant:

$$G[x, y, z, u, v, w] = -\frac{1}{2}\begin{vmatrix} 0 & 1 & 1 & 1 & 1 \\ 1 & 0 & v & x & z \\ 1 & v & 0 & u & y \\ 1 & x & u & 0 & w \\ 1 & z & y & w & 0 \end{vmatrix}\,. \tag{D.6}$$

The three body decay rate is then:

$$\Gamma_3 = \frac{1}{2\sqrt{s}} \frac{1}{(2\pi)^5} R_3(s)\,. \tag{D.7}$$

With Lorentz invariant phase space integral :

$$R_3(s) = \frac{8\pi^2}{32s}\int ds_1 ds_2 \Theta[-G(s_1, s_2, s, m_2^2, m_1^2, m_3^2)]\,, \tag{D.8}$$

where $\Theta(x)$ is the heavyside step-function.

E The Trace Technique and Spin Sums

This section follows the discussion in [3]. When calculating the squares of matrix elements involving external on-shell fermions it is a common feature to obtain a combination of fermion currents from which a trace can be formed. Employing the following identities we demonstrate how spin sums can be calculated:

$$\sum_{r=1}^{2} = v_r \bar{v}_r = \not{p} - m\,, \tag{E.1}$$

$$\sum_{s=1}^{2} = u_s \bar{u}_s = \not{p} + m\,, \tag{E.2}$$

makes spin sums easy to do.

Take as an example the process $e^-(p_1) + e^+(p_2) \to e^+(p_3) + e^-(p_4)$: The matrix element in Feynmann guage: $\epsilon = 0$ is:

$$i\mathcal{M} = \bar{v}(p_2)\left(-ie\gamma^\mu\right)u(p_1)\left(\frac{-i\left(g_{\mu\nu}\right)}{k^2}\right)\bar{u}(p_4)\left(-ie\gamma^\nu\right)v(p_3)\,. \tag{E.3}$$

We find the matrix element squared:

$$|\mathcal{M}|^2 = \frac{e^4}{k^4}\left[\bar{v}_\alpha(p_2)\gamma^\mu_{\alpha\beta}u_\beta(p_1)\right]\left[\bar{u}_\rho(p_4)\gamma_{\mu\rho\sigma}v_\sigma(p_3)\right] \times \left[\bar{u}_\alpha(p_1)\gamma^\mu_{\alpha\beta}v_\beta(p_2)\right]\left[\bar{v}_\rho(p_3)\gamma_{\mu\rho\sigma}u_\sigma(p_4)\right]\,. \tag{E.4}$$

Since spinor indices keeps track of matrix multiplication for us, we are free to move the elements of this equation around. Using that for a square matrix M, $M_i i = Tr[M]$, we can see that this product of matrices reduces to the product of two traces:

$$\sum_{Spins}|\mathcal{M}|^2 = \frac{e^4}{k^4}\left[\not{p}_1 + m\right]_{\beta i}\left[\not{p}_2 - m\right]_{j\alpha}\gamma^\mu_{\alpha\beta}\gamma^\nu_{ij} \times \left[\not{p}_3 - m\right]_{\sigma n}\left[\not{p}_4 + m\right]_{m\rho}\gamma_{\nu nm}\gamma_{\mu\rho\sigma}\,. \tag{E.5}$$

$$\sum_{Spins}|\mathcal{M}|^2 = \frac{e^4}{k^4}Tr\left(\left[\not{p}_1 + m\right]\gamma^\nu\left[\not{p}_2 - m\right]\gamma^\mu\right) \times Tr\left(\left[\not{p}_3 - M\right]\gamma_\nu\left[\not{p}_4 + M\right]\gamma_\mu\right)\,. \tag{E.6}$$

Where the dirac slash notation has been used, $\not{p} = \gamma^\mu p_\mu$.

The identities taken from [3] in Table 7 can then be used to obtain the final matrix element squared in terms of the momentum of involved particles.

$Tr(\mathbb{I})$	4
$Tr(\prod^{n=\text{odd}} \gamma^\mu)$	0
$Tr(\gamma^\mu\gamma^\nu)$	$4g^{\mu\nu}$
$Tr(\gamma^\mu\gamma^\nu\gamma^\rho\gamma^\sigma)$	$4g^{\mu\nu}g^{\rho\sigma} - 4g^{\mu\rho}g^{\nu\sigma} + 4g^{\mu\sigma}g^{\nu\rho}$
$Tr(\gamma^5 \prod^{n=\text{odd}} \gamma^\mu)$	0
$Tr(\gamma^5)$	0
$Tr(\gamma^5\gamma^\mu\gamma^\nu)$	0
$Tr(\gamma^5\gamma^\mu\gamma^\nu\gamma^\rho\gamma^\sigma)$	$4i\epsilon^{\mu\nu\rho\sigma}$

Table 7: Trace Identities from [3]. $\epsilon^{\mu\nu\rho\sigma}$ is the Levi-Cevita anti symmetric tensor.

The chiral basis $\{\mathbb{I}, P_\pm, \gamma^\mu P_\pm, \sigma^{\mu\nu}\}$, forms a complete basis for the γ^μ-matrix space. Because of this Table 8 contains all combinations of fermion bilinears in the chiral basis calculated using Table 7.

Interference	Result
$\bar{\psi}_{k_1}\gamma^\mu P_\pm\chi_{k_2}(\bar{\psi}_{k_1}P_\pm\chi_{k_2})^\dagger$	$2m_\chi k_1^\mu$
$\bar{\psi}_{k_1}\gamma^\mu P_\pm\chi_{k_2}(\bar{\psi}_{k_1}P_\mp\chi_{k_2})^\dagger$	$2m_\psi k_2^\mu$
$\bar{\psi}_{k_1}\gamma^\mu P_\pm\chi_{k_2}(\bar{\psi}_{k_1}\gamma^\nu P_\pm\chi_{k_2})^\dagger$	$2k_1^\nu k_2^\mu + 2k_1^\mu k_2^\nu - 2k_1\cdot k_2 g^{\mu\nu} \pm 2i\epsilon^{\mu\nu\sigma\rho}k_{1,\sigma}k_{2,\rho}$
$\bar{\psi}_{k_1}\gamma^\mu P_\pm\chi_{k_2}(\bar{\psi}_{k_1}\gamma^\nu P_\mp\chi_{k_2})^\dagger$	$2m_\psi m_\chi g^{\mu\nu}$
$\bar{\psi}_{k_1}\gamma^\mu P_\pm\chi_{k_2}(\bar{\psi}_{k_1}\sigma^{\mu\nu}\chi_{k_2})^\dagger$	$6im_\chi k_1^\nu - 6im_\psi k_2^\nu$
$\bar{\psi}_{k_1}\gamma^\mu P_\pm\chi_{k_2}(\bar{\psi}_{k_1}\mathbb{I}\chi_{k_2})^\dagger$	$2m_\chi k_1^\mu + 2m_\psi k_2^\mu$

Table 8: Table of all possible interferences of fermion bilinears in the chiral basis.$\epsilon^{\mu\nu\rho\sigma}$ is the Levi-Cevita anti symmetric tensor.

F Dimensional regularization

This section is based on discussions in Ref. [7] There are many approaches to regulating divergences in loop diagrams in quantum field theory. One of the most commonly employed methods is dimensional regularization.

Take for example the photon vacuum energy loop integral:

$$-i\Pi = \int \frac{d^4l}{(2\pi)^2} \frac{(-i\gamma^\mu_{ab}e)(\gamma^\mu l_\mu + m)_{bc}(-i\gamma^\mu_{cd}e)(\gamma^\mu(l-p)_\mu + m)_{da}}{[l^2 - m^2 + i\epsilon][(l-p)^2 - m^2 + i\epsilon]}\,. \tag{F.1}$$

This loop integral is divergent in four dimension but taking the dimension to be $d = 4 - 2\epsilon$ we can compute the integral. Afterward we can then get physical result by taking the limit of

$d \to 4$. We find:

$$-i\Pi = \mu^{2\epsilon} \int \frac{d^d l}{(2\pi)^2} \frac{(-i\gamma^\mu_{ab} e)(\gamma^\mu l_\mu + m)_{bc}(-i\gamma^\mu_{cd} e)(\gamma^\mu (l-p)_\mu + m)_{da}}{[l^2 - m^2 + i\epsilon][(l-p)^2 - m^2 + i\epsilon]}\,, \tag{F.2}$$

here μ^ϵ is added to keep the units correct when going to $d = 4 - 2\epsilon$ dimensions. From here one uses Feynman parametrization, Eq. F.3 to obtain an appropriate form in order to use the loop integral master equation in dimensional regularization Eq. F.5

$$\frac{1}{A_1 \cdots A_n} = \int_1^1 d\alpha_1 \cdots d\alpha_n \frac{\Gamma(n)\delta(1 - \alpha_1 - \cdots - \alpha_n)}{[\alpha_1 A_1 + \cdots + \alpha_n A_n]^n}\,. \tag{F.3}$$

Where:

$$\Gamma(n) = \int_0^\infty x^{n-1} e^{-x} dx\,, \tag{F.4}$$

is the extension of the factorial function to complex numbers[40].

$$\int \frac{d^d k}{(2\pi)^d} \frac{k^{2a}}{(k^2 - \Delta)^b} = i(-1)^{a-b} \frac{1}{\Delta^{a-b-\frac{d}{2}}} \frac{\Gamma(a + \frac{d}{2})\Gamma(b - a - \frac{d}{2})}{\Gamma(b)\Gamma(\frac{d}{2})}\,. \tag{F.5}$$

In the limit $\epsilon \to 0$ the Γ-function can be expanded as[2]:

$$\Gamma(\epsilon) = \frac{1}{\epsilon} - \gamma_E + \mathcal{O}(\epsilon)\,. \tag{F.6}$$

Where $\gamma_E = 0.5772$ is known as the Euler-Mascheroni constant.

References

[1] M. Peskin and D. Schroeder, *An Introduction to Quantum Field Theory*. Advanced book classics, Avalon Publishing, 1995.

[2] M. D. Schwartz, *Quantum field theory and the standard model*. Cambridge University Press, 2014.

[3] M. Thomson, *Modern Particle Physics*. Modern Particle Physics, Cambridge University Press, 2013.

[4] M. Cepeda *et al.*, "Report from Working Group 2: Higgs Physics at the HL-LHC and HE-LHC," *CERN Yellow Rep. Monogr.*, vol. 7, pp. 221–584, 2019.

[5] "Standard Model Summary Plots June 2021," tech. rep., CERN, Geneva, Jul 2021. All figures including auxiliary figures are available at https://atlas.web.cern.ch/Atlas/GROUPS/PHYSICS/PUBNOTES/ATL-PHYS-PUB-2021-032.

[6] G. Aad *et al.*, "Combined measurements of Higgs boson production and decay using up to 80 fb^{-1} of proton-proton collision data at $\sqrt{s} = 13$ TeV collected with the ATLAS experiment," *Phys. Rev. D*, vol. 101, no. 1, p. 012002, 2020.

[7] J. F. Donoghue, E. Golowich, and B. R. Holstein, *Dynamics of the standard model*, vol. 35. Cambridge university press, 2014.

[8] B. Henning, X. Lu, and H. Murayama, "How to use the Standard Model effective field theory," *JHEP*, vol. 01, p. 023, 2016.

[9] T. Corbett, O. J. P. Éboli, and M. C. Gonzalez-Garcia, "Inverse amplitude method for the perturbative electroweak symmetry breaking sector: The singlet Higgs portal as a study case," *Phys. Rev. D*, vol. 93, no. 1, p. 015005, 2016.

[10] P. J. Mohr, B. N. Taylor, and D. B. Newell, "Codata recommended values of the fundamental physical constants: 2010," *Rev. Mod. Phys.*, vol. 84, pp. 1527–1605, Nov 2012.

[11] C. Patrignani *et al.*, "Review of Particle Physics," *Chin. Phys. C*, vol. 40, no. 10, p. 100001, 2016.

[12] J. Konya and N. Nagy, *Nuclear and Radiochemistry*. Elsevier insights, Elsevier Science, 2012.

[13] J. Goldstone, "Field Theories with Superconductor Solutions," *Nuovo Cim.*, vol. 19, pp. 154–164, 1961.

[14] B. Grzadkowski, M. Iskrzynski, M. Misiak, and J. Rosiek, "Dimension-Six Terms in the Standard Model Lagrangian," *JHEP*, vol. 10, p. 085, 2010.

[15] B. Henning, X. Lu, and H. Murayama, "How to use the standard model effective field theory," 2015.

[16] S. Weinberg, "Baryon and Lepton Nonconserving Processes," *Phys. Rev. Lett.*, vol. 43, pp. 1566–1570, 1979.

[17] I. Brivio, Y. Jiang, and M. Trott, "The SMEFTsim package, theory and tools," *JHEP*, vol. 12, p. 070, 2017.

[18] T. Corbett, O. J. P. Eboli, J. Gonzalez-Fraile, and M. C. Gonzalez-Garcia, "Robust Determination of the Higgs Couplings: Power to the Data," *Phys. Rev. D*, vol. 87, p. 015022, 2013.

[19] C. Hays, A. Helset, A. Martin, and M. Trott, "Exact SMEFT formulation and expansion to $\mathcal{O}(v^4/\Lambda^4)$," *JHEP*, vol. 11, p. 087, 2020.

[20] A. Helset, A. Martin, and M. Trott, "The geometric standard model effective field theory," *Journal of High Energy Physics*, vol. 2020, Mar 2020.

[21] T. Corbett, "The Feynman rules for the SMEFT in the background field gauge," *JHEP*, vol. 03, p. 001, 2021.

[22] A. Firan and R. Stroynowski, "Internal conversions in Higgs decays to two photons," *Phys. Rev. D*, vol. 76, p. 057301, 2007.

[23] Y. Sun, H.-R. Chang, and D.-N. Gao, "Higgs decays to gamma l+ l- in the standard model," *JHEP*, vol. 05, p. 061, 2013.

[24] R. Akbar, I. Ahmed, and M. J. Aslam, "Lepton Polarization Asymmetries of $H \to \gamma\tau^+\tau^-$ Decays in Standard Model," *PTEP*, vol. 2014, no. 9, p. 093B03, 2014.

[25] A. Abbasabadi, D. Bowser-Chao, D. A. Dicus, and W. W. Repko, "Radiative Higgs boson decays H —> fermion anti-fermion gamma," *Phys. Rev. D*, vol. 55, pp. 5647–5656, 1997.

[26] A. Kachanovich, U. Nierste, and I. Nišandžić, "Higgs boson decay into a lepton pair and a photon revisited," *Phys. Rev. D*, vol. 101, no. 7, p. 073003, 2020.

[27] G. Passarino, "Higgs Boson Production and Decay: Dalitz Sector," *Phys. Lett. B*, vol. 727, pp. 424–431, 2013.

[28] T. Han and X. Wang, "Radiative Decays of the Higgs Boson to a Pair of Fermions," *JHEP*, vol. 10, p. 036, 2017.

[29] T. Corbett and T. Rasmussen, "Higgs decays to two leptons and a photon beyond leading order in the smeft," 2021.

[30] E. Byckling and K. Kajantie, *Particle Kinematics*. A Wiley-Interscience publication, Wiley, 1973.

[31] T. Hahn, "Cuba—a library for multidimensional numerical integration," *Computer Physics Communications*, vol. 168, no. 2, pp. 78–95, 2005.

[32] P. A. Zyla *et al.*, "Review of Particle Physics," *PTEP*, vol. 2020, no. 8, p. 083C01, 2020.

[33] I. Dubovyk, A. Freitas, J. Gluza, T. Riemann, and J. Usovitsch, "Electroweak pseudo-observables and Z-boson form factors at two-loop accuracy," *JHEP*, vol. 08, p. 113, 2019.

[34] K. Olive, "Review of particle physics," vol. 40, p. 100001, oct 2016.

[35] H. H. Patel, "Package-x 2.0: A mathematica package for the analytic calculation of one-loop integrals," *Computer Physics Communications*, vol. 218, pp. 66–70, 2017.

[36] I. Brivio, "Smeftsim 3.0 — a practical guide," *Journal of High Energy Physics*, vol. 2021, Apr 2021.

[37] A. Kachanovich, U. Nierste, and I. Nisandzic, "Higgs decay into a lepton pair and a photon: a roadmap to $\mathbf{H} \to \mathbf{Zfl}$ discovery and probes of new physics," 2021.

[38] J. de Blas, J. C. Criado, M. Perez-Victoria, and J. Santiago, "Effective description of general extensions of the Standard Model: the complete tree-level dictionary," *JHEP*, vol. 03, p. 109, 2018.

[39] E. da Silva Almeida, A. Alves, O. J. P. Éboli, and M. C. Gonzalez-Garcia, "Electroweak legacy of the lhc run ii," 2021.

[40] P. J. Davis, "Leonhard euler's integral: A historical profile of the gamma function: In memoriam: Milton abramowitz," *The American Mathematical Monthly*, vol. 66, no. 10, pp. 849–869, 1959.